

Advancements in Photovoltaic Cell and System Technologies

Lead Guest Editor: Daniel T. Cotfas

Guest Editors: Dezso Sera, Eleni Kaplani, Petru A. Cotfas, and Alireza Rezaniakolaei





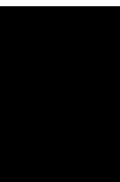
Advancements in Photovoltaic Cell and System Technologies

International Journal of Photoenergy

Advancements in Photovoltaic Cell and System Technologies

Lead Guest Editor: Daniel T. Cotfas

Guest Editors: Dezso Sera, Eleni Kaplani, Petru A. Cotfas,
and Alireza Rezaniakolaei



Copyright © 2019 Hindawi Limited. All rights reserved.

This is a special issue published in "International Journal of Photoenergy." All articles are open access articles distributed under the Creative Commons Attribution License, which permits unrestricted use, distribution, and reproduction in any medium, provided the original work is properly cited.

Chief Editor

Giulia Grancini, Italy




Editorial Board

Mohamed S.A. Abdel-Mottaleb, Egypt
Angelo Albini, Italy
Alberto Álvarez-Gallegos, Mexico
Vincenzo Augugliaro, Italy
Detlef W. Bahnemann, Germany
Simona Binetti, Italy
Fabio Bisegna, Italy
Thomas M. Brown, Italy
Joaquim Carneiro, Portugal
Yatendra S. Chaudhary, India
Yong Chen, China
Věra Cimrová, Czech Republic
Gianluca Coccia, Italy
Juan M. Coronado, Spain
P. Davide Cozzoli, Italy
Dionysios D. Dionysiou, USA
Abderrazek Douhal, Spain
Mahmoud M. El-Nahass, Egypt
Polycarpos Falaras, Greece
Chris Ferekides, USA
Paolo Fornasiero, Italy
Manuel Fuentes Conde, Spain
Germà Garcia-Belmonte, Spain
Elisa Isabel Garcia-Lopez, Italy
Mohammed Ashraf Gondal, Saudi Arabia
Pierluigi Guerriero, Italy
Michael D. Heagy, USA
Wing-Kei Ho, Hong Kong
Jürgen Hüpkes, Germany
Adel A. Ismail, Kuwait
Chun-Sheng Jiang, USA
Zaiyong Jiang, China
Cooper H. Langford, Canada
Yuanzuo Li, China
Manuel Ignacio Maldonado, Spain
Santolo Meo, Italy
Claudio Minero, Italy
Antoni Morawski, Poland
Fabrice Morlet-Savary, France
Mohammad Muneer, India
Maria da Graça P. Neves, Portugal
Tsuyoshi Ochiai, Japan
Kei Ohkubo, Japan
Leonardo Palmisano, Italy

Dillip K. Panda, USA
Thierry Pauporté, France
Juan Manuel Peralta-Hernández, Mexico
Philippe Poggi, France
Carlo Renno, Italy
Francesco Riganti-Fulginei, Italy
Leonardo Sandrolini, Italy
Jinn Kong Sheu, Taiwan
Kishore Sridharan, India
Zofia Stasicka, Poland
Elias Stathatos, Greece
Jegadesan Subbiah, Australia
K. R. Justin Thomas, India
Nikolai V. Tkachenko, Finland
Koray Ulgen, Turkey
Ahmad Umar, Saudi Arabia
Thomas Unold, Germany
Mark van Der Auweraer, Belgium
Wilfried G.J.H.M. Van Sark, The Netherlands
Thomas Edwin Vandervelde, USA
Xuxu Wang, China
Huiqing Wen, China
Yanfa Yan, USA
Jiangbo Yu, USA

Contents



Advancements in Photovoltaic Cell and System Technologies

Daniel T. Cotfas , Dezso Sera, Eleni Kaplani , Petru A. Cotfas , and Alireza Rezaniakolaei
Editorial (2 pages), Article ID 8129137, Volume 2019 (2019)




Multiconcept Methods to Enhance Photovoltaic System Efficiency

D. T. Cotfas  and P. A. Cotfas 
Review Article (14 pages), Article ID 1905041, Volume 2019 (2019)




Comparative Study of Two Commercial Photovoltaic Panels under Natural Sunlight Conditions

Daniel T. Cotfas  and Petru A. Cotfas 
Research Article (10 pages), Article ID 8365175, Volume 2019 (2019)


Determination of Technological Features of a Solar Photovoltaic Cell Made of Monocrystalline Silicon P+PNN+

Cristian-Petre Fluieraru , Gabriel Predușcă, Horia Andrei, Emil Diaconu, Petru Adrian Cotfas , and Daniel Tudor Cotfas 
Research Article (14 pages), Article ID 7945683, Volume 2019 (2019)


Experimental Study of Thermal Effect of Lacquer Coating for PV-Trombe Wall System Combined with Phase Change Material in Summer

Chenglong Luo , Wu Zou, Dan Sun, Lijie Xu , Jie Ji , and Mengyin Liao
Research Article (10 pages), Article ID 7918782, Volume 2019 (2019)




Assessment of the Use of PV Panels with Energy Accumulation Option for Riga City Office Building

Kristina Berzina, Inga Zicmane , and Konstantins Kasperuks
Research Article (11 pages), Article ID 9592746, Volume 2019 (2019)

Investigation of Repurposed Material Utilization for Environmental Protection and Reduction of Overheat Power Losses in PV Panels

Ammar Alkhalidi , Mohamad K. Khawaja, and Abdel Ghaffar Al Kelany
Research Article (9 pages), Article ID 2181967, Volume 2019 (2019)

Preparation of Nano-Ag-TiO₂ Composites by Co-60 Gamma Irradiation to Enhance the Photocurrent of Dye-Sensitized Solar Cells

Le Thanh Nguyen Huynh , Viet Hai Le, Thanh Long Vo, Thi Kim Lan Nguyen, Quoc Hien Nguyen , and Thai Hoang Nguyen 
Research Article (8 pages), Article ID 5737952, Volume 2019 (2019)

Editorial

Advancements in Photovoltaic Cell and System Technologies

Daniel T. Cotfas ¹, **Dezso Sera**,² **Eleni Kaplani** ³, **Petru A. Cotfas** ¹,
and **Alireza Rezaniakolaei**²

¹*Electronics and Computers Department, Transilvania University of Brasov, Romania*

²*Department of Energy Technology, Aalborg University, Denmark*

³*Engineering, Faculty of Science, University of East Anglia, UK*

Correspondence should be addressed to Daniel T. Cotfas; dtcotfas@unitbv.ro

Received 28 November 2019; Accepted 29 November 2019; Published 5 December 2019

Copyright © 2019 Daniel T. Cotfas et al. This is an open access article distributed under the Creative Commons Attribution License, which permits unrestricted use, distribution, and reproduction in any medium, provided the original work is properly cited.

Renewable energy undergoes a continuous development and improvement being driven by the growth in energy demand, the need to reduce pollution, and the increase in investment and policies at national and international levels. The photovoltaic solar energy lately became an important pillar for renewable energy to reach global and European targets in the share of renewable electricity. The first target for the energy generated by photovoltaic systems is 10% from the total European electricity production until 2020 [1], and until 2050, 60% from electricity generation has to be from photovoltaic solar energy and wind [2].

The global cumulative installed PV capacity reached over 500 GW in the end of 2018 following an exponential growth [3, 4]. In 2018, the 100 GW of a new added PV capacity has been reached for the first time; this was also the third consecutive year when PV had by far the largest new capacity addition among all energy technologies. This trend is expected to continue [3–5]. The price of the PV module is continuously decreasing, so at each doubling of the production, the price goes down by 24% [5, 6]. All of these are possible due to the common effort of the researchers, R&D centers, industry communities, and government policies.

There is ongoing interdisciplinary research on the design of advanced photovoltaic technologies and photovoltaic systems contributing to the increase in cell and module efficiency, PV system reliability and durability, maximization of solar energy harvested, and overall system yield. Furthermore, advanced PV-based configurations and hybrid systems, including PV, Solar Thermoelectric Generators

(STEG), PV/T, and concentrated or conventional PV systems, integrated with STEG, STC, and energy storage can lead to an increase in the electrical and thermal energy generated and in system lifetime.

This special issue includes articles within the scope of advancements in photovoltaic cell and system technologies. These range from articles addressing the increase in photovoltaic cell efficiency through advancements in their structure or composition and enhancements in photovoltaic module performance targeting the decrease in photovoltaic cell temperature by passive cooling using recyclable materials or phase change materials. Optimal solutions for a wide range of applications are presented along with concepts for enhancing the efficiency of the photovoltaic systems and the final energy yield, including among others sun-tracking systems, reflective and refractive systems, the most commonly applied cooling methods, and maximum power point tracking techniques.

Conflicts of Interest

The editors declare that they have no conflicts of interest regarding the publication of this special issue.

*Daniel T. Cotfas
Dezso Sera
Eleni Kaplani
Petru A. Cotfas
Alireza Rezaniakolaei*

References

- [1] *EERA Joint Programme Photovoltaic Solar Energy*, November 2019, <https://www.eera-set.eu/>.
- [2] IRENA, *Global energy transformation: a roadmap to 2050 (2019 edition)*, International Renewable Energy Agency, Abu Dhabi, 2019.
- [3] IEA, *Snapshot of global PV markets, Report IEA-PVPS*, 2019.
- [4] SolarPower Europe, *Global Market Outlook For Solar Power / 2019 – 2023*, 2019.
- [5] *Renewables 2019 Global Status Report*, REN21 Secretariat, Paris, 2019.
- [6] *Photovoltaics Report, Fraunhofer Institute for Solar Energy Systems, ISE with support of PSE GmbH*, 2019, <https://www.ise.fraunhofer.de>.

Review Article

Multiconcept Methods to Enhance Photovoltaic System Efficiency

D. T. Cotfas  and **P. A. Cotfas** 

Electrical Engineering and Computer Science Faculty, Transilvania University of Brasov, Romania

Correspondence should be addressed to D. T. Cotfas; dtecotfas@unitbv.ro

Received 18 April 2019; Revised 16 October 2019; Accepted 6 November 2019; Published 25 November 2019

Academic Editor: Jegadesan Subbiah

Copyright © 2019 D. T. Cotfas and P. A. Cotfas. This is an open access article distributed under the Creative Commons Attribution License, which permits unrestricted use, distribution, and reproduction in any medium, provided the original work is properly cited.

The main goal of this paper is to review the most important methods previously developed to enhance the efficiency and increase the lifetime of photovoltaic panels. The methods to increase the solar radiation incident on photovoltaic panels, as well as the cooling and the maximum power point tracker methods, are concisely presented in this paper. The pros and cons analysis reveals that the methods to enhance the power generated by the photovoltaic panels are strongly dependent on geographical location, climatic conditions, and the materials used. This review paper is also of interest for engineers who attempt to identify the most adequate solutions to maximize the energy output of photovoltaic systems for each location.

1. Introduction

The electricity demand has greatly increased in recent years due to economy and population growth in developing countries, a gradual rise in comfort levels in well-developed countries, the demand for more goods and services, and the increase in the number of electric vehicles for public transportation and electric cars [1]. India's energy demand will increase the global one with 30% and only a part of the Chinese industry will increase the electricity demand with 20% by 2040, according to the International Energy Agency [1]. The increase in electricity demand leads to rising levels of pollution. This can be prevented if the electricity is produced by using renewable energy.

The photovoltaic systems (PV) which convert the solar energy in electric systems are the most important systems from the renewable energy ones. The added solar PV capacity worldwide in 2017 was 98 GW, and the total installed PV capacity by the end of 2017 was 402 GW [2].

The electric power generated by the photovoltaic panels can be increased if their efficiency is enhanced. Moreover, if PV lifetime is also increased, the total amount of the electricity generated is further grown.

The efficiency of the most important photovoltaic panels varies from 10% to 38% if the photovoltaic cells and panels are measured under Standard Test Conditions (STC)—air mass (AM) 1.5, temperature 25°C, and irradiance 1000 W/m². The comparison between the most efficient photovoltaic cells and PV panels is presented in Table 1. The efficiency of the PV panels is smaller than the PV cells used for its construction. In the case of aSi, the difference is very small, while for Perovskite, it is high, this being explained by the fact that the technology is still young. The Perovskite cell is a promising candidate for a very good efficiency as well as the multijunction cells. Thus, one way to increase efficiency is to find new proper materials to make better photovoltaic cells.

In order to ensure the necessary energy amount, the maximum power (P_{\max}) generated by the photovoltaic panels has to increase. This can be achieved by the production process following the research results and through extrinsic methods which are the topic of this paper because the panels' users can bring improvements. For the first type issue, an example is to maximize the active area of the photovoltaic cells. The Maxeon third generation photovoltaic cells have fingers and bus bars, which have been moved from the front face on the back one; thus, all contacts are on the back of the cell. Thus, the

TABLE 1: Efficiency of the PV cells and panels measured under STC [3].

Material	Efficiency (%)						
	mSi	a-Si/nc-Si	GaAs	CIGS	Perovskite	CdTe	InGaP/GaAs/InGaAs
PV cell	26.7 [4]	12.7 [5]	29.1 [6]	22.9 [7]	20.9 [8]	21.0 [9]	37.9 [10]
PV panel	24.4 [4]	12.3 [11]	25.1 [12]	19.2 [13]	11.6 [14]	18.6 [15]	31.2 [16]

entire front area is active. The energy generated from the Maxeon photovoltaic system is higher by over 30% than other photovoltaic systems for the same area used during the last 25 years [17].

For this study, it is important to identify, describe, and discuss pros and cons of the methods and their results to enhance the performance of existing photovoltaic panels in work environment. The parameters of the photovoltaic panels are given after their testing in STC conditions, which are very rarely reached in real conditions. It is important to add something to obtain the maximum power specified by the producer or to exceed this amount.

The maximum power generated by the photovoltaic panels increases with the solar radiation which falls on them. This issue can be solved by using sun tracker systems [18–20], which reflect the solar radiation on photovoltaic panels [21, 22] and solar concentrating systems [23]. All these solutions cause other problems which have to be solved in order to obtain real improvements. One of the most important problems is that the temperature of the photovoltaic panels increases with the irradiance growth, and in concentration systems, the acceptable functioning temperature for photovoltaic cells is very easily exceeded especially for high concentration rates [24, 25]. The maximum power generated by the monocrystalline silicon cell decreases with around $0.45\%/^{\circ}\text{C}$ [24], and the lifetime also decreases [26]. The cooling methods, passive as well as active ones, are used to reduce the temperature of the photovoltaic cell. The uniformity of the temperature on the photovoltaic panel surface is very important for the PV to work properly, and the cooling methods must ensure this. Another problem that arises is whether the cooling method is sustainable from the economic perspective. Does the additional energy generated due to the cooling system used cover its extra cost? The extra lifetime of the photovoltaic panels, ensured by the cooling system, is important to be taken into consideration, also from the economic point of view. Therefore, the cooling system is absolutely necessary for the photovoltaic cells in concentrated light systems.

It is also very important to use all the power which can be generated by the photovoltaic panels to enhance the performance of the system, and thus, the use of the maximum power point tracking (MPPT) becomes a necessity.

Other factors which can have negative consequences for the PV panel energy output are dust, shade, humidity, wind speed, direction, and tilt angle [25].

The paper is structured in five sections, as follows: the methods to increase the solar radiation which falls on the PV panels are presented in Section 2. In Section 3, the methods to increase the power generated by the PV panels using cooling are discussed. Section 4 provides in a concise

manner the maximum power point tracking methods. The last section is dedicated to discussions and conclusions.

2. Methods to Increase the Solar Radiation Which Falls on the PV Panels

2.1. Sun Tracker Systems. Theoretically, the solar radiation falling on the PV panels increases by 41% when the dual axis sun tracker is used [18], but the increase in generated energy varies between 10% and 45% in comparison with fixed systems [19, 20]. The energy consumed by the PV system to follow the sun when the tracking system is used varies between 2% and 5% from the generated energy. If the processes for the sun tracker are not optimized, this can be even higher [20]. The sun tracker systems are more complex than the fixed systems, and the maintenance is more expensive. The sun tracker is absolutely necessary for the concentrated light systems.

The main types of the sun trackers and the gain in power in comparison with the fixed PV system are presented in Table 2.

The power gain when the sun tracker is used is strongly dependent on the type of trackers, the location [29], seasons, months, day types [27, 34], and the PV panel technologies. The most widely known classification of the sun trackers is in function of the axis number: with single axis and dual axis (Figure 1). For example, for the dual-axis sun tracker based on MPPT, the gain is 28.8% in winter, 33.6% in spring, 43.6% in summer, and 38.3% in winter [35].

The power gain depends on the PV panel technologies. The gain for four PV types when a dual axis with algorithm is used is 17% for amorphous silicon panels, 18% for monocrystalline silicon panels, 5% for polycrystalline silicon panels, and 20% for CIS panels [37]. The power gain also depends on the seasons of the year and implicitly on the month. The experimental results for the gain obtained using a dual-axis sun tracker active system, in Patras, Greece, are 31.11% for April, 32.78% for May, 36.85% for June, and 34.2% for July (Figure 2) [38].

2.2. Reflective Systems. The maximum power generated by the photovoltaic panels can be increased if the reflected solar radiation falls on the photovoltaic panels. This can be obtained in natural-passive reflectance and artificial-active reflectance modes.

2.2.1. Passive Reflectance. The solar radiation is reflected by the surface. The albedo provides the information about the solar radiation amount which is reflected by each type of surface. The albedo for different types of surfaces is presented in Table 3 [39–41].

TABLE 2: Sun tracker types and gain.

Type	Description	Gain in power	Ref.
Single axis	(1) The rotation is on E-W direction, and on N-S, the panel is tilted at 30°. It is an active tracker, based on closed-loop (two photodiodes are used).	15.3%—cloudy day 16.2%—partially clear day 23.2%—clear day	[27]
	(2) The rotation is on N-S direction. It is an active tracker, based on closed-loop (algorithm). The system movement is electromechanical.	20%	[28]
	(3) The rotation is on E-W direction, and it is an active tracker with algorithms. The fixed system is near earth for site A, is one of the 90 sun trackers but deactivated for site B, and is tilted at 30° for site C.	37.7% site A 30.4% site B 31.5% site C	[29]
	(4) The rotation is on E-W direction, and it is an active tracker based on closed-loop (sensors).	45%	[30]
	(5) The rotation is on N-S direction, and it is a passive tracker based on two bimetallic strips.	23%	[31]
	(6) Tracker with three positions (fixed angles) for morning, noon, and afternoon.	24.5%	[32]
Dual axis	(1) It is an active tracker with a tracking algorithm. The system movement is electromechanical.	42.6%	[33]
	(2) Equatorial sun tracker. It is an active tracker with sensors.	108 Whr/m ² —cloudy day 603 Whr/m ² —clear day	[34]
	(3) It is an active tracker based on MPPT.	37.1%	[35]
	(4) It is an active tracker based on an algorithm.	24.59%	[36]

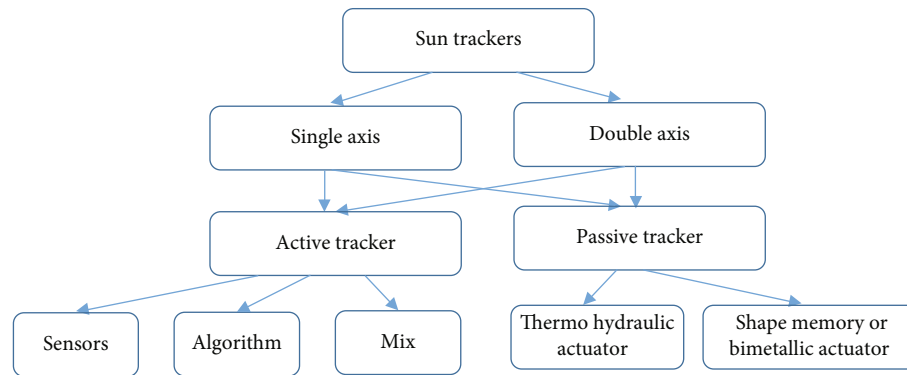


FIGURE 1: Classification of sun trackers.

The additional irradiance which falls on the photovoltaic panels depends on the albedo, the shape of the reflective surface, and the tilt angle of the PV panels.

There are some studies on the increasing maximum power generated by the photovoltaic panels using the passive reflectance. The photovoltaic panels which are mounted on a flat large roof or large flat land can receive additional solar radiation by reflection. The roofs are generally covered with waterproof materials which have a small reflection, such as bituminous membrane (BM) and cement slabs (Table 3). Nowadays, there are waterproof materials with high reflection, such as white tiles or white waterproof materials, which have an albedo above 70%. Also, the roof and the land in winter can be covered with snow which has the albedo of up to 92%.

D.T. Cotfas and P.A. Cotfas proposed a simple method to increase the power generated by the PV panels [21].

The expanded polystyrene was used to simulate the white waterproof material or snow. The albedo of the expanded polystyrene (EP) is over 80%. Two “twin” photovoltaic panels are used to study the effect of the reflected solar radiation, one being placed on the expanded polystyrene to receive the solar reflected radiation from EP and another to receive the solar reflected radiation from the bituminous membrane [21]. The comparison of the maximum power generated by PV panels with solar reflected radiation from the bituminous membrane BMR and from the expanded polystyrene EPR is presented in Figure 3. The comparison is made for different solar global radiation values from 100 W/m² to 1000 W/m², measured with a pyranometer placed in the same plane with the PV panels on a clear day. The gain in percentages for the maximum power of the PV panel with EPR varies from 8% at 100 W/m² irradiance to 17% at 1000 W/m² irradiance. The gain in power, function of the irradiance, is linear (Figure 4).

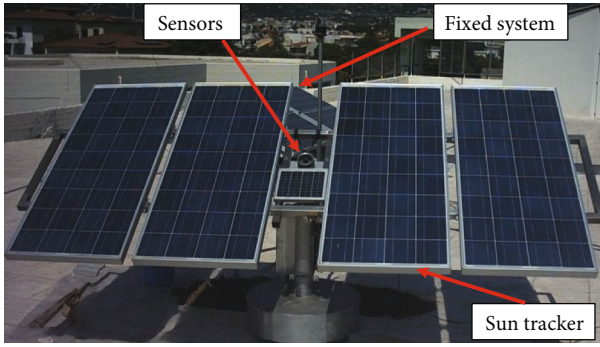


FIGURE 2: Dual-axis sun tracker active and fixed system, Patras, Greece.

TABLE 3: Albedo values.

Surface	Albedo (%)
Dry soil (dark)	9
Bituminous membrane	13
Cement slabs	15
Green grass	23
Concrete	25
Concrete (milky)	46
Old snow	45-50
White tiles	71
Aluminum foil	75
White painted concrete	60-80
Expanded polystyrene	83
Fresh snow	90-92

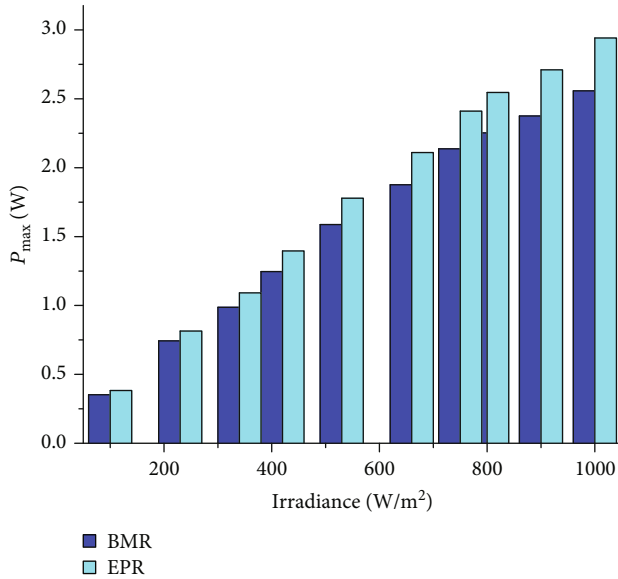


FIGURE 3: P_{\max} generated by the two PV panels.

Meyta and Savrasov have obtained an increase by 7.3% in the current generated by the monocrystalline photovoltaic minipanel when it is placed on the ground covered with snow [40].

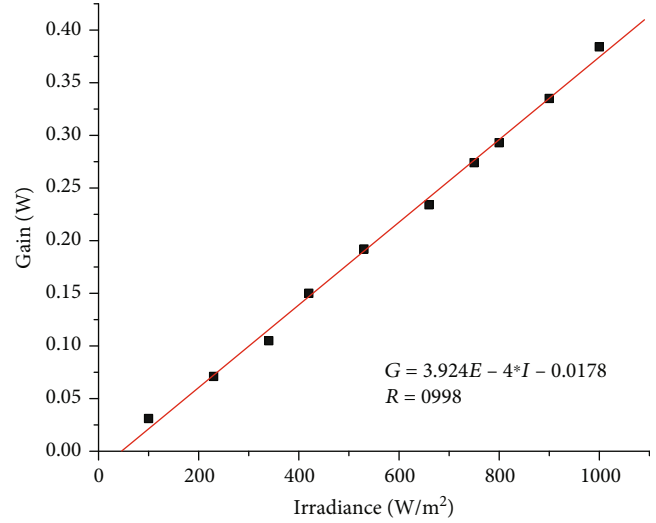


FIGURE 4: Gain in P_{\max} for PV panel in EPR case.

The passive reflectance plays a very important role in radiation gain for the bifacial photovoltaic panels. The gain in power of the bifacial PV panels in comparison with monofacial PV panels is reported to be between 13% and 35% for sunny days and between 40% and 70% for cloudy days. The variation is determined by the height at which the photovoltaic panels are mounted from the ground [41, 42]. The height influences the amount of the solar radiation reflected which falls mainly on the back of the panels and also on their front. Chiodetti et al. calculated the influence of the albedo for the power generated by the rear side of the bifacial PV panels [43]. They obtained that the contribution of the albedo is of 68.1% for 20% albedo, 81% for 40% albedo, and 86.5% for 60% albedo.

2.2.2. Active Reflectance. The reflected solar radiation which falls on the photovoltaic panels can be artificially increased by using different methods. One method is to use mirrors (glass mirrors or anodized aluminum), but reflective surfaces, such as aluminum foil or zinc tiles, can be used in order to reduce the system price. The concentration rate for these methods is very low, up to maximum 3 times.

These systems can use from one mirror to four mirrors [44]. The most used systems are those using two mirrors, and they are called V-troughs [45–49].

The V-trough systems generally have to be used with sun tracker systems. The systems with one or two mirrors (Figure 5) can be used with or without the sun tracker [50]. The inclination angle of the mirrors is very important to maximize the gain. Kostić et al. calculated the optimal inclination angle of the mirrors towards the PV panel. The optimal angle was found 66° [51].

Arshad et al. measured the gain in power for the system with mirrors without the sun tracker. The measured power of the PV monocrystalline silicon panel without mirrors is 24.84 W. They obtained 28.84 W for the panel with one mirror, 31.25 W for the system with two mirrors, and 36.93 W for the system with three mirrors [44]. The gain for the last system in comparison with the first is 48.7%.

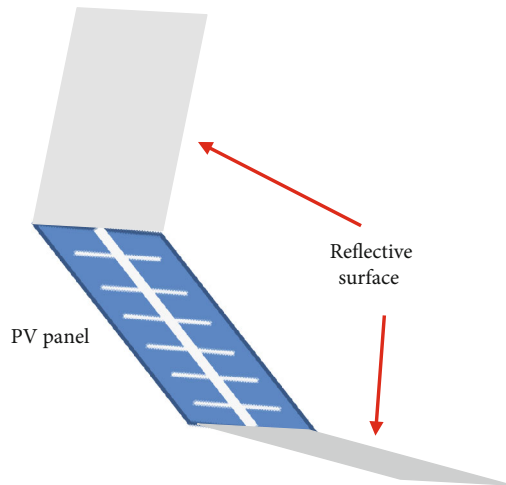


FIGURE 5: PV panel with mirror system.

The gain in power when the V-trough systems is used is concisely presented in Table 4.

2.3. Refractive Systems. The Fresnel lens is the best candidate and the most used for refractive concentration light (Figure 6). The rate of concentration can vary from low concentration, of up to 10 suns, to high concentration, of up to 2000 suns [23]. The polycarbonate Fresnel lens is widely used due to its lower cost and greater toughness in comparison to methyl methacrylate. The latter is more resistant to scratch [53] and has only longitudinal chromatic aberration [23]. The spherical and chromatic aberrations decrease the optical efficiency at the high concentration rate [54]. There are some solutions to reduce the chromatic aberrations and increase the performance of the Fresnel lens, such as using a hybrid refractive/diffractive design and using two different optical materials [54, 55]. Zhou et al. obtained a 98.5% transmittance [56] by using antifogging and antireflective coating for the Fresnel lens. Another problem of the Fresnel lens is the angular acceptance which is acceptable for low concentration rates and low for high concentration rates. The solution proposed by Akisawa et al. is a dome-shaped lens [57].

3. PV Panel Cooling Methods

The maximum power generated by the PV panels is strongly influenced by their temperature. The temperature growth has a negative influence on the electrical energy produced by photovoltaic cells. The percentage of the maximum power decreasing if the temperature rises by one degree for four photovoltaic cells is presented in Figure 7 [24]. The most widespread PV panels, monocrystalline and polycrystalline silicon, have the highest maximum power temperature coefficient. In semiarid and arid regions, the temperature of PV panels reaches more than 80°C [58].

All methods presented in the previous section of the paper increase the solar radiation received by PV panels which leads to rise in their temperature and lifetime reduction. Thus, continuous efforts to improve or find new methods to cool PV panels are necessary.

The main cooling methods of the photovoltaic panels are presented in Figure 8.

3.1. Air Cooling. The natural air flow is the most common method for cooling the PV panels due to its simplicity, no extra materials being needed, and the cost being relatively low. However, cooling of photovoltaic panels can be improved if on the back of PV panels metallic materials with fins are mounted to ensure a very good air circulation [59–61]. By using natural air flow between the building vertical walls and PV system mounted on them, the temperature of the photovoltaic panels can be maintained at less than 40°C [61] which is smaller with almost 20°C than the average.

The forced air circulation is an active method to cool the photovoltaic panels. There are more methods to force the air circulation, such as open channel beneath, steel plate with an air channel underneath, and array of air ducts underneath the PV panels with optimum fins [62, 63]. Teo et al. using the array ducts significantly decrease the temperature of the photovoltaic panels, and their efficiency increases between 12 and 14% [62].

3.2. Water Cooling. The cooling with water of the photovoltaic panels has been studied since the end of the 1960s, when the first hybrid PVT panels were build (photovoltaic panel and solar thermal collector), and this technology underwent a rapid development after the 1990s. Nowadays, there is a multitude of types of PVT, such as with natural and forced water circulation, using nonconcentrated and concentrated sunlight, glazing and without glazing, with and without absorber plate, and other types [64].

These hybrid panels can produce electric energy and thermal energy in almost the same space. He et al. studied a PVT which consists of a monocrystalline silicon panel placed on the absorber plate with a water pipe attached beneath. The water circulation is a natural one. The efficiency of the photovoltaic panel is comparable with the one that does not have a solar collector, and for the solar collector, the efficiency is around 40%. The efficiency of the hybrid system is much higher than that of a conventional system [65]. Yang and Yin found that the maximum power of the PV panel in hybrid systems increases with 23% in comparison with PV panel alone, and the solar thermal collector generates 661 W/m² [66]. Xu et al. proposed a concentrated PVT system. The Fresnel lenses and an optical prism are used to concentrate the sunlight up to 1090 suns. The efficiency of the photovoltaic cells is 28%, and the thermal efficiency is 60% [67].

The temperature of the photovoltaic panels can be reduced using the water which flows on the panels or is sprayed on them. Krauter proposed a method to cool the photovoltaic cell using the water flow on the surface of the panel. The results show that the efficiency of the PV panels increases with 10.3%. The water flow, 4.4l/min, is achieved using a pump and 12 nozzles placed on the top of the PV panel assuring the distribution of the water. The photovoltaic cell temperature decreases up to 22°C which increases the lifetime of the PV panels. The water film reduces the reflection by 2-3.6%. The gain of the system is 9% if the pump

TABLE 4: V-trough system.

Description	Gain (%)	Rate of concentration	Reference
Ya'acob et al. made a comparative study using three monocrystalline silicon photovoltaic systems: fix (F), dual-axis sun tracker (DST), and V-trough system with sun tracker (V); the rated power of all three systems is 1 kW	DST to F is 9.4 V to DST is 23.4 V to F is 32.8	2	[48]
Hu and Yachi proposed an innovative V system with tracker for each mirror	70 to the panel without mirror	—	[49]
Tina and Scandura compared the power generated by two photovoltaic systems: one is a single-axis tracking system (azimuth) (SA) and the second is a dual-axis tracking system with mirrors (M)	M to SA is 34	1.81	[51]
Solanki et al. proposed a system which consists of 6 monocrystalline silicon panels, each of them being placed in a V system	7.7 to the panels without mirrors	2	[46]
Maiti et al. study two 10 W photovoltaic panels placed on V-trough. One PV panel is cooled with PCM material, and the second is not. A manual sun tracker on East-West direction is used. The panels are tilted at 18.9° to the horizontal, which is the optimum angle	55 to the panels without mirrors and PCM	2	[47]
Singh et al. compared the generated power of two systems: one is V-trough system and the other is compound parabolic concentrator (CPC). Four monocrystalline silicon photovoltaic cell series connected are used for each concentrator	V to CPC is 17.2 at the specific tilt angle 30°	2.2	[52]

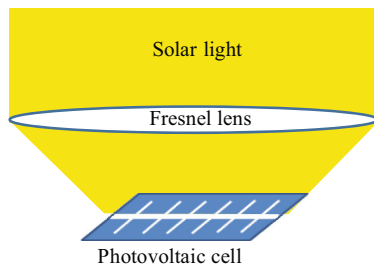


FIGURE 6: Fresnel light concentration system.

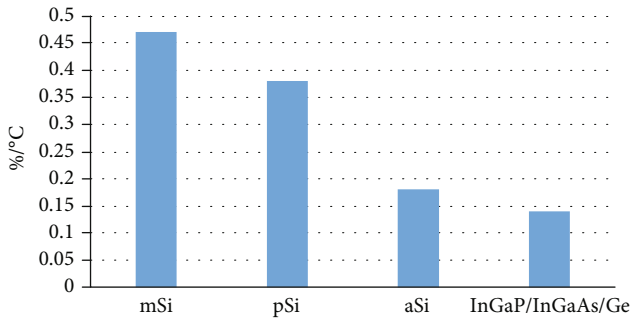


FIGURE 7: The decrease percentage in maximum power for different types of photovoltaic cells.

consumption is taken into account [68]. Moharram et al. developed a water spray system to cool the photovoltaic panels [69]. The system consists of six PV panels, a water tank, a centrifugal pump, 120 water nozzles for spraying water, and a system to recover the water. The temperature of the photovoltaic cells is decreased at 35°C when the spraying system is used [69]. Abdolzadeh and Ameri also studied the cooling system based on the water spray technique. The working temperature of the PV panels is 37.5°C when the ambient temperature is 33°C and the flow is 501/h [70].

Clot et al. studied the behavior of the PV single crystalline silicon panel submerged in water [71]. The temperature of the PV panel which operates in natural conditions is around 70°C, but the temperature decreases at 30°C if it is submerged at 4 cm. The efficiency of the panel submerged increases with 11%. This increase is limited by water absorption. If the PV panel is submerged at 40 cm, the efficiency decreases with 23%.

The PV floating is another possibility to reduce the temperature of the photovoltaic panels. Cazzaniga et al. [72] described the PV floating plant which works in low rate concentrated light; the photovoltaic panels have been cooled using water sprinklers. Sacramento et al. used two polycrystalline silicon panels to compare their behavior when one is ground mounted and the other is water floating [73]. The efficiency of the water floating PV panel is higher than that for the other PV panel with 12.5%.

Water with different nanoparticles is successfully used to reduce the temperature of the photovoltaic cells and to increase the performance of the photovoltaic thermal hybrid systems [74, 75]. Several nanoparticles such as Boehmite (AlOOH-xH₂O), Aluminum oxide (Al₂O₃), Zinc Oxide (ZnO) and Titanium Oxide (TiO₂), Magnetite (Fe₃O₄), Silicon carbide (SiC), and Copper Oxide (CuO) are used at different weight fractions.

Karami and Rahimi used water-based Boehmite with 0.01 wt% to cool the photovoltaic panels, and the gain in efficiency is 27% [74]. Hussien et al. used Al₂O₃-water nanofluid with concentration ratio 0.3% for improving the performance of the hybrid PV/T panel. The tests are performed at 1000 W/m² and mass flow rate of 0.2 L/s for 24 min. The temperature of the photovoltaic panel decreases from almost 79°C to 35°C. The efficiency of the PV panel increases from 8% without nanofluid to 12%, with it, which means a 50% growth [76]. The photovoltaic panel illuminated at 917 W/m² is cooled using the water, TiO₂/water, ZnO/water, and Al₂O₃/water, and the concentration ratio

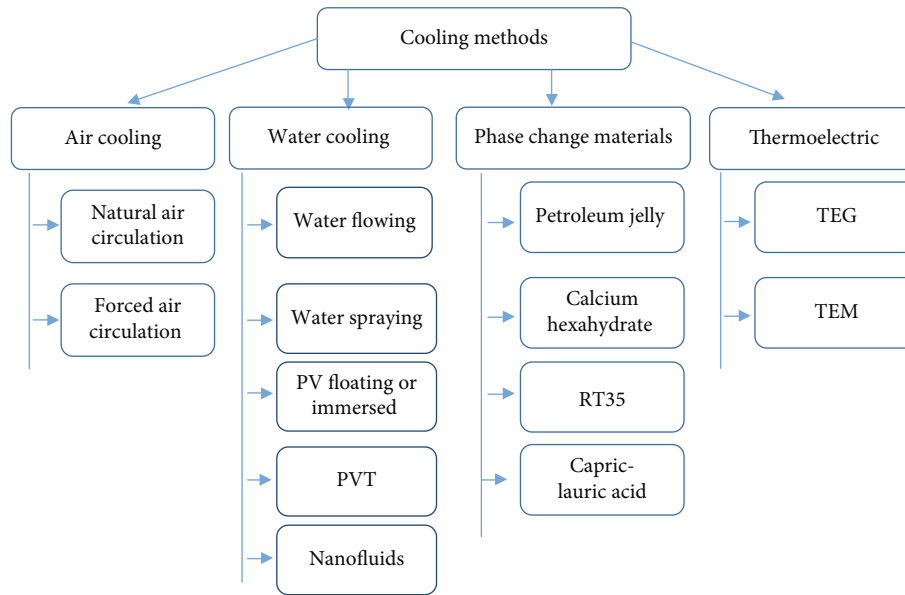


FIGURE 8: The main cooling methods.

was 0.2%. The best enhancement in electrical efficiency was found for $\text{Al}_2\text{O}_3/\text{water}$ 6.36%, and the lowest was for water 5.48% [77]. Rostami et al. used simultaneous nanofluids and ultrasound to cool the photovoltaic panels. The study took into account variation of the nanoparticle concentration from 0.01% to 0.8% and the flow rate from $0.4\text{ m}^3/\text{h}$ to $12.5\text{ m}^3/\text{h}$, and the level of illumination is $1000\text{ W}/\text{m}^2$. The experiment takes 50 minutes. The PV temperature is highly influenced by the flow rate and the concentration rate of the nanoparticles. For 0.8% concentration rate, the PV temperature decreases from 49°C to 24°C , when the flow rate increases from $0.4\text{ m}^3/\text{h}$ to $12.5\text{ m}^3/\text{h}$, and from 36°C to 24°C , when the concentration rate varies from 0.01% to 0.8% at $12.5\text{ m}^3/\text{h}$ flow rate [75].

3.3. PCM. The phase change materials (PCM) have the properties to absorb the excess heat and maintain the PV panels at constant and uniform temperature [78]. There are different PCM materials able to reduce the temperature of the PV panels and to ensure a homogenous distribution of the heat on all photovoltaic panel surface, some of them being noted in Figure 4. Hasan et al., using different PCM materials, obtained a temperature reduction for PV panels ranging between 10°C and 18°C [79]. Biwole et al., using PCM materials, could maintain the PV panel temperature under 40°C for 80 min at $1000\text{ W}/\text{m}^2$ irradiance [80]. Indartono et al. improved the efficiency of the roof integrated photovoltaic panels (10 W) with 21.6% and with 6% for the stand-alone panel using PCM (petroleum jelly material) [81]. The temperature of the PV panels can be reduced with 21°C for Pakistan and 10°C for Ireland when salt hydrate is used [82].

Al-Waeli et al. tested and compared three PV/T systems: one with water, the second with water and PCM, and the third with PCM and nano-SiC-water nanofluid. The results show that the third system has the best performance. The efficiency varies from 13.7% for PCM and nanofluid and 11.4% for PCM and water to 8.5% for water. The electric

power generated varies from 81.3 W (first system) to 111.3 W (third system) [83]. Sardarabadi et al. found that the gain in electricity is higher than 13% when PCM/nanofluids are used in PV/T panels [84].

3.4. Thermoelectric. The thermoelectric generator (TEG) has been considered a promising part of the PV-TEG hybrid system since the early 2000s. The thermoelectric module can be used to extract a part of the heat of the PV panels and convert it into electric energy based on Seebeck effect. This device can be used to cool the PV panels by consuming the electric energy, based on Peltier effect.

Benghanem et al. cooled the PV panels from the semi-arid and arid regions using one TEG for each panel. The necessary energy to power the TEGs is generated by an additional photovoltaic panel [58]. Cotfas et al. used TEG to build a PV-TEG-STC hybrid system and to study it in natural sunlight conditions [85]. The temperature of the photovoltaic cell was reduced with 19°C , and the power generated increased with 11%. The temperature distribution of the photovoltaic cell shows a very small variation of the heat which has a positive effect on the lifetime of the photovoltaic cells (Figure 9).

Mahmoudinezhad et al. studied the behavior under low concentration of the hybrid system which consists of GaInP/GaInAs/Ge multijunction photovoltaic cell and Bi_2Te_3 thermoelectric generator [86]. The temperature of the multijunction photovoltaic cell increases only up to 120°C at 39 suns due to the heat extracted by the thermoelectric generator. Kil et al. determined a gain about 3% for the power generated by a PV cell used in the hybrid system in comparison with the PV cell alone for a concentrated rate of 50 suns [87].

4. MPPT Methods

In order to make maximum use of the output of the PV panels, the DC load has to intersect the current voltage characteristic in the maximum power point. In real operation

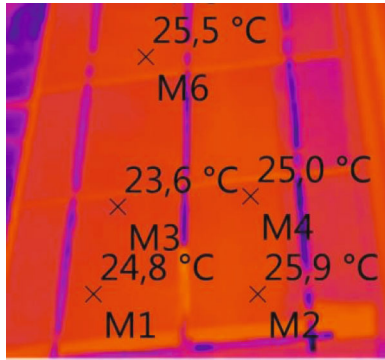


FIGURE 9: The temperature distribution [85].

conditions, this rarely happens due to the load mismatch, the variation of the solar radiation, and temperature. This problem can be overcome by using DC/DC or DC/AC converter with MPP controller [88].

A lot of MPPT methods are being developed, each of them with its own applications and limitations [89, 90]. They depend on whether the PV panels are used in stand-alone or grid connected systems. A classification of the main MPPT methods is presented in Figure 10.

Karami et al. give some criteria to choose the best MPPT technique for an application such as the following [88].

Implementation: some methods are very simply implemented, for example, the constant voltage; others are more complex, such the methods based on artificial intelligence. For implementation, it is also important that the irradiation and temperature are uniform. The success of the MPPT depends on whether there is shadow or not on the PV panels.

Sensors: the number of sensors must be limited, but sufficient; there are in general four sensors for temperature, solar radiance, voltage, and current. Using simple methods, such as constant voltage or constant current, the number can be reduced at one.

Efficiency: there are methods which have a simple value and methods which allow oscillations around the maximum power point. The losses can become important and can influence the costs.

Cost: cost depends on the complexity of the circuit and method [88].

5. Discussion and Conclusions

The performance of the photovoltaic panels can be enhanced if the solar radiation falling on them is increased, the photovoltaic panels are cooled, and smart electronic circuits are used.

The important issue for increasing the irradiance on the photovoltaic panels through sun trackers, active reflectance, and concentration systems is that these systems use mobile parts and the temperature of the photovoltaic panel increases when more solar radiation falls on it. Therefore, the systems are more complex, and questions appear which refer to the additional cost, the energy consumption to move the system, maintenance, the losses in case the system does

not work properly or is broken, and which the gain in produced energy is.

The answers for these issues are the following:

The gain: it depends on the sun tracker system type, for single axis the gain is 10–25% and 25–45% for double axis; geographical location where the PV system is placed; technology; and materials used for photovoltaic panels. Table 5 comparatively presents the annual energy generated by the 1 kW PV plant with fixed panels and the 1 kW PV plant with the dual-axis sun tracker. Three technologies are considered, such as mSi, CIS, and CdTe, and four locations. The gain between the annual energy generated by PV plants placed in Kaunas and Marbella is also calculated. Data used for this comparison is obtained from the Photovoltaic Geographical Information System [91]. The gain can be improved by reflections especially in the morning and in the evening especially in case of dual-axis sun trackers.

Energy consumption: it is 3.5% in average from the total energy generated, if the sun tracker process is optimized, if not, it can be over 5%. It also depends on the speed and accuracy of the positioning.

Losses: they depend on the problems which appear. The worst case is when the PV system remains blocked for optimum position towards East or West. In this case, the losses are over 95% from the energy generated per day. In the case of concentration systems, the losses depend on the accuracy of the sun trackers due to the fact that their performance is a function of the acceptance angle, which plays a very important role.

Costs: it is an important factor which must be taken into account when considering whether to implement the sun tracker system or not. It depends on the type of the sun tracker systems, as the cost to produce 1 kWp varies from \$600 to \$1900 for dual axis and varies from \$135 to \$930 for single axis. The variation appears due to the producers, the components, and the accuracy. Singh et al. assert that the cost for PV fixed photovoltaic panels varies between \$2 and \$2.4/watt. The supplementary cost for single-axis systems is around \$1.17/watt for dual axis systems, and it is \$0.36/watt comparatively for single axis [19].

Maintenance: it has to be made regularly in order to avoid losses. It is a factor which increases the costs of the PV systems.

In case of fixed photovoltaic systems, it is very important to choose the tilt angle and orientation (azimuth) of the system. The optimum choice of both leads to an increase in generated energy, due to the growth in incident solar radiation and self-cleaning. The fixed PV panel grid connected has to be mounted at the optimum annual tilt angle, because the yearly energy must be maximized. Rhodes et al. et al. calculated for Austin, USA, the optimal annual tilt angle and the azimuth angle, which are 28° and 188°, respectively [92].

The calculation of the tilt angle for stand-alone applications, such as home systems or solar garden lamps, has to consider other factors, among which the most important is the solar radiation in critical periods of the year. Cotfas et al. et al. developed a prototype for intelligent solar garden lamps in the Steinel project [93]. The critical period for such devices is from October to March. By analyzing the solar radiation for

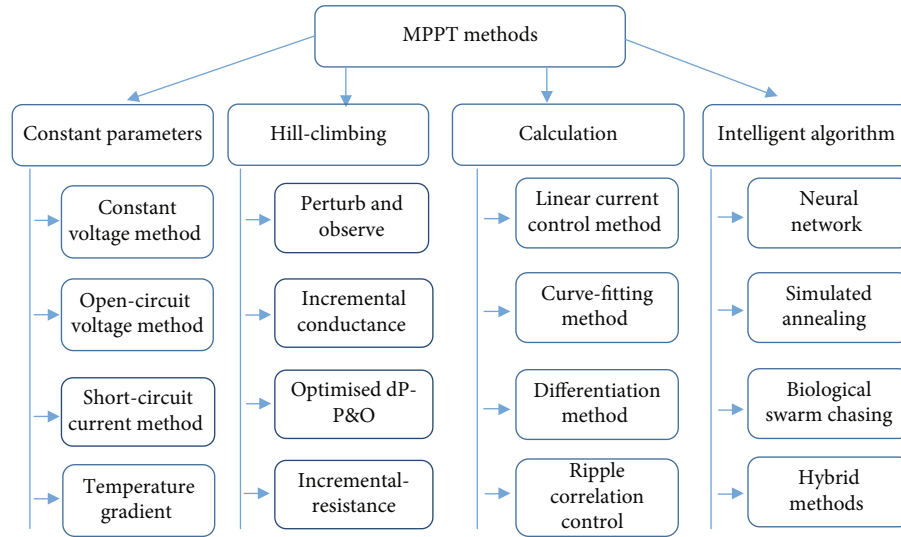


FIGURE 10: The main MPPT methods.

TABLE 5: Comparison of annual energy generated by 1 kW PV plant.

Location	Geographical coordinates	Optimal angle	Annual energy generated (kW)								
			mSi			CIS			CdTe		
			Fix	DST	Gain (%)	Fix	DST	Gain (%)	Fix	DST	Gain (%)
Heraklion, Greece	Lat. 35°34'	28°	1650	2330	41.2	1630	2290	40.4	1680	2390	42.3
	Lon. 25°13'										
Brasov, Romania	Lat. 45°65'	36°	1130	1470	30.1	1100	1430	30	1130	1490	31.8
	Lon. 25°61'										
Kaunas, Lithuania	Lat. 54°89'	38°	930	1230	32.2	909	1200	32	918	1230	33.9
	Lon. 23°90'										
Marbella, Spain	Lat. 36°50'	32°	1720	2430	41.3	1690	2390	41.4	1760	2510	42.6
	Lon. -4°88'										
Gain between Kaunas and Marbella		(kW)	790	1200		781	1190		842	1280	
		%	84.5	97.5		85.9	99.2		91.7	104	

these months, it was concluded that the best solution for the optimum angle was 55°. This solution is validated through experiments, where three small photovoltaic panels, mono-crystalline, polycrystalline and amorphous silicon are measured at different angles. The best solution of the solar garden lamp is the monocrystalline photovoltaic panels. The difference between the consumed energy and the energy generated by the photovoltaic panel is negative for all six critical months if the panel is horizontal and for four months (November-February) if the panel is tilted at the optimum annual angle and is positive or zero if the panel is tilted at 55°. Moreover, the chosen tilt angle has the following advantages: generated maximum energy in months with problems in terms of solar radiation, the additional radiation by reflection is incident on the PV panel; improvement of self-cleaning; and temperature reduction for the summer months.

Quesada et al. proposed a strategy for sun tracker system function of the weather: in case of clear sky or only partly

sunny, the sun tracker has to work normally; for cloudy days, the sun tracker must be positioned with the PV panels horizontally; and for snowy days, the PV panels have to be at the optimum angle [94].

A method proposed by paper authors to reduce energy consumption for sun tracker systems is to move the position of the system discretely, not continuously, using a mathematical algorithm, for example, once per hour. The first position on the East-West axis is at 7.5° westwards from the optimal position at sunrise time. The temperature of the PV panels in this case is lower than that for the PV panels directly oriented towards the sun, which leads to the increase of generated power from the temperature point of view. This increase can partially compensate for the losses due to the positioning mismatch between the PV panels for certain periods of time. This method cannot be used for sun tracker systems used for concentrated PV systems, where the PV panels must be permanently oriented directly towards the sun (Figure 11).



FIGURE 11: Concentration PV plan Evora, Portugal.

The sun trackers increase the solar incident radiation, but the temperature of the photovoltaic panels also increases. There are studies on this for different types of sun trackers or technologies [43, 95]. Ya'acob et al. concluded that the maximum difference between the average daily temperature PV fixed panel and PV panels mounted on a dual-axis sun tracker is 3.8°C , and between a fixed one and a V-trough concentrator, it is 6.1°C . These differences are higher (more than 15°C) in the morning and evening because the mobile PV panels received more solar radiation.

There are some issues which have to be analyzed when the cooling is used to decrease the temperature of the photovoltaic panels among which the temperature distribution, the extra costs, the location, and the sustainability.

Temperature distribution: uniform temperature distribution on the photovoltaic panels is a key parameter to maximize the power generated by the photovoltaic panels and to increase their lifetime. The nonuniform temperature distribution has as effect growth in the photovoltaic cell temperature, increase in series resistance, fill factor decrease, and maximum power reduction [78]. There are several methods which assure the uniform cooling of the PV panel: direct immersion, phase change material, heat sinks, jet impingement, thermoelectric generators, and microchannels [78, 85]. Bahaidarah shows that if impingement cooling is used instead of the rectangular channel heat exchanger, the temperature nonuniformity is reduced from an average of 3.55°C to 1.81°C [96].

Costs: Baloch et al. calculated that the cost of the uncooled PV system is 282.9 whereas for cooled, it is 328.9. Levelled cost of energy (LCE) is calculated to be 1.95 (€/kWh) for an uncooled PV system and 1.57 (€/kWh) for cooled [97].

Location: the energy generated by the PV system is dependent on the location. The temperature of the PV system depends on the location; in arid areas, the PV temperature can exceed 85°C . The cooling system must be more efficient for these areas. Another problem is which type can be successfully used. For arid areas, thermoelectric generators prove to be a suitable choice.

The extracted heat can be converted in thermal or electric energy by using cooling methods, such as PVT or PV-TEG, and the energy generated by the PV panels due to their cooling can increase with around 7.5% [24]. The electrical and thermal efficiencies of nonconcentrated PVT systems are in the range of 10–12% and 50–70%, respectively. In case of

the submerging method to cool the PV panel, the optimum depth varies from 2 to 4 cm. The disadvantages for this method are that the efficiency of the PV panels decreases over time due to the ionized water and in the cloudy days the generated power is lower than that for ground PV panels.

The multiple PCM (multiple melting points) could be a very good solution for cooling and for homogenous heat distribution. PCM with a low melting point (25°C) can reduce the PV panel temperature more than PCM with a high melting point (over than 30°C), but for short periods, and hot spots can appear on the PV panel surface. The disadvantages of the PCM are that the absorptive capabilities of material degrade over time and they do not have the same efficiency worldwide. They are more efficient in hot regions than in cold regions.

Although there are plenty of MPPT methods, two of them are most frequently used, Perturb and Observe (P&O) and incremental conductance (IC). Recently, new methods have been developed using algorithms from the field of artificial intelligence.

The methods from the constant parameter family are the simplest ones to implement, very fast but unstable. In case of the open circuit voltage method, the maximum voltage V_{MPP} is calculated by multiplying V_{oc} with k_{oc} , the range of k_{oc} being 0.73–0.8, 0.76 for monocrystalline silicon PV panel. The accuracy of the method depends of the choice of k_{oc} . The short circuit method is analog with the open circuit voltage method. In this case, the maximum current is obtained by multiplying the short circuit current with k_{sc} . The value of k_{sc} varies between 0.85 and 0.92, for polycrystalline silicon photovoltaic panels being 0.85. The P&O and IC methods are net superior to open circuit voltage and short circuit current methods for the majority of irradiance levels. However, the open circuit voltage method performs better at low solar radiation than the P&O and IC methods. To improve the MPPT efficiency, the open circuit voltage method can be combined with one of the two Hill climb methods obtaining a MPPT hybrid method, which can perform with high efficiency for all irradiance levels.

MPPT methods, which use algorithms from artificial intelligence, are more efficient, very fast, and stable. For example, the biological swarm chasing method has an efficiency of around 12% higher than the P&O method [98].

The solar radiation and temperature can vary rapidly. In this case, the IC method is a better solution than the P&O method. The demerit of the IC method is the high time of computation. The intelligent algorithms can be a very promising MPPT method to solve the problem for rapid changes of temperature and solar radiation. The implementation of one method must take into consideration several factors, such as efficiency, cost, the simplicity or difficulty of algorithm implemented, hardware availability, and convergence time.

Problems for the MPPT appear in case of the photovoltaic panels which are partially shaded. This case is commonly met; for example, Eftichios and Gosumbonggot and Fujita show that 10% of the energy is lost because over 41% from panels which are mounted on roofs in Germany are affected by shading [99, 100]. Another study shows that not detecting the maximum power leads to loss of 70% from the energy produced by PV systems [101].

There are multiple local maximum power values for shading cases and only one global maximum in normal case, without shading. Therefore, in shading cases, it is very important to determine the correct global maximum power. The conventional MPPT algorithms, such as constant voltage or short circuit current method, cannot detect the changes determined by shading or find the maximum power. Mohapatra et al. affirm that an accurate mathematical model is not available for shading conditions [89]. The correct global maximum power in shading conditions can be obtained using the new methods based on artificial intelligence or improved conventional methods such as perturbation, observation, or incremental conductance.

The improvement of consecrated MPPT leads to their aim fulfillment, but some issues appear as the tracking time is high [100]; results are good for short time, but results for long time are not presented [102]; the oscillation problem is still present when the system operates in rapid solar radiation changes and temperature variation [103–105]; the electronic circuit becomes increasingly complex due to additional control circuit, switches, and sensors, which eventually lead to cost increase. The methods which use artificial intelligence present almost the same issues in terms of complexity and cost implementation, but they can reduce the computational time due to increased speed and the accuracy. These are reached using improved PSO (particle swarm optimization) or hybrid bioinspired algorithms [106, 107], the oscillation also reducing. The premature convergence is a problem for the bioinspired algorithms. Mirjalili et al. proposed the salp swarm algorithm (SSA) which uses a control parameter and assures the convergence through the adaptive mechanism [108]. Wan et al. improved the performance of the SSA algorithm using the grey wolf optimization algorithm in order to provide a better leader structure but which keeps the adaptive mechanism [109]. They compare the results in terms of time convergence and maximum power of the PVs obtained for one consecrated method P&O, and three algorithms PSO, SSA, and SSA-GWO. The consecrated method P&O gives better results for the uniform irradiance case from the time convergence point of view (0.48 s) than PSO (0.72 s) and SSA (0.58 s) algorithms, but not for SSA-GWO (0.46 s) algorithm [109]. The maximum power determined through P&O is the lowest one due to the oscillations. In the case of one pattern with three local maximum points, the P&O determined the global maximum very fast in comparison with the other three ones, but the accuracy is the lowest. Thus, the time for the P&O is 0.15 while for SSA-GWO it is 0.53 s, but the P_{\max} is 34.64 W for P&O and 44.55 W for SSA-GWO [109]. By using bioinspired algorithms or the hybrid algorithms, the power fluctuations are reduced, the global maximum power point is rapidly but accurately determined, and they can be successfully used for partial shading and for rapid changes in irradiance.

Conflicts of Interest

The authors declare that they have no conflicts of interest. The authors are employed at Transilvania University of Brasov.

References

- [1] March 2019, <https://www.iea.org/weo2018/electricity/>.
- [2] J. L. Sawin, K. Seyboth, and F. Sverrisson, *Renewables 2018 Global Status Report*, REN21 Secretariat, Paris, France, 2018, March 2019, http://www.ren21.net/wp-content/uploads/2018/06/17-8652_GSR2018_FullReport_web_-1.pdf.
- [3] M. A. Green, Y. Hishikawa, E. D. Dunlop et al., “Solar cell efficiency tables (version 53),” *Progress in Photovoltaics: Research and Applications*, vol. 27, no. 1, pp. 3–12, 2019.
- [4] K. Yoshikawa, H. Kawasaki, W. Yoshida et al., “Silicon heterojunction solar cell with interdigitated back contacts for a photoconversion efficiency over 26%,” *Nature Energy*, vol. 2, no. 5, article 17032, 2017.
- [5] T. Matsui, H. Sai, T. Suezaki et al., “Development of highly stable and efficient amorphous silicon based solar cells,” in *Proc. 28th European Photovoltaic Solar Energy Conference*, pp. 2213–2217, Paris, France, September 2013.
- [6] B. M. Kayes, H. Nie, R. Twist et al., “27.6% conversion efficiency, a new record for single-junction solar cells under 1 sun illumination,” in *2011 37th IEEE Photovoltaic Specialists Conference*, Seattle, WA, USA, June 2011.
- [7] J. L. Wu, Y. Hirai, T. Kato, H. Sugimoto, and V. Bermudez, “New world record efficiency up to 22.9% for Cu (In,Ga) (Se,S)2 thin-film solar cells,” in *7th World Conference on Photovoltaic Energy Conversion (WCPEC-7)*, Waikoloa, HI, USA, June 2018.
- [8] W. S. Yang, J. H. Noh, N. J. Jeon et al., “Solar cells. High-performance photovoltaic perovskite layers fabricated through intramolecular exchange,” *Science*, vol. 348, no. 6240, pp. 1234–1237, 2015.
- [9] First Solar Press Release, *First Solar Builds the Highest Efficiency Thin Film PV Cell on Record*, 2014.
- [10] K. Sasaki, T. Agui, K. Nakaido, N. Takahashi, R. Onitsuka, and T. Takamoto, *Proceedings, 9th International Conference on Concentrating Photovoltaics Systems*, Miyazaki, Japan, 2013.
- [11] J. S. Cashmore, M. Apolloni, A. Braga et al., “Improved conversion efficiencies of thin-film silicon tandem (MICROMORPH™) photovoltaic modules,” *Solar Energy Materials and Solar Cells*, vol. 144, pp. 84–95, 2016.
- [12] P. J. Verlinden, *Will we have >22% efficient multi-crystalline silicon solar cells?*, PVSEC 26, Singapore, 2016.
- [13] H. Sugimoto, “High efficiency and large volume production of CIS-based modules,” in *2014 IEEE 40th Photovoltaic Specialist Conference (PVSC)*, Denver, CO, USA, June 2014.
- [14] “Toshiba news,” September 2017, https://www.toshiba.co.jp/rdc/rd/detail_e/e1709_02.html.
- [15] First Solar Press Release, *First solar achieves world record 18.6% thin film module conversion efficiency*, 2015.
- [16] T. Takamoto, H. Washio, and H. Juso, “Application of InGaP/GaAs/InGaAs triple junction solar cells to space use and concentrator photovoltaic,” in *2014 IEEE 40th Photovoltaic Specialist Conference (PVSC)*, Denver, CO, USA, June 2014.
- [17] <https://global.sunpower.com/solar-panel-products/sunpower-maxeon-solar-panels>.
- [18] S. Yilmaz, H. Riza Ozcalik, O. Dogmus, F. Dincer, O. Akgol, and M. Karaaslan, “Design of two axes sun tracking controller

- with analytically solar radiation calculations,” *Renewable and Sustainable Energy Reviews*, vol. 43, pp. 997–1005, 2015.
- [19] R. Singh, S. Kumar, A. Gehlot, and R. Pachauri, “An imperative role of sun trackers in photovoltaic technology: a review,” *Renewable and Sustainable Energy Reviews*, vol. 82, pp. 3263–3278, 2018.
- [20] W. Nsengiyumva, S. G. Chen, L. Hu, and X. Chen, “Recent advancements and challenges in Solar Tracking Systems (STS): a review,” *Renewable and Sustainable Energy Reviews*, vol. 81, pp. 250–279, 2018.
- [21] D. T. Cotfas and P. A. Cotfas, “A simple method to increase the amount of energy produced by the photovoltaic panels,” *International Journal of Photoenergy*, vol. 2014, Article ID 901581, 6 pages, 2014.
- [22] L. T. Kostic, Z. T. Pavlovic, and S. M. Krasic, “The effect of four flat plate reflectors on light energy-harvesting system characteristics,” *Facta Universitatis - Series: Physics, Chemistry and Technology*, vol. 13, no. 3, pp. 171–180, 2015.
- [23] K. Shanks, S. Senthilarasu, and T. K. Mallick, “Optics for concentrating photovoltaics: trends, limits and opportunities for materials and design,” *Renewable and Sustainable Energy Reviews*, vol. 60, pp. 394–407, 2016.
- [24] D. T. Cotfas, P. A. Cotfas, and O. M. Machidon, “Study of temperature coefficients for parameters of photovoltaic cells,” *International Journal of Photoenergy*, vol. 2018, Article ID 5945602, 12 pages, 2018.
- [25] L. Idoko, O. Anaya-Lara, and A. McDonald, “Enhancing PV modules efficiency and power output using multi-concept cooling technique,” *Energy Reports*, vol. 4, pp. 357–369, 2018.
- [26] D. T. Cotfas, P. A. Cotfas, D. I. Floroian, and L. Floroian, “Accelerated life test for photovoltaic cells using concentrated light,” *International Journal of Photoenergy*, vol. 2016, Article ID 9825683, 7 pages, 2016.
- [27] G. C. Lazaroiu, M. Longo, M. Roscia, and M. Pagano, “Comparative analysis of fixed and sun tracking low power PV systems considering energy consumption,” *Energy Conversion and Management*, vol. 92, pp. 143–148, 2015.
- [28] A. Al-Mohamad, “Efficiency improvements of photo-voltaic panels using a Sun-tracking system,” *Applied Energy*, vol. 79, no. 3, pp. 345–354, 2004.
- [29] G. Chicco, J. Schlabbach, and F. Spertino, “Performance of grid-connected photovoltaic systems in fixed and sun-tracking configurations,” in *2007 IEEE Lausanne Power Tech*, pp. 677–682, Lausanne, Switzerland, July 2007.
- [30] I. Sefa, M. Demirtas, and İ. Çolak, “Application of one-axis sun tracking system,” *Energy Conversion and Management*, vol. 50, no. 11, pp. 2709–2718, 2009.
- [31] M. J. Clifford and D. Eastwood, “Design of a novel passive solar tracker,” *Solar Energy*, vol. 77, no. 3, pp. 269–280, 2004.
- [32] B. J. Huang and F. S. Sun, “Feasibility study of one axis three positions tracking solar PV with low concentration ratio reflector,” *Energy Conversion and Management*, vol. 48, no. 4, pp. 1273–1280, 2007.
- [33] C. Sungur, “Multi-axes sun-tracking system with PLC control for photovoltaic panels in Turkey,” *Renewable Energy*, vol. 34, no. 4, pp. 1119–1125, 2009.
- [34] J. F. Lee, N. A. Rahim, and Y. A. al-Turki, “Performance of dual-axis solar tracker versus static solar system by segmented clearness index in Malaysia,” *International Journal of Photoenergy*, vol. 2013, Article ID 820714, 13 pages, 2013.
- [35] H. Fathabadi, “Novel high accurate sensorless dual-axis solar tracking system controlled by maximum power point tracking unit of photovoltaic systems,” *Applied Energy*, vol. 173, pp. 448–459, 2016.
- [36] H. Fathabadi, “Novel high efficient offline sensorless dual-axis solar tracker for using in photovoltaic systems and solar concentrators,” *Renewable Energy*, vol. 95, pp. 485–494, 2016.
- [37] M. Badea, A. S. Moraru, I. Visa, G. B. Burduhos, and M. Comsit, “Command-control-monitoring of a dual-axis tracking photovoltaic platform,” in *7th IFAC Conference on Manufacturing Modelling, Management, and Control International Federation of Automatic Control*, Saint Petersburg, Russia, June 2013.
- [38] D. T. Cotfas, P. Cotfas, S. Kaplanis, D. Ursutiu, and C. Samoila, “Sun tracker system vs fixed system,” *Bulletin of the Transilvania University of Brasov Series III: Mathematics, Informatics, Physics*, vol. 1, no. 50, pp. 545–552, 2008.
- [39] D. T. Cotfas, S. Kaplanis, P. A. Cotfas, D. Ursutiu, and C. Samoila, “A new albedometer based on solar cells,” in *Proc. World Renewable Energy Congress X*, A. Sayigh, Ed., Glasgow, 2008.
- [40] R. V. Meyta and F. V. Savrasov, “To study the influence of snow cover on the power generated by photovoltaic modules,” *IOP Conference Series: Materials Science and Engineering*, vol. 81, article 012110, 2015.
- [41] T. C. R. Russell, R. Saive, A. Augusto, S. G. Bowden, and H. A. Atwater, “The influence of spectral albedo on bifacial solar cells: a theoretical and experimental study,” *IEEE Journal of Photovoltaics*, vol. 7, no. 6, pp. 1611–1618, 2017.
- [42] C. E. Valdivia, C. T. Li, A. Russell et al., “Bifacial photovoltaic module energy yield calculation and analysis,” in *2017 IEEE 44th Photovoltaic Specialist Conference (PVSC)*, Washington, DC, USA, June 2017.
- [43] M. Chiodetti, A. Lindsay, P. Dupeyrat et al., “PV bifacial yield simulation with a variable albedo model,” in *32nd European Photovoltaic Solar Energy Conference and Exhibition*, Munich, Germany, 2016.
- [44] R. Arshad, S. Tariq, M. U. Niaz, and M. Jamil, “Improvement in solar panel efficiency using solar concentration by simple mirrors and by cooling,” in *2014 International Conference on Robotics and Emerging Allied Technologies in Engineering (iCREATE)*, Islamabad, Pakistan, April 2014.
- [45] W. A. M. Al-Shohani, R. Al-Dadah, S. Mahmoud, and A. Algareu, “Optimum design of V-trough concentrator for photovoltaic applications,” *Solar Energy*, vol. 140, pp. 241–254, 2016.
- [46] C. S. Solanki, C. S. Sangani, D. Gunashekar, and G. Antony, “Enhanced heat dissipation of V-trough PV modules for better performance,” *Solar Energy Materials and Solar Cells*, vol. 92, no. 12, pp. 1634–1638, 2008.
- [47] S. Maiti, S. Banerjee, K. Vyas, P. Patel, and P. K. Ghosh, “Self regulation of photovoltaic module temperature in V-trough using a metal-wax composite phase change matrix,” *Solar Energy*, vol. 85, no. 9, pp. 1805–1816, 2011.
- [48] M. E. Ya’acob, H. Hizam, H. Abdul Rahman, W. Z. Wan Omar, M. T. Htay, and A. H. M. A. Rahim, “A simple approach in estimating the effectiveness of adapting mirror concentrator and tracking mechanism for PV arrays in the tropics,” *International Journal of Photoenergy*, vol. 2014, Article ID 341863, 7 pages, 2014.

- [49] J. Hu and T. Yachi, "Photovoltaic systems with solar tracking mirrors," in *2013 International Conference on Renewable Energy Research and Applications (ICRERA)*, Madrid, Spain, October 2013.
- [50] O. K. Ahmed and S. M. Bawa, "Reflective mirrors effect on the performance of the hybrid PV/thermal water collector," *Energy for Sustainable Development*, vol. 43, pp. 235–246, 2018.
- [51] G. M. Tina and P. F. Scandura, "Case study of a grid connected with a battery photovoltaic system: V-trough concentration vs. single-axis tracking," *Energy Conversion and Management*, vol. 64, pp. 569–578, 2012.
- [52] H. Singh, M. Sabry, and D. A. G. Redpath, "Experimental investigations into low concentrating line axis solar concentrators for CPV applications," *Solar Energy*, vol. 136, pp. 421–427, 2016.
- [53] Z. Mathys and P. J. Burchill, "Influence of location on the weathering of acrylic sheet materials," *Polymer Degradation and Stability*, vol. 55, no. 1, pp. 45–54, 1997.
- [54] F. E. Sahin and M. Yilmaz, "High concentration photovoltaics (HCPV) with diffractive secondary optical elements," *Photonics*, vol. 6, no. 2, p. 68, 2019.
- [55] F. Languy, K. Fleury, C. Lenaerts et al., "Flat Fresnel doublets made of PMMA and PC: combining low cost production and very high concentration ratio for CPV," *Optics Express*, vol. 19, Supplement 3, pp. A280–A294, 2011.
- [56] G. Zhou, J. He, and L. Xu, "Antifogging antireflective coatings on Fresnel lenses by integrating solid and mesoporous silica nanoparticles," *Microporous and Mesoporous Materials*, vol. 176, pp. 41–47, 2013.
- [57] A. Akisawa, M. Hiramatsu, and K. Ozaki, "Design of dome-shaped non-imaging Fresnel lenses taking chromatic aberration into account," *Solar Energy*, vol. 86, no. 3, pp. 877–885, 2012.
- [58] M. Benganem, A. A. Al-Mashraqi, and K. O. Daffallah, "Performance of solar cells using thermoelectric module in hot sites," *Renewable Energy*, vol. 89, pp. 51–59, 2016.
- [59] Z. A. Haidar, J. Orfi, and Z. Kaneesamkandi, "Experimental investigation of evaporative cooling for enhancing photovoltaic panels efficiency," *Results in Physics*, vol. 11, pp. 690–697, 2018.
- [60] L. Mei, D. Infield, U. Eicker, and V. Fux, "Thermal modelling of a building with an integrated ventilated PV façade," *Energy and Buildings*, vol. 35, no. 6, pp. 605–617, 2003.
- [61] D. Sato and N. Yamada, "Review of photovoltaic module cooling methods and performance evaluation of the radiative cooling method," *Renewable and Sustainable Energy Reviews*, vol. 104, pp. 151–166, 2019.
- [62] H. G. Teo, P. S. Lee, and M. N. A. Hawlader, "An active cooling system for photovoltaic modules," *Applied Energy*, vol. 90, no. 1, pp. 309–315, 2012.
- [63] R. Mazón-Hernández, J. R. García-Cascales, F. Vera-García, A. S. Káiser, and B. Zamora, "Improving the electrical parameters of a photovoltaic panel by means of an induced or forced air stream," *International Journal of Photoenergy*, vol. 2013, Article ID 830968, 10 pages, 2013.
- [64] W. He, Y. Zhang, and J. Ji, "Comparative experiment study on photovoltaic and thermal solar system under natural circulation of water," *Applied Thermal Engineering*, vol. 31, no. 16, pp. 3369–3376, 2011.
- [65] S. S. Joshi and A. S. Dhoble, "Photovoltaic -thermal systems (PVT): technology review and future trends," *Renewable and Sustainable Energy Reviews*, vol. 92, pp. 848–882, 2018.
- [66] D. Yang and H. Yin, "Energy conversion efficiency of a novel hybrid solar system for photovoltaic, thermoelectric and heat utilization," *IEEE Transactions on Energy Conversion*, vol. 26, no. 2, pp. 662–670, 2011.
- [67] N. Xu, J. Ji, W. Sun, W. Huang, J. Li, and Z. Jin, "Numerical simulation and experimental validation of a high concentration photovoltaic/thermal module based on point-focus Fresnel lens," *Applied Energy*, vol. 168, pp. 269–281, 2016.
- [68] S. Krauter, "Increased electrical yield via water flow over the front of photovoltaic panels," *Solar Energy Materials and Solar Cells*, vol. 82, no. 1-2, pp. 131–137, 2004.
- [69] K. A. Moharram, M. S. Abd-Elhady, H. A. Kandil, and H. el-Sherif, "Enhancing the performance of photovoltaic panels by water cooling," *Ain Shams Engineering Journal*, vol. 4, no. 4, pp. 869–877, 2013.
- [70] M. Abdolzadeh and M. Ameri, "Improving the effectiveness of a photovoltaic water pumping system by spraying water over the front of photovoltaic cells," *Renewable Energy*, vol. 34, no. 1, pp. 91–96, 2009.
- [71] M. Rosa-Clot, P. Rosa-Clot, G. M. Tina, and P. F. Scandura, "Submerged photovoltaic solar panel: SP2," *Renewable Energy*, vol. 35, no. 8, pp. 1862–1865, 2010.
- [72] R. Cazzaniga, M. Rosa-Clot, P. Rosa-Clot, and G. M. Tina, "Floating tracking cooling concentrating (FTCC) systems," in *2012 38th IEEE Photovoltaic Specialists Conference*, pp. 514–517, Austin, TX, USA, June 2012.
- [73] E. M. do Sacramento, P. C. M. Carvalho, J. C. de Araújo, D. B. Riffel, R. M. da Cruz Corrêa, and J. S. P. Neto, "Scenarios for use of floating photovoltaic plants in Brazilian reservoirs," *IET Renewable Power Generation*, vol. 9, no. 8, pp. 1019–1024, 2015.
- [74] N. Karami and M. Rahimi, "Heat transfer enhancement in a hybrid microchannel-photovoltaic cell using Boehmite nanofluid," *International Communications in Heat and Mass Transfer*, vol. 55, pp. 45–52, 2014.
- [75] Z. Rostami, M. Rahimi, and N. Azimi, "Using high-frequency ultrasound waves and nanofluid for increasing the efficiency and cooling performance of a PV module," *Energy Conversion and Management*, vol. 160, pp. 141–149, 2018.
- [76] H. A. Hussien, M. Hasanuzzaman, A. H. Noman, and A. R. Abdulmunem, "Enhance photovoltaic/thermal system performance by using nanofluid," in *3rd IET International Conference on Clean Energy and Technology (CEAT) 2014*, Kuching, Malaysia, November 2014.
- [77] A. K. Suresh, S. Khurana, G. Nandan, G. Dwivedi, and S. Kumar, "Role on nanofluids in cooling solar photovoltaic cell to enhance overall efficiency," *Materials Today: Proceedings*, vol. 5, no. 9, pp. 20614–20620, 2018.
- [78] H. M. S. Bahaidarah, A. A. B. Baloch, and P. Gandhidasan, "Uniform cooling of photovoltaic panels: a review," *Renewable and Sustainable Energy Reviews*, vol. 57, pp. 1520–1544, 2016.
- [79] A. Hasan, S. J. McCormack, M. J. Huang, and B. Norton, "Evaluation of phase change materials for thermal regulation enhancement of building integrated photovoltaics," *Solar Energy*, vol. 84, no. 9, pp. 1601–1612, 2010.
- [80] P. H. Biwole, P. Eclache, and F. Kuznik, "Phase-change materials to improve solar panel's performance," *Energy and Buildings*, vol. 62, pp. 59–67, 2013.
- [81] Y. S. Indartono, A. Suwono, and F. Y. Pratama, "Improving photovoltaics performance by using yellow petroleum jelly

- as phase change material,” *International Journal of Low-Carbon Technologies*, vol. 11, no. 3, pp. 333–337, 2014.
- [82] A. Hasan, S. J. McCormack, M. J. Huang, and B. Norton, “Energy and cost saving of a photovoltaic-phase change materials (PV-PCM) system through temperature regulation and performance enhancement of Photovoltaics,” *Energies*, vol. 7, no. 3, pp. 1318–1331, 2014.
- [83] A. H. A. Al-Waeli, K. Sopian, M. T. Chaichan et al., “Evaluation of the nanofluid and nano-PCM based photovoltaic thermal (PVT) system: an experimental study,” *Energy Conversion and Management*, vol. 151, pp. 693–708, 2017.
- [84] M. Sardarabadi, M. Passandideh-Fard, M. J. Maghrebi, and M. Ghazikhani, “Experimental study of using both ZnO/water nanofluid and phase change material (PCM) in photovoltaic thermal systems,” *Solar Energy Materials & Solar Modules*, vol. 161, pp. 62–69, 2017.
- [85] D. T. Cotfas, P. A. Cotfas, D. Ciobanu, and O. M. Machidon, “Characterization of photovoltaic-thermoelectric-solar collector hybrid systems in natural sunlight conditions,” *Journal of Energy Engineering*, vol. 143, no. 6, article 04017055, 2017.
- [86] S. Mahmoudinezhad, S. Ahmadi Atouei, P. A. Cotfas, D. T. Cotfas, L. A. Rosendahl, and A. Rezanian, “Experimental and numerical study on the transient behavior of multi-junction solar cell-thermoelectric generator hybrid system,” *Energy Conversion and Management*, vol. 184, pp. 448–455, 2019.
- [87] T. H. Kil, S. Kim, D. H. Jeong et al., “A highly-efficient, concentrating-photovoltaic/thermoelectric hybrid generator,” *Nano Energy*, vol. 37, pp. 242–247, 2017.
- [88] N. Karami, N. Moubayed, and R. Outbib, “General review and classification of different MPPT techniques,” *Renewable and Sustainable Energy Reviews*, vol. 68, pp. 1–18, 2017.
- [89] A. Mohapatra, B. Nayak, P. Das, and K. B. Mohanty, “A review on MPPT techniques of PV system under partial shading condition,” *Renewable and Sustainable Energy Reviews*, vol. 80, pp. 854–867, 2017.
- [90] J. Hahm, J. Baek, H. Kang, H. Lee, and M. Park, “Matlab-based modeling and simulations to study the performance of different MPPT techniques used for photovoltaic systems under partially shaded conditions,” *International Journal of Photoenergy*, vol. 2015, Article ID 979267, 10 pages, 2015.
- [91] April 2019, http://re.jrc.ec.europa.eu/pvg_tools/en/tools.html.
- [92] J. D. Rhodes, C. R. Upshaw, W. J. Cole, C. L. Holcomb, and M. E. Webber, “A multi-objective assessment of the effect of solar PV array orientation and tilt on energy production and system economics,” *Solar Energy*, vol. 108, pp. 28–40, 2014.
- [93] March 2019, <https://www.steinel.de/en/lights-floodlights/solar-lights/xsolar-l-s-silver.html>.
- [94] G. Quesada, L. Guillon, D. R. Rousse, M. Mehrtash, Y. Dutil, and P. L. Paradis, “Tracking strategy for photovoltaic solar systems in high latitudes,” *Energy Conversion and Management*, vol. 103, pp. 147–156, 2015.
- [95] B. G. Burduhos, I. Visa, A. Duta, and M. Neagoe, “Analysis of the conversion efficiency of five types of photovoltaic modules during high relative humidity time periods,” *IEEE Journal of Photovoltaics*, vol. 8, no. 6, pp. 1716–1724, 2018.
- [96] H. M. S. Bahaidarah, “Experimental performance investigation of uniform and non-uniform cooling techniques for photovoltaic systems,” in *2015 IEEE 42nd Photovoltaic Specialist Conference (PVSC)*, pp. 14–19, New Orleans, Louisiana, USA, June 2015.
- [97] A. A. B. Baloch, H. M. S. Bahaidarah, P. Gandhidasan, and F. A. Al-Sulaiman, “Experimental and numerical performance analysis of a converging channel heat exchanger for PV cooling,” *Energy Conversion and Management*, vol. 103, pp. 14–27, 2015.
- [98] L.-R. Chen, C.-H. Tsai, Y.-L. Lin, and Y.-S. Lai, “A biological swarm chasing algorithm for tracking the PV maximum power point,” *IEEE Transactions on Energy Conversion*, vol. 25, no. 2, pp. 484–493, 2010.
- [99] E. Koutroulis and F. Blaabjerg, “A new technique for tracking the global maximum power point of PV arrays operating under partial-shading conditions,” *IEEE Journal of Photovoltaics*, vol. 2, no. 2, pp. 184–190, 2012.
- [100] J. Gosumbonggot and G. Fujita, “Partial shading detection and global maximum power point tracking algorithm for photovoltaic with the variation of irradiation and temperature,” *Energies*, vol. 12, no. 2, p. 202, 2019.
- [101] S. Daraban, D. Petreus, C. Morel, and M. Machmoum, “A novel global MPPT algorithm for distributed MPPT systems,” in *2013 15th European Conference on Power Electronics and Applications (EPE)*, pp. 1–10, Lille, France, September 2013.
- [102] L. Gao, R. A. Dougal, S. Liu, and A. P. Iotova, “Parallel-connected solar PV system to address partial and rapidly fluctuating shadow conditions,” *IEEE Transactions on Industrial Electronics*, vol. 56, no. 5, pp. 1548–1556, 2009.
- [103] A. Jubaer, “An enhanced adaptive P&O MPPT for fast and efficient tracking under varying Environmental Conditions,” *IEEE Transactions on Industrial Electronics*, vol. 9, no. 3, pp. 1487–1496, 2008.
- [104] K. Ş. Parlak and H. Can, “A new MPPT method for PV array system under partially shaded conditions,” in *2012 3rd IEEE International Symposium on Power Electronics for Distributed Generation Systems (PEDG)*, pp. 437–441, Aalborg, Denmark, June 2012.
- [105] R. Alik, A. Jusoh, and N. A. Shukri, “An improved perturb and observe checking algorithm MPPT for photovoltaic system under partial shading condition,” in *2015 IEEE Conference on Energy Conversion (CENCON)*, Johor Bahru, Malaysia, October 2015.
- [106] K. Sundareswaran, S. Peddapati, and S. Palania, “MPPT of PV systems under partial shaded conditions through a colony of flashing fireflies,” *IEEE Transactions on Energy Conversion*, vol. 29, no. 2, pp. 463–472, 2014.
- [107] K. Sundareswaran, V. Vignesh kumar, and S. Palani, “Application of a combined particle swarm optimization and perturb and observe method for MPPT in PV systems under partial shading conditions,” *Renewable Energy*, vol. 75, pp. 308–317, 2015.
- [108] S. Mirjalili, A. H. Gandomi, S. Z. Mirjalili, S. Saremi, H. Faris, and S. M. Mirjalili, “Salp swarm algorithm: a bio-inspired optimizer for engineering design problems,” *Advances in Engineering Software*, vol. 114, pp. 163–191, 2017.
- [109] Y. Wan, M. Mao, L. Zhou, Q. Zhang, X. Xi, and C. Zheng, “A novel nature-inspired maximum power point tracking (MPPT) controller based on SSA-GWO algorithm for partially shaded photovoltaic systems,” *Electronics*, vol. 8, no. 6, p. 680, 2019.

Research Article

Comparative Study of Two Commercial Photovoltaic Panels under Natural Sunlight Conditions

Daniel T. Cotfas  and Petru A. Cotfas 

Electrical Engineering and Computer Science Faculty, Transilvania University of Brasov, Romania

Correspondence should be addressed to Daniel T. Cotfas; dtcotfas@unitbv.ro

Received 21 March 2019; Revised 24 July 2019; Accepted 14 October 2019; Published 22 November 2019

Academic Editor: Giulia Grancini

Copyright © 2019 Daniel T. Cotfas and Petru A. Cotfas. This is an open access article distributed under the Creative Commons Attribution License, which permits unrestricted use, distribution, and reproduction in any medium, provided the original work is properly cited.

Photovoltaic (PV) panels are used for both standalone applications and grid-connected systems. In the former case, the PV panels used vary in size, from very small, for smart solar garden lamps, to standard, in order to ensure the necessary electric energy for a house. For these cases, it is very important to choose the best solution in terms of photovoltaic cell materials. In this paper, a comparative study of two commercial photovoltaic panels, monocrystalline and amorphous silicon, is presented. The two photovoltaic panels are measured in natural conditions, during two years, in Brasov, Romania. The emphasis is placed upon the maximum power generated by the two panels, but the cost and the lifetime are also taken into consideration. The gain in average maximum power for the monocrystalline silicon panel varies from 1.9 times for low irradiance to 2.4 times higher than the one obtained from the amorphous silicon panel, during the test period. The temperature of the monocrystalline silicon panels is lower than that of the amorphous silicon panel in the majority of measurements. The degradation rate determined in two years is 1.02% for the monocrystalline silicon panel and 1.97% for the amorphous silicon panel.

1. Introduction

Different types of photovoltaic cells and panels were created over time in order to improve the performance, to reduce the cost and the amount of the materials used, and also to increase their application possibilities. The photovoltaic cells are classified into four groups generally referred to as generations [1]. For the first generation, the most representative is the monocrystalline silicon (mSi) photovoltaic cell, whose theoretical efficiency limit is around 32% [2–4]. The polycrystalline silicon (pSi), amorphous silicon (aSi), CdTe, and CIGS are the most important photovoltaic cells from the second generation [1, 2]. The third generation is represented by the organic or polymer, dye-sensitized solar cell DSSC and multijunction photovoltaic cells [1, 5]. “Inorganics-in-organics” is the fourth generation [5]. The photovoltaic cells obtained by incorporating the inorganic components led to the improvements of the low-cost thin film. The next generation of photovoltaic cells will be based on the new discoveries, such as nanotube and graphene, to improve the performance of the PVs [1].

The performance of different types of photovoltaic panels was largely studied [6–19]. From two to six types were taken into account in these studies. Most of them are made under natural conditions, only two being based on the simulation model [14, 19]. Some parameters are used to study the performance of the PV panels, namely, P_{\max} (maximum power), MAE (mean array efficiencies), CF (capacity factors), and PR (performance ratio) (International Electrotechnical Commission Standard IEC-61724 [20]) [21–24].

The performance of the photovoltaic panels, such as monocrystalline, polycrystalline, and amorphous silicon, cadmium tellurium, copper-indium-diselenide, and copper-indium-gallium-selenide, is studied for a location, a region, or a country. Carr and Pryor made a study for five different photovoltaic panels, among which are crystalline silicon and aSi, at Perth, Western Australia. The efficiency of the laser-grooved buried contact crystalline Si module varies between 11.5% and 12.5% on one year, and for triple junction, it is almost half [6]. Bashir et al. studied three types of photovoltaic panels in Taxila, Pakistan for winter months taking into account the efficiency and the performance ratio.

The average efficiency of the monocrystalline panel was almost 2.3 times higher than that of the amorphous panel, while the average performance ratio of aSi is almost 1.3 times better than of the monocrystalline panel [7]. Dolara et al. studied mono and polycrystalline panels in Milano to achieve a forecast model for the power generated by panel function of weather [8]. The parameters and the degradation of crystalline photovoltaic panels using the I-V characteristics are studied for Adrar, from the southern part of Algeria [10]. The performance of different photovoltaic panels is studied for different climates, such as Mediterranean climate (Malaga, Spain), temperate mountain climate (Brasov, Romania) [13], milder climate with long winter (Grimstad, Norway) [15], and semiarid climate (Amman, Jordan) [16]. Ito et al. studied six different types of photovoltaic panels from the life cycle analysis in Hokuto, Japan [17]. Amin et al. achieved a comparative study for different photovoltaic panels under Malaysian weather [9]. Dias et al. analyzed the models to estimate PV energy and proposed a new one based on results obtained from six types of photovoltaic panels among which are amorphous silicon and monocrystalline silicon in Brazil [14]. Six photovoltaic subsystems located in Madrid were analyzed based on the performance and the degradation rate. They find out that the CdTe/CdS technology has 2% in the first two years while the monocrystalline technology has the lowest rate [25]. Komoni et al. analyzed the performance of two panels, mono and polycrystalline connected on a grid, and obtained that the monocrystalline panel has a higher performance which generated 1328.21 kWh/kWp compared with 1286.57 kWh/kWp generated from polycrystalline panels [26]. The monocrystalline, polycrystalline, and amorphous silicon panels were tested in Casablanca, Morocco, and the results show that the monocrystalline panel has the best efficiency in both types of day, clear and cloudy [27]. Kumar et al. analyzed through simulation the performance of the three photovoltaic panels integrated in the buildings and obtained that CdTe is the best technology [28]. Ameer et al. studied three grid-connected photovoltaic technologies (monocrystalline, polycrystalline, and amorphous silicon) in the region of Ifrane, Morocco. They found out that the monocrystalline silicon and the polycrystalline silicon have almost the same performance during 51 months and the amorphous silicon has the lowest performance [29].

Although researchers developed many types of photovoltaic cells, the crystalline photovoltaic cells dominate the market and there is a trend of steady growth. Therefore, the market share is around 93% [30]. The amorphous silicon photovoltaic cell is another major component of the silicon family, with a market share around 50% from all thin-film photovoltaic cells until 2011 [31], afterwards decreasing, CdTe thus becoming leader [32], but the aSi photovoltaic cells remain the most widely used in small applications.

Considering the aspects mentioned above, this comparative study is focused upon two of the most commonly used photovoltaic panels from their group: monocrystalline and amorphous silicon. The previous aforementioned studies are focused on medium and large applications, while the tar-

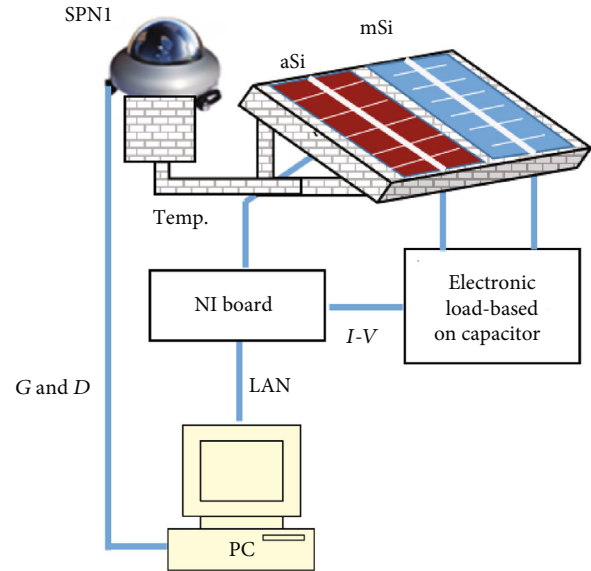


FIGURE 1: System setup with the two commercial photovoltaic panels.

get of this study is their utilization for standalone small applications, such as smart solar garden lamps, and by extrapolation for home photovoltaic systems. Moreover, in all studies mentioned before the photovoltaic panels had the backside free, not covered as in this study. The performance of the two photovoltaic panels is studied during two years in Brasov, Romania, at latitude 45.655°N and longitude 25.597°E. The measurements were made in outdoor conditions, taking into account the temperature of the panels and the solar radiation.

2. The Experimental Setup

The space for photovoltaic panel in small applications is limited, and its working conditions can be different in comparison with normal PV power plants. For smart solar garden lamps, the area of the photovoltaic panels has to be as small as possible. Therefore, it is important for comparison that the PV panels have the same area. The two photovoltaic panels under testing were chosen to have the sizes of 10 cm × 10 cm, which can be suitable for small applications.

The two PV panels, monocrystalline and amorphous silicon, were mounted on the same support tilted at 55°.

The solar radiation is measured using the SPN1 pyranometer. SPN1 measured the global solar radiation (G), and the diffuse solar radiation (D) is calculated. This information is very useful for determining the days or the period when the sky is cloudy. The standard uncertainty for the global radiation is 0.35 W/m².

The schema of the experimental setup is presented in Figure 1.

The current-voltage characteristics, I - V , of monocrystalline and amorphous silicon panels are measured using the capacitor technique [33].

The electronic load based on the capacitor technique is developed in our laboratory and permits the measurement

TABLE 1: The month optimum angle for Brasov and the month average irradiance at optimum angles 35°, 44°, 55°, and 64°.

Month	Jan	Feb	Mar	Apr	May	Jun	Jul	Aug	Sep	Oct	Nov	Dec
Opt. tilt (°)	63	55	44	29	16	9	13	25	40	55	64	65
G_{opt} (Wh/m ² /day)	1910	2550	4070	4570	4970	5100	5480	5260	4310	3830	2600	1640
$G_{[44]}$ (Wh/m ² /day)	2010	2630	4100	4470	4760	4830	5220	5110	4320	3960	2760	1730
$G_{[55]}$ (Wh/m ² /day)	2090	2660	4040	4250	4390	4390	4770	4800	4210	4020	2870	1800
$G_{[63]}$ (Wh/m ² /day)	2100	2640	3900	3980	4010	3950	4320	4450	4030	3970	2890	1820

of the I - V characteristics in the same time, using the data acquisition board from National Instruments. The voltage is measured with 0.1 mV standard uncertainty and the current with 0.08 mA standard uncertainty. The temperature of the photovoltaic panels is measured using two sensors, LM 35 (the typical accuracy is $\pm 0.4^\circ\text{C}$), which are mounted on the back of each PV panel. The solar radiation is measured simultaneously with the I - V characteristics of the photovoltaic panels. The program to perform the measurement and the control is realized in the LabVIEW software. The I - V characteristics of the photovoltaic panels, the temperatures, and the solar radiation are measured at five minutes each. The data is saved, and using a suitable program developed by the authors, it is processed in order to perform the comparison.

3. Theoretical Considerations

The maximum power (P_{max}) generated by the photovoltaic panels is the most important parameter to perform the comparison between the PV panels, in cases of small applications. The maximum power is determined using the power voltage characteristic, P - V , of the photovoltaic panels obtained from the I - V characteristic. The one-diode mathematical model, which is used to analyze the I - V characteristic, is described in [34]

$$I = I_{\text{ph}} - I_0 \left(e^{V + IR_s / nV_T} - 1 \right) - \frac{V + IR_s}{R_{\text{sh}}}, \quad (1)$$

where I_{sc} is the short circuit current, I_0 is the reverse saturation current, q represents the elementary charge, n is the ideality factor of diode, k is the Boltzmann constant, T is the panels' temperature, R_s represents the series resistance, and R_{sh} represents the shunt resistance.

Another parameter used for comparison is the efficiency of the photovoltaic panels and it is calculated using

$$\eta = \frac{P_{\text{max}}}{A \times I_s}, \quad (2)$$

where P_{max} is the maximum power, A represents the area of the photovoltaic panels, and I_s is the solar irradiance.

4. Results and Discussion

The measurements of the two photovoltaic panels are performed on the roof of the Transilvania University of Brasov throughout a two-year duration.

The goal of the PV power plants is to maximize the energy amount for the entire year, but for the PV panel used in smart solar garden lamps, the goal is to assure the energy so that the lamps work uninterruptedly for the entire year, even when there are periods without sun.

The tilt angle for the PV panel in the case of the smart solar garden lamp was chosen, analyzing the data obtained using the free PVGIS software and the Climate-SAF PVGIS database [35], see Table 1. So, the PV panel inclination was chosen, 55°, to maximize the amount of energy in the months when the ratio between the energy needed and the generated energy is critical taking into account the purpose of this study. The critical months are from October to February. In this period, the night is longer than the day, and the period when the smart lamp is turned on is higher than for the rest of year. For the other months, the energy generated by the photovoltaic panels is generally over the needed energy. There are other considerations for the use of tilted PV panels, such as increase in the quantity of the solar radiation falling on PV panels through reflections especially during winter (the worst period from the energy point of view) when the albedo of the fresh snow is around 90% and the self-cleaner process is improved at this tilt.

A simple way to compare the performance of the PV panels is to take into account the maximum power of the two photovoltaic panels given by manufacturers, who performed the measurements in standard test conditions (STC): irradiance 1000 W/m², air mass 1.5, and temperature 25°C. These conditions are rarely encountered in natural environment, and it is better to perform the comparison using the values obtained for the PV panels under natural sunlight illumination.

The maximum power generated by the PV panels and consequently their efficiency are considered for comparison because the area of the photovoltaic panels is limited and equal for the two PV panels taken into account. The maximum power and the efficiency are function of irradiance and time.

First of all, the two photovoltaic panels were measured under natural sunlight at different tilt angles on the N-S axis from 0 to 90 degrees and the azimuth angle is taken 0 degree to determine the angle effect. The horizontal solar radiation during measurements was $550 \pm 5 \text{ W/m}^2$. The measurements

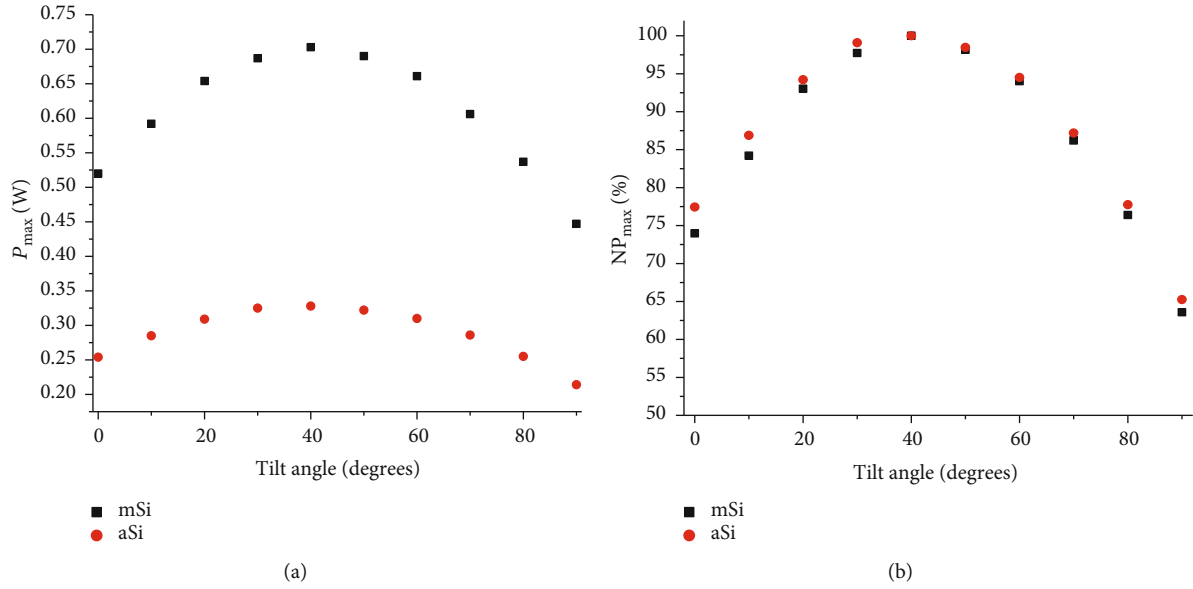


FIGURE 2: Performance comparison of the PV panels vs. tilt angle: (a) the maximum power and (b) the normalized power.

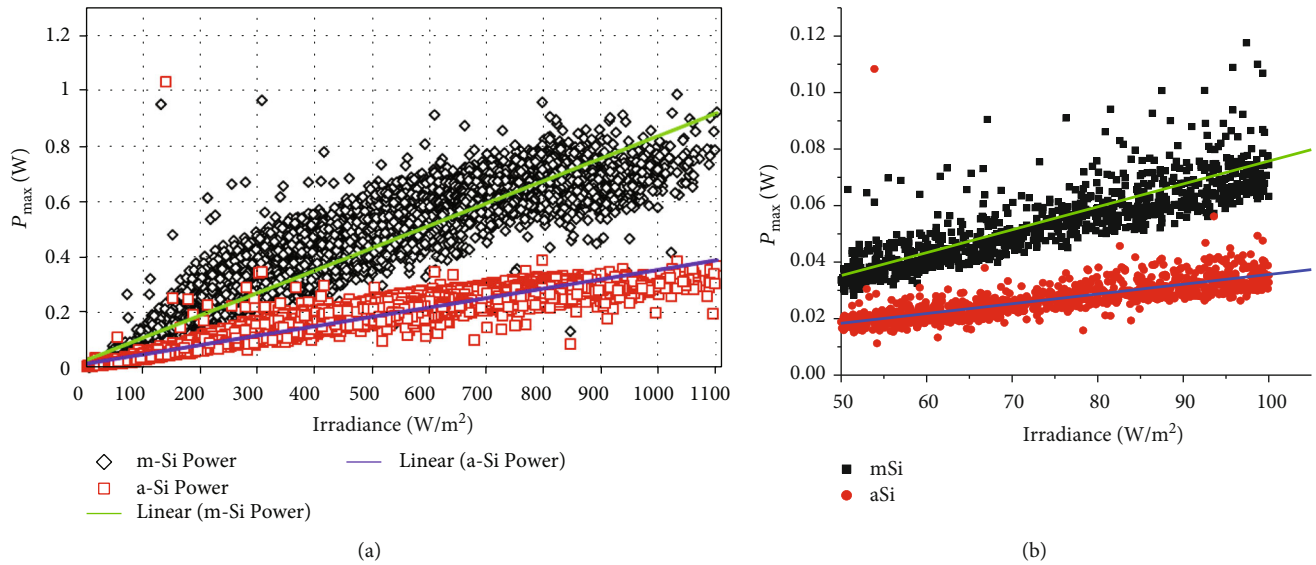


FIGURE 3: The maximum power of the two PV panels. (a) Irradiance from 0 to 1100 W/m^2 . (b) Irradiance from 50 to 100 W/m^2 .

were performed using a sun tracker, in September when for Brasov the optimum mathematical tilt angle is 40 degrees, see Table 1. The sun tracker system consists of a tripod and a pan/tilt device J-PT-1008-D which can work with an 8 kg load and move the panels on two axis. The pan/tilt device is controlled using the NI myRIO device, and two encoders are used for feedback. The sun is followed using the mathematical algorithm.

The maximum power generated by the two photovoltaic panels is presented in Figure 2(a) and the normalized power (NP_{\max}) in Figure 2(b), being calculated as the ratio between P_{\max} obtained for different angles and P_{\max} at 40°.

The maximum value for P_{\max} is obtained at 40 degrees for both photovoltaic panels which correspond to the optimum angle for September in Brasov. The maximum power gener-

ated by the monocrystalline silicon panel is over two times higher than the maximum power generated by the aSi photovoltaic panel, from 2.04 at 0° to 2.14 at 40°. The normalized power of the aSi panel is slightly bigger than that of the monocrystalline silicon panel, Figure 2(b), proving that the aSi panel has better performance in NP_{\max} for small values of the solar radiation, but in our case, this is less important because the monocrystalline silicon (mSi) panel generates power around two times higher than aSi even for small values of solar radiation.

The distribution of the maximum power generated by the two photovoltaic panels, tilted at 55°, on two years' duration function of the irradiance is presented in Figure 3(a). The temperature correction for maximum power is not taken into account to have the real behaviour of the two

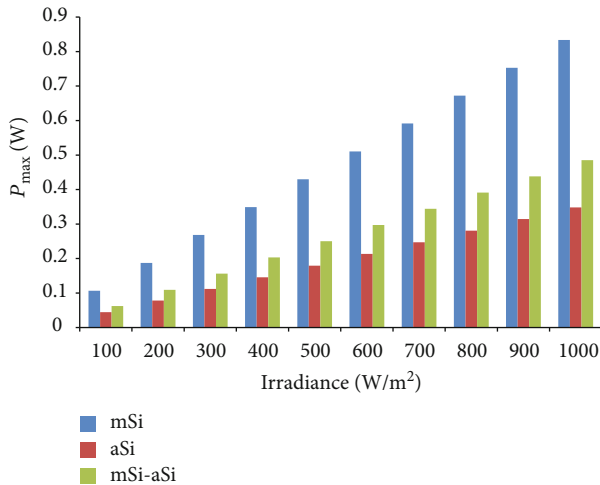


FIGURE 4: The average maximum power vs. illumination levels.

photovoltaic panels over the two years of measurement. An almost linear distribution of the maximum power function of the irradiance can be observed. The slope of the linear fit for the monocrystalline silicon panel maximum power is bigger than the one for aSi, meaning that the gain in maximum power for mSi increases for high values of irradiance. Figure 3(b) shows the distribution of the PV maximum power for small irradiance from 50 to 100 W/m². The monocrystalline silicon PV panel generates 35.24 mW at 50 W/m² while the aSi generates 18.34 mW. These values are obtained using the linear fit equation for the two PV panels. The monocrystalline silicon panel gain in power is almost two times larger than that for aSi.

The better performance of the monocrystalline silicon photovoltaic panel in comparison with the amorphous silicon panel is due to its efficiency. The high efficiency is obtained because the technology is very well developed and the highest quality silicon is used, the purity is 99.9999%. The monocrystalline silicon cell has the photoactive absorber stable, but an indirect energy band gap. This can be over-passed using surface texturing, suitable antireflection coating, and effective surface passivation.

The dependency of the maximum power average generated by the two photovoltaic panels on the irradiance is considered to have a better image (Figure 4). The difference between the average maximum power generated by the monocrystalline silicon panel and the aSi panel is also presented in Figure 4.

The values of the difference are higher than the values of the aSi maximum power for all irradiance values considered. By analyzing the results for the average maximum power function of the illumination levels, a gain is observed for the mSi panel which varies from 2.4 times at 1000 W/m² to 2.393 times at 100 W/m². The same behaviour is observed when the measurements were made only in a clear sky day (Figure 2(a)). The difference in maximum power is under two times for irradiance under 100 W/m² because the amorphous photovoltaic panel has good light absorbing characteristics in low irradiance. This result is in concordance with the one found by Bashir et al. [7].

In the following, analysis is made for day types in order to obtain data for specific conditions. Therefore, two days, one clear and one cloudy, were considered in winter and in summer. Figure 5 shows the maximum power variation for the four days: 6 January 2014 (Figure 5(a)), 9 January 2014 (Figure 5(b)), 3 August 2015 (Figure 5(c)), and 22 August 2015 (Figure 5(d)).

The shape of the curves for the maximum power generated by both photovoltaic panels for each of the considered days is almost the same.

The difference between the maximum powers of the two PV panels is higher for high values of irradiance. The power difference is higher in clear days than in cloudy days. The maximum power generated by the monocrystalline silicon panel can be almost three times higher than that generated by the aSi panel in clear days especially in winter, when the temperature of the monocrystalline silicon cells is smaller than the temperature of the aSi cells. This is an advantage for mSi because its maximum power temperature coefficient is -0.47% and for aSi it is -0.18% [36], and the gain in maximum power generated by monocrystalline silicon cells increases with the maximum power generated by aSi. The aSi panel is less sensitive at temperature variation than the monocrystalline silicon panel.

There are small deviations for some points which could appear due to measurement conditions which are detailed below. The difference in gain for the same type of days can be explained due to the temperature variation in the photovoltaic panels especially for cloudy days when the influence of the spectrum is high. The two panels respond differently both in temperature (see above the temperature coefficients) and spectrum. The spectral response for monocrystalline silicon cells is between 350 nm and 1200 nm with a maximum response for around 1100 nm, and for amorphous silicon cells, it is between 300 nm and 800 nm with a maximum response for around 500 nm. The part of solar spectrum is influenced by the clouds and the atmospheric conditions. Song et al. show that the relative decrease of the solar radiation on cloudy days is higher for wavelengths over 800 nm where decreasing is more than 70%, whereas below this wavelength value it is smaller than 50% [37]. This explains the better behaviour for the aSi panel in cloudy days when the gain of the monocrystalline silicon panel is smaller than for clear days.

Taking into account the amplitude of the gain, even on cloudy days where this is almost two times higher, it is clear that the mSi panels are the best choice in case the area is the same for both PV panels.

The solar global and diffuse radiation for the four days are shown in Figure 6. By analyzing these graphs together with the data for the maximum power generated by the PV panels, the same behaviour for radiation and power can be observed.

The solar diffuse radiation is almost equal with the solar global radiation, as can be seen in Figures 6(b) and 6(d), for the entire day, proving that the sky was cloudy on these days.

The variation of the photovoltaic panel temperature is presented in Figure 7(a) for a winter day (6 January 2014) and Figure 7(b) for a summer day (3 August 2015). The

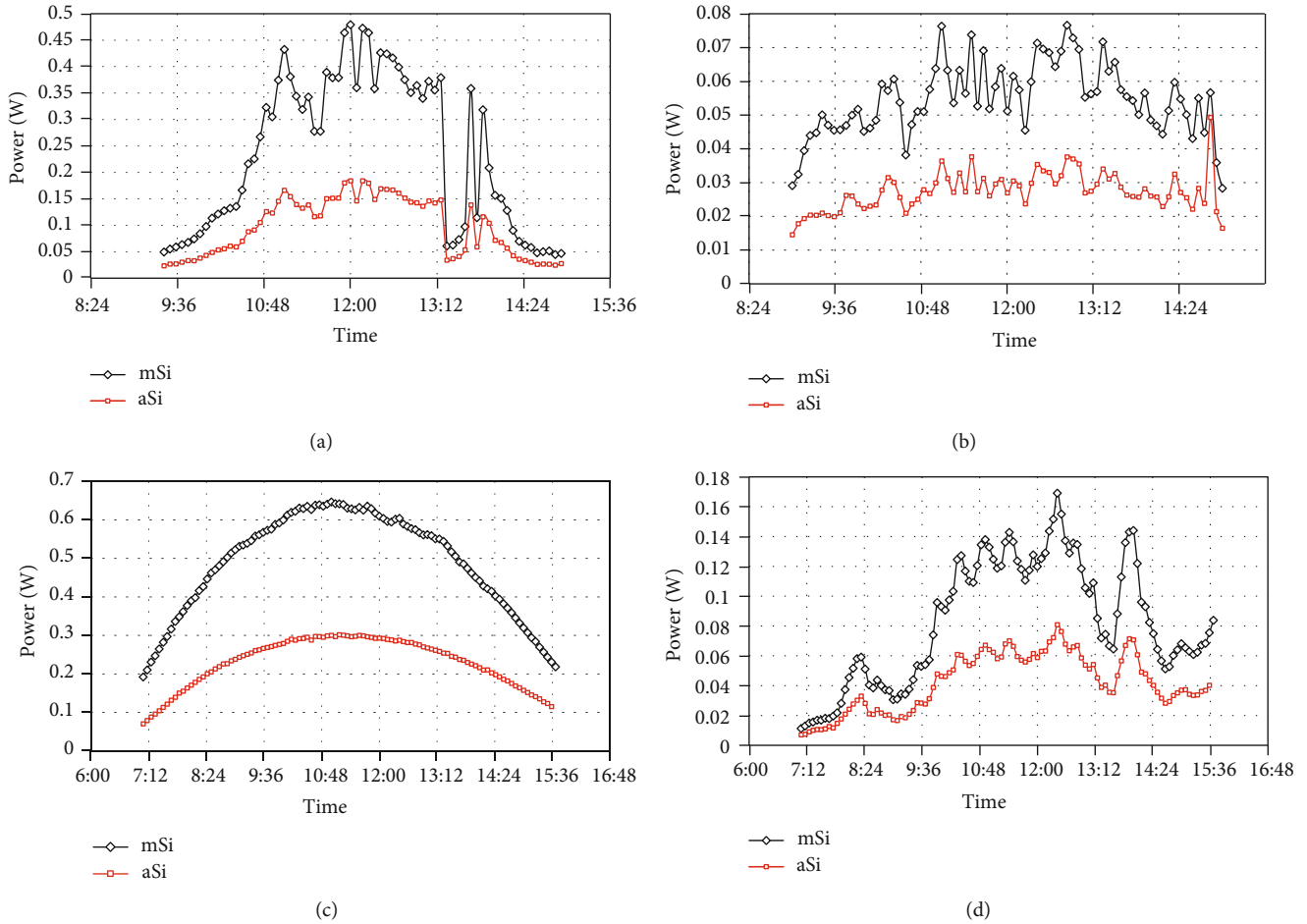


FIGURE 5: The maximum power generated by the two PV panels: (a) winter clear day, (b) winter cloudy day, (c) summer clear day, and (d) summer cloudy day.

temperature of the aSi panel in both cases is a little higher than the temperature of the monocrystalline silicon panel.

In general, the photovoltaic panels used for small applications do not have a free backside. For solar garden lamps, they have on the back the electronic circuit and the support for the light source.

The two photovoltaic panels analyzed have in the back a wooden support which is a thermal insulator to simulate the real work conditions.

The temperature difference between the two photovoltaic panels appears due to the better efficiency of the monocrystalline silicon panel, which is two times higher than the one of the aSi panel, the area of the two PV panels being the same and the PV back being covered. So, the heat dissipation effect is reduced compared to the case of PV panels for large applications, when the back of PV panels is free and the area of the aSi panel is almost two times bigger than the area of the mSi panel [7]. In the last case, the heat convection between the air and panel surface is better than that for the case under study. The higher temperature of the aSi panel is compensated by the lower power temperature coefficient [24, 36].

The behaviour of the efficiency for the two photovoltaic panels is the same as the maximum power because the areas

of the PV panels are equal and the irradiance is the same. The average efficiency for the minimum and maximum irradiance is presented in Table 2. There are significant differences from the STC efficiency, in accordance with other studies [9]. The efficiency calculated in natural conditions is influenced by the temperature of the photovoltaic panels, humidity, spectrum of sunlight, and also dust and dirt, as PV panels are naturally cleaned.

Using the current-voltage characteristics measured, in the future work, the parameters for both photovoltaic panels can be determined. They can be compared in function of the solar irradiance and the temperature. Also, other photovoltaic panels are going to be measured and compared. The behaviour of the photovoltaic panels when they are covered with dust and snow will be taken into account in a future study.

The comparison between the two photovoltaic panels is incomplete without taking into consideration the lifetime and the cost. For mSi photovoltaic systems, it is known that after 10 years the power generated represents 92% from the initial state and after 25 years the power is 82.5%. By analyzing the research literature for the lifetime behaviour of the two types of photovoltaic panels, the median degradation rate found is 0.36%/year for the monocrystalline silicon

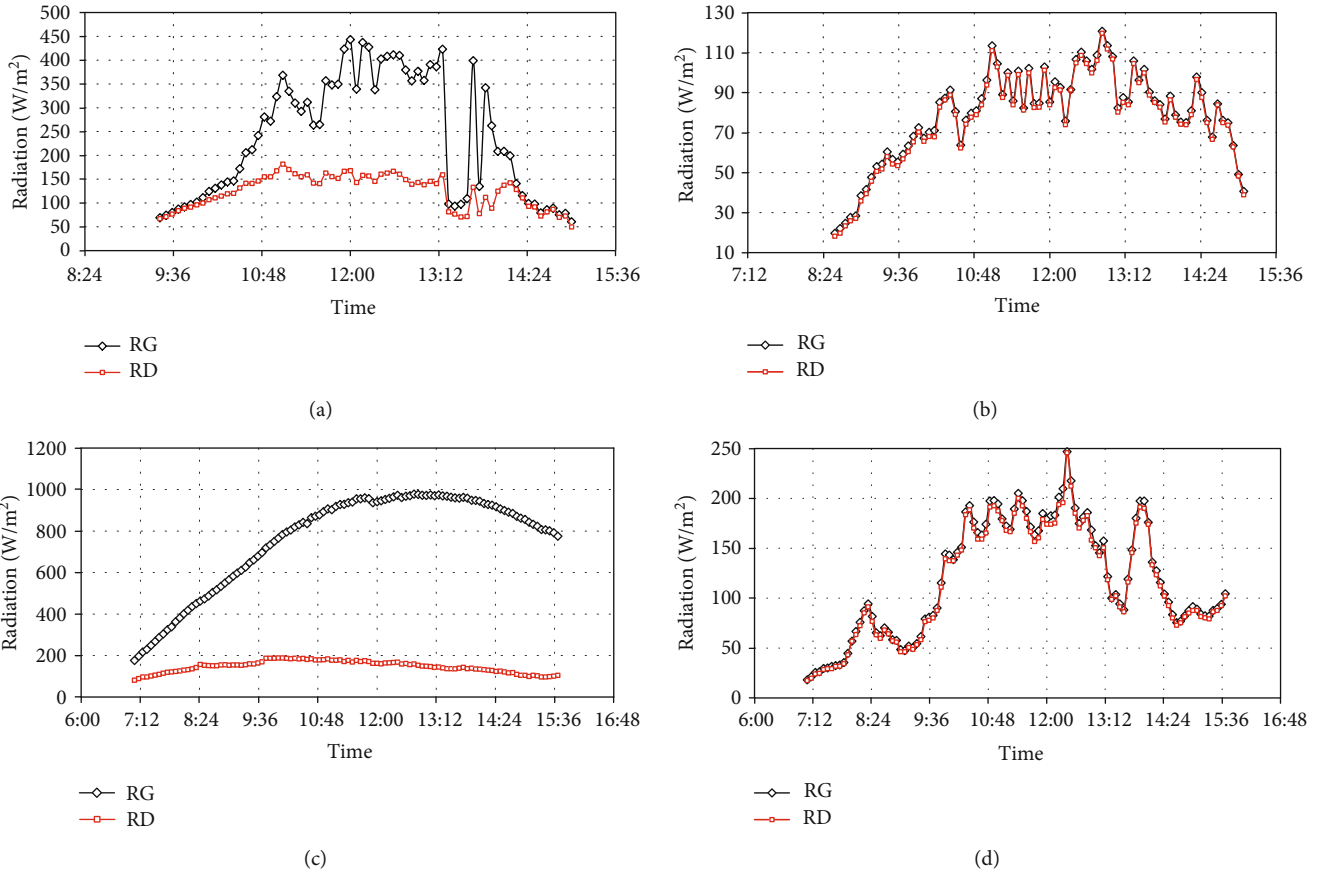


FIGURE 6: The solar global (RG) and diffuse radiation (RD): (a) winter clear day, (b) winter cloudy day, (c) summer clear day, and (d) summer cloudy day.

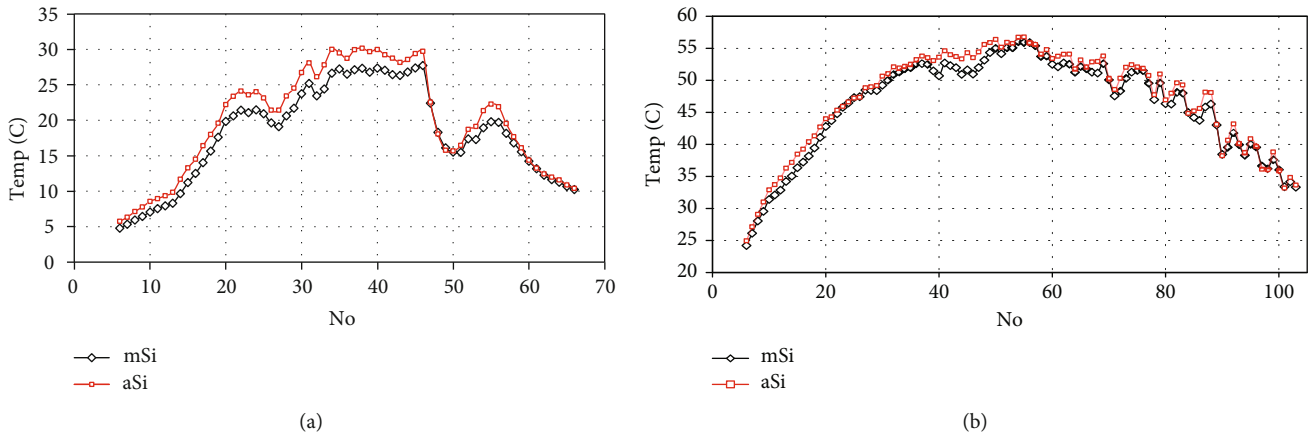


FIGURE 7: The temperature of the two photovoltaic panels: (a) winter day and (b) summer day.

photovoltaic panels, 0.87%/year for the amorphous silicon photovoltaic panels manufactured after 2000, 0.47%/year for the monocrystalline silicon panel, and 0.96% for the aSi panels manufactured before 2000 [38]. For the photovoltaic panels manufactured after 2000, the median degradation rate decreases with 10% for the aSi panels and with 20% for the monocrystalline silicon panels compared to that for panels manufactured before 2000.

The degradation rate is influenced by climate conditions, geographical relief, and so on. Therefore, it is important to study the lifetime behaviour of the PV panels for particular conditions. After two years, the degradation rate of the monocrystalline silicon panel is 1.02%, and for the aSi panel, it is 1.97% for this study. The monocrystalline silicon panel has an advantage on the long term because the degradation rate is almost two times smaller than that for the aSi panel.

TABLE 2: Mean efficiency for the two photovoltaic panels.

Irradiance (W/m ²)	Average efficiency (%)	
	mSi	aSi
100	10.66	4.45
1000	8.34	3.48

The aSi photovoltaic panel has a lower cost than the monocrystalline silicon panel, but the difference is not significant. The medium price for the aSi panel is 0.84 \$/W, while for mSi it is 1.1 \$/W [19]. The lowest price is 0.69 \$/W for aSi and 0.75 \$/W for mSi [39]. The lower price for the aSi photovoltaic panel is an advantage, but in addition to this price, the supplementary cost for the mounting must also be taken into consideration because for the same power an almost double area is needed.

The price for the two photovoltaic panels used, which are commercial panels, is almost the same with the lowest price. The common solar garden lamps use PV panels with a very small area because the required energy is very low, and consequently, the cost becomes a secondary aspect. It can be important for smart solar garden lamps, such as XSolar L-S [40], for whose prototype the authors contributed, where the necessary energy is in the order of watts.

5. Conclusions

The performance analysis for two commercial photovoltaic panels, monocrystalline and amorphous silicon, with small sizes 10 cm × 10 cm, was performed and presented. The experimental setup to measure the *I-V* characteristics of the two photovoltaic panels, the solar global radiation, and the temperature of the PV panels and the software for data processing were developed.

The maximum power of the PV panels is the parameter taken into account to achieve the comparison because the area of the PV panels is the same. Firstly, the maximum power generated by the two photovoltaic panels and the normalized power are measured for tilts between 0° and 90° on the N-S direction in order to have an initial image of their behaviour. Then, the panels were tilted at 55° which is the optimum angle for the critical period in the case of the solar garden lamps. The *I-V* characteristics of the two panels are measured during two years and are used to determine the maximum power of them. Also, the temperature of the two panels is measured during the test period. Comparing the average maximum power generated by the two panels shows that the average maximum power of the monocrystalline silicon panel is over two times higher than the one generated by the amorphous silicon panel. This value increases to almost three on clear winter days due to the temperature decrease of the monocrystalline silicon panel. The gain is over 1.9 times even for very low irradiance, under 100 W/m². The difference in temperature between the amorphous silicon panel and the monocrystalline silicon panel is higher in winter days than in summer days. It is positive during the measurement period. Therefore, the monocrystalline silicon panel is space efficient, analyzing the maximum power generated by the two photovoltaic panels.

The median degradation rate is another advantage for the panel which is almost two times lower than the one for aSi. The cost and the maximum power temperature coefficient are lower for the aSi photovoltaic panel which can be an advantage. However, the cost of the aSi system increases because it is necessary to double the area to obtain the same power generated as in the monocrystalline Si case.

Taking into consideration these aspects, the monocrystalline silicon panel is the most suitable for the applications with limited space, such as smart and common solar garden light.

The behaviour of the parameters, such as the short circuit current, the reverse saturation current, the ideality factor of diode, the series resistance, and the shunt resistance, for the two photovoltaic panels will be analyzed in the future work using the *I-V* characteristics and different parameter extraction methods.

Data Availability

Some of the data used in this work are available in Annex and the rest can be provided upon request from authors (email addresses dtcofas@unitbv.ro and pcofas@unitbv.ro).

Disclosure

A first version of the paper was presented at the international conference for Alternative Energy Sources, Materials and Technologies (AESMT'18), Plovdiv, Bulgaria.

Conflicts of Interest

The authors are employed at Transilvania University of Brasov.

Supplementary Materials

Annex: the maximum power and the normalized power for the two monocrystalline and amorphous photovoltaic panels measured in function of the tilt angles are given. Also, the average maximum power of the monocrystalline and amorphous photovoltaic panels is calculated for different values of the irradiance which varies from 100 W/m² to 1000 W/m², the two panels being tilted at 55°. The maximum power for different tilt angles (monocrystalline and amorphous panels). (*Supplementary Materials*)

References

- [1] Next generation solar cells, *The Future of Renewable Energy* <http://mnre.gov.in>.
- [2] F. H. Alharbi and S. Kais, "Theoretical limits of photovoltaics efficiency and possible improvements by intuitive approaches learned from photosynthesis and quantum coherence," *Renewable and Sustainable Energy Reviews*, vol. 43, pp. 1073–1089, 2015.
- [3] M. A. Green, Y. Hishikawa, E. D. Dunlop, D. H. Levi, J. Hohl-Ebinger, and A. W. Y. Ho-Baillie, "Solar cell efficiency tables (version 52)," *Progress in Photovoltaics: Research and Applications*, vol. 26, no. 7, pp. 427–436, 2018.

- [4] D. M. Bagnal and M. Boreland, "Photovoltaic technologies," *Energy Policy*, vol. 36, no. 12, pp. 4390–4396, 2008.
- [5] K. D. G. I. Jayawardena, L. J. Rozanski, C. A. Mills, M. J. Belia-tis, N. A. Nismya, and S. R. P. Silva, "Inorganics-in-organics': recent developments and outlook for 4G polymer solar cells," *Nanoscale*, vol. 5, no. 18, pp. 8411–8427, 2013.
- [6] A. J. Carr and T. L. Pryor, "A comparison of the performance of different PV module types in temperate climates," *Solar Energy*, vol. 76, no. 1-3, pp. 285–294, 2004.
- [7] M. A. Bashir, H. M. Ali, S. Khalil, M. Ali, and A. M. Siddiqui, "Comparison of performance measurements of photovoltaic modules during winter months in Taxila, Pakistan," *International Journal of Photoenergy*, vol. 2014, Article ID 898414, 8 pages, 2014.
- [8] A. Dolar, S. Leva, and G. Manzolini, "Comparison of different physical models for PV power output prediction," *Solar Energy*, vol. 119, pp. 83–99, 2015.
- [9] N. Amin, C. W. Lung, and K. Sopian, "A practical field study of various solar cells on their performance in Malaysia," *Renewable Energy*, vol. 34, no. 8, pp. 1939–1946, 2009.
- [10] M. Sadok and A. Mehdaoui, "Outdoor testing of photovoltaic arrays in the Saharan region," *Renewable Energy*, vol. 33, no. 12, pp. 2516–2524, 2008.
- [11] M. Ohmukai and A. Tsuyoshi, "Comparison between amorphous and tandem silicon solar cells in practical use," *Journal of Power and Energy Engineering*, vol. 05, no. 04, pp. 9–14, 2017.
- [12] C. Canete, J. Carretero, and M. Sidrach-de-Cardona, "Energy performance of different photovoltaic module technologies under outdoor conditions," *Energy*, vol. 65, pp. 295–302, 2014.
- [13] I. Visa, B. Burduhos, M. Neagoe, M. Moldovan, and A. Duta, "Comparative analysis of the infield response of five types of photovoltaic modules," *Renewable Energy*, vol. 95, pp. 178–190, 2016.
- [14] C. L. A. Dias, D. A. C. Branco, M. C. Arouca, and L. F. L. Legey, "Performance estimation of photovoltaic technologies in Brazil," *Renewable Energy*, vol. 114, pp. 367–375, 2017.
- [15] O. M. Midtgard, T. O. Sætre, G. Yordanov, A. G. Imenes, and C. L. Nge, "A qualitative examination of performance and energy yield of photovoltaic modules in southern Norway," *Renewable Energy*, vol. 35, no. 6, pp. 1266–1274, 2010.
- [16] M. R. Abdelkader, A. Al-Salaymeh, Z. Al-Hamamre, and F. Sharaf, "A comparative analysis of the performance of monocrystalline and polycrystalline PV cells in semi-arid climate conditions: the case of Jordan," *Jordan Journal of Mechanical and Industrial Engineering*, vol. 4, pp. 543–552, 2010.
- [17] M. Ito, M. Kudo, M. Nagura, and K. Kurokawa, "A comparative study on life-cycle analysis of 20 different pv modules installed at a Hokuto mega-solar plant," in *25th European Photovoltaic Solar Energy Conference and Exhibition/5th World Conference on Photovoltaic Energy Conversion*, Valencia, Spain, January 2011.
- [18] A. Bianchini, M. Gambuti, M. Pellegrini, and C. Sacconi, "Performance analysis and economic assessment of different photovoltaic technologies based on experimental measurements," *Renewable Energy*, vol. 85, pp. 1–11, 2016.
- [19] A. A. Hossam El-din, C. F. Gabra, and A. H. H. Ali, "A comparative analysis between the performances of monocrystalline, polycrystalline and amorphous thin film in different temperatures at different locations in Egypt," in *1st Africa Photovoltaic Solar Energy Conference and Exhibition*, Durban, March 2014.
- [20] International Electrotechnical Commission (IEC), "International Standard IEC-61724: Photovoltaic System Performance Monitoring," *Guidelines for Measurement, Data Exchange and Analysis*, 1998.
- [21] M. E. Başoğlu, A. Kazdaloğlu, T. Erfidan, M. Z. Bilgin, and B. Çakir, "Performance analyzes of different photovoltaic module technologies under İzmit, Kocaeli climatic conditions," *Renewable and Sustainable Energy and Reviews*, vol. 52, pp. 357–365, 2015.
- [22] A. Balaska, A. Tahri, F. Tahri, and A. B. Stambouli, "Performance assessment of five different photovoltaic module technologies under outdoor conditions in Algeria," *Renewable Energy*, vol. 107, pp. 53–60, 2017.
- [23] A. Abdallah, D. Martinez, B. Figgis, and O. El Daif, "Performance of silicon heterojunction photovoltaic modules in Qatar climatic conditions," *Renewable Energy*, vol. 97, pp. 860–865, 2016.
- [24] D. A. Quansah and M. S. Adaramola, "Assessment of early degradation and performance loss in five co-located solar photovoltaic module technologies installed in Ghana using performance ratio time-series regression," *Renewable Energy*, vol. 131, pp. 900–910, 2019.
- [25] T. A. Guerra, J. A. Guerra, B. O. Taberero, and G. C. García, "Comparative energy performance analysis of six primary photovoltaic technologies in Madrid (Spain)," *Energies*, vol. 10, no. 6, p. 772, 2017.
- [26] V. Komoni, A. Gebremedhin, and N. Ibrahim, "A comparison of the performance of mono-Si and poly-Si photovoltaic modules operating under Kosovo climate condition," *Journal of Renewable and Sustainable Energy*, vol. 10, no. 1, article 013504, 2018.
- [27] E. Karami, M. Rafi, A. Haibaoui, A. Ridah, B. Hartiti, and P. Thevenin, "Performance analysis and comparison of different photovoltaic modules technologies under different climatic conditions in Casablanca," *Journal of Fundamentals of Renewable Energy and Applications*, vol. 07, no. 03, pp. 1–6, 2017.
- [28] N. M. Kumar, K. Sudhakar, and M. Samykan, "Performance comparison of BAPV and BIPV systems with c-Si, CIS and CdTe photovoltaic technologies under tropical weather conditions," *Case Studies in Thermal Engineering*, vol. 13, article 100374, 2019.
- [29] A. Ameur, A. Sekkat, K. Loudiyi, and M. Aggour, "Performance evaluation of different photovoltaic technologies in the region of Ifrane, Morocco," *Energy for Sustainable Development*, vol. 52, pp. 96–103, 2019.
- [30] P. J. Ribeyron, "Crystalline silicon solar cells: better than ever," *Nature Energy*, vol. 2, no. 5, article 17067, 2017.
- [31] "Amorphous silicon will continue to dominate thin-film PV market," November 2018, <http://www.renewableenergyfocus.com/view/1131/amorphous-silicon-will-continue-to-dominate-thin-film-pv-market/>.
- [32] Fraunhofer ISE, *Photovoltaics Report*, Fraunhofer ISE, Freiburg, 2014, November 2018, <http://www.ise.fraunhofer.de>.
- [33] D. T. Cotfas and P. A. Cotfas, "PV innovative techniques and experimental test sets," in *Renewable Energy Systems: Theory, Innovations and Intelligent Applications*, S. Kaplanis and E. Kaplani, Eds., pp. 525–546, Nova Science Publishers, USA, 2013.

- [34] D. T. Cotfas, P. A. Cotfas, and S. Kaplanis, "Methods to determine the dc parameters of solar cells: a critical review," *Renewable and Sustainable Energy Reviews*, vol. 28, pp. 588–596, 2013.
- [35] November 2018, <http://re.jrc.ec.europa.eu/pvgis/apps4/pvest.php>.
- [36] D. T. Cotfas, P. A. Cotfas, and O. M. Machidon, "Study of temperature coefficients for parameters of photovoltaic cells," *International Journal of Photoenergy*, vol. 2018, Article ID 5945602, 12 pages, 2018.
- [37] X. Song, E. L. Miller, and D. Garmire, *Experimental study of solar spectrum impact on solar cells*, *Technical Proceedings of the 2010 Clean Technology Conference and Trade Show*, University of Hawaii at Manoa, US, 2010.
- [38] D. C. Jordan and S. R. Kurtz, "Photovoltaic Degradation Rates—an Analytical Review," *Progress in Photovoltaics Research and Applications*, vol. 21, no. 1, pp. 12–29, 2013.
- [39] V. Alfonso <http://www.josre.org/wp-content/uploads/2012/10/Photovoltaics-Choices-Costs-and-Benefits-by-Victor-Alfonso.pdf>.
- [40] April 2019, <https://www.steinel.de/en/lights-floodlights/solar-lights/xsolar-l-s-silver.html>.

Research Article

Determination of Technological Features of a Solar Photovoltaic Cell Made of Monocrystalline Silicon P⁺PNN⁺

Cristian-Petre Fluieraru ¹, **Gabriel Predușcă**,¹ **Horia Andrei**,¹ **Emil Diaconu**,¹
Petru Adrian Cotfas ² and **Daniel Tudor Cotfas** ²

¹Department of Electronics, Telecommunications, and Energy Engineering, University Valahia of Târgoviște, Str. Aleea Sinaia, Nr. 13, RO-130004 Târgoviște, Romania

²Department of Electronics and Computer, University Transilvania of Brasov, Str. Universitatii, Nr. 1, Brasov, Romania

Correspondence should be addressed to Cristian-Petre Fluieraru; cristi2006tg@yahoo.com

Received 6 April 2019; Accepted 26 September 2019; Published 19 November 2019

Academic Editor: Leonardo Palmisano

Copyright © 2019 Cristian-Petre Fluieraru et al. This is an open access article distributed under the Creative Commons Attribution License, which permits unrestricted use, distribution, and reproduction in any medium, provided the original work is properly cited.

The development in the field of semiconductor materials and electronic devices has a great impact on systems with renewable energy sources. Determination of the functional parameters of photovoltaic solar cells is essential for the subsequent usage of these semiconductor devices. Research was made on type P⁺PNN⁺ monocrystalline silicon wafers. Crystallographic measurements of the photovoltaic solar cell were made by means of FESEM-FIB Auriga Workstation. Initial data were selected from the study of models found in the specialized literature. The experimental results were compared to classical mathematical models. Measurements made on the photovoltaic solar cell were realised in laboratory conditions on the NI-ELVIS platform produced by National Instruments.

1. Introduction

Absorption of photons under certain conditions in a semiconductor plate creates electrical power. The principle of conversion is based on the fact that in a semiconductor the electrons removed from the nucleus can be transformed into free conducting electrons in motion. This creates a positive load and a negative carrier simultaneously.

If there is a potential difference in the semiconductor material due to a p-n junction, then this load carrier can be forced to direct to an external circuit and thus an electric power can be produced. In the case of crystalline silica, the electric charge carriers that have been obtained can only reach this potential barrier due to thermal vibrations. No other force can lead them in this direction. This means that loaded particles will have to survive until they reach the potential barrier. The resulting lifetime is one of the key factors for the efficiency of photovoltaic energy production [1].

The physical effect was first observed by Becquerel in 1839 when he obtained power by exposing silver electrodes

to radiation in an electrolyte. The effect was further described by Adams and Day in 1877 [2, 3]. They noticed that the exposure of selenium electrodes to radiation produces electrical voltage thus allowing them to obtain electrical power. Until 1949, when the semiconductor appeared, the photovoltaic effect was not used. Then in 1954, in the US, Chapin developed the first solar cell based on crystalline silicon, which had a 6% efficiency (very good for those times) [4]. In the coming years, efficiency has increased to 10%.

The main reason for the spread of the application of the photovoltaic effect to energy sources was the oil crisis of 1973. Since that time, specific research institutes have emerged around the world. At the beginning of the 1980s, it was recognized that the efficiency of solar cells is very important for reducing the cost of alternative energy systems. From this point on, research and development have been focused on achieving greater efficiency. For the future, it is expected that with the disappearance of fossil fuels, the Sun will be one of the few inexhaustible sources of energy widely used.

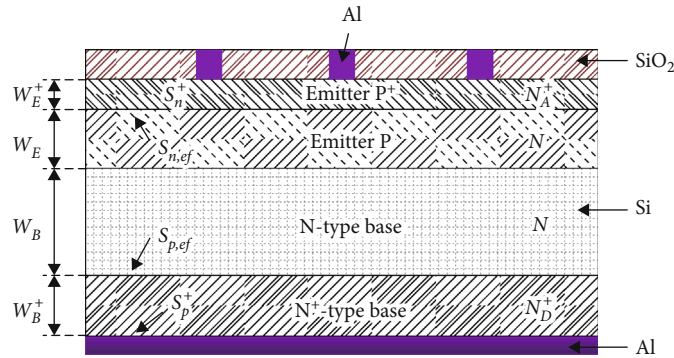


FIGURE 1: The structure of the analysed photovoltaic cell.

The efficiency record is 24-27% and is owned by a monocrystalline silicon solar cell using very complex technology [5, 6].

Cells currently commercially produced have an efficiency of between 14% and 16%. In particular cases, cells that stretch on larger surfaces have an efficiency of between 17% and 19% [7, 8].

In general, the efficiency of photovoltaic energy conversion is very limited of physical causes [9]. Approximately 24% of the solar radiation has a wavelength so large that it cannot be absorbed. In addition, 33% is lost as heat. The following 15-20% losses occur because the cell voltage reaches only 70% of the value corresponding to the energy range [10].

From the recent literatures, it was found that there are no studies on parasitic resistance and characteristics of PV cells made of monocrystalline silicon P^+PNN^+ .

This study aims to determine the technological characteristics of PV cell monocrystalline silicon P^+PNN^+ . The present work has five sections. Section 1 covers a review of the literature. Section 2 is based on the experimental setup and methodology of the studied PV cell. Determination and analysis of technological parameters of the studied PV cell are discussed in Section 3. Afterwards, the experimental results are interpreted in Section 4 and compared to theoretical ones. Section 4 provides concluding remarks.

2. Experimental Setup and Methodology

Monocrystalline silicon solar photovoltaic cells are the most stable from the family of photovoltaic cells made of silicon [10–15].

The processing of monocrystalline silicon for obtaining semiconductor devices for solar photovoltaic cells is a complex manufacturing process [16–18]. The studied cells are manufactured at ICPE-Bucharest, and they are type P^+PNN^+ solar photovoltaic cells (see Figures 1 and 2). There were type p silicon wafers used for its manufacturing. The production flow chart contains a couple of basic stages, each of it containing a few specific operations with longer or shorter processing times for semiconductor structures, such as photolithography and multiple high-temperature chemical processes. The attributes of semiconductor silicon devices are strongly influenced by temperature [19].

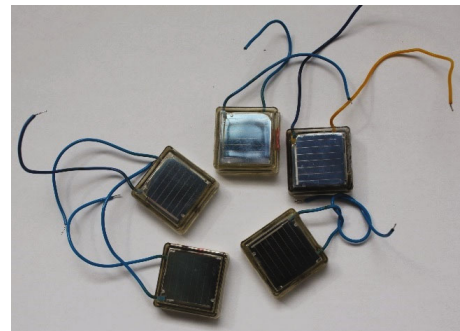


FIGURE 2: Photovoltaic cell type P^+PNN^+ .

Semiconductor junctions lay at the foundation of manufacturing and functioning of the majority of semiconductor device categories. Related to conversion efficiency and power output, it is considered that the best results are obtained for the photovoltaic solar cells with p-n junctions [20]. Hence, if two semiconductor materials such as type p and type n are put in contact, they create the p-n junction of the material. Practically, this represents the separation area between the two regions [21], the type p semiconductor being doped with acceptor atoms (for instance, boron) and the type n semiconductor being doped with donor atoms (for instance, phosphorus). Pursuant to the diffusion of majority carriers in the junction area, there appears an area of positive spatial charge in layer n and an area of negative charge in layer p. In this situation, the electric field oriented from layer n to layer p appears [20, 22–24].

Crystallographic measurements of the photovoltaic solar cell were made by means of Auriga FESEM-FIB Workstation equipment. In Figure 3, the SEM analysis in a longitudinal section on a metallic face at a resolution of $100 \mu\text{m}$ is presented.

X-ray diffraction is an analytic technique which offers structural and chemical information about the crystallography of a range of various materials [25], such as the crystallographic structure of the material, structural analysis of the material, surface analysis of the material, analysis of thin layers, and transformation due to the influence of temperature (see Figures 4 and 5) [25–27]. Graphics data processing was made by the representation of data acquired using a D8 DISCOVER diffractometer, Bruker AXS GmbH.

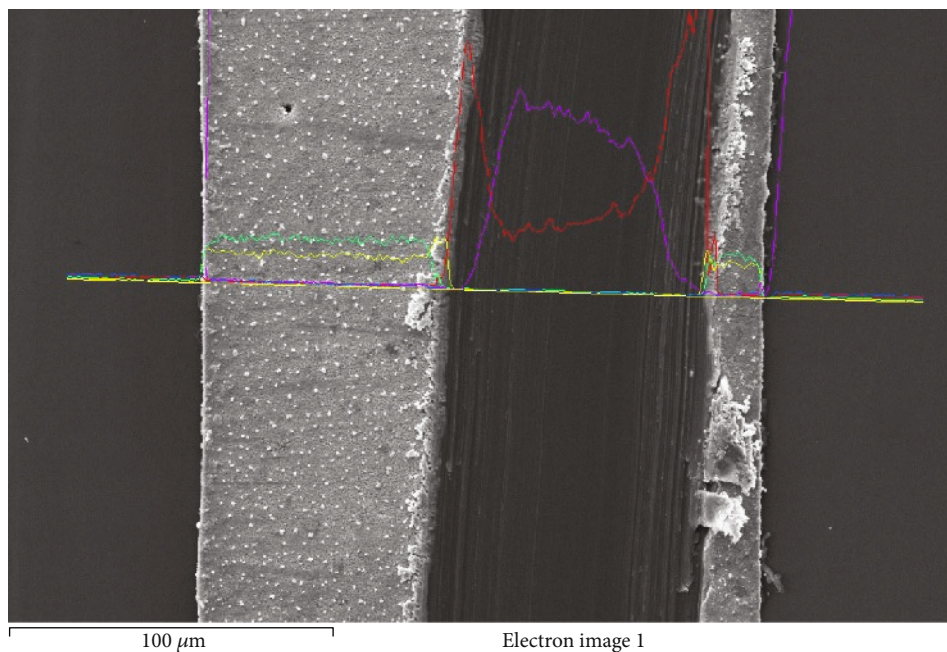


FIGURE 3: SEM analysis in a longitudinal section at a resolution of 100 μm .

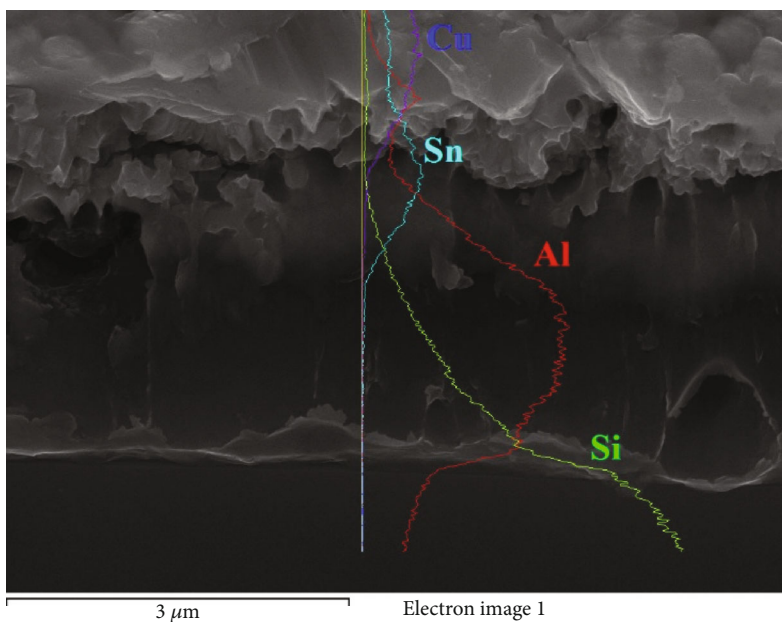


FIGURE 4: SEM and EDX for the upper part of the metal-faced layer of a photovoltaic solar cell.

Silicon is one of the hardest materials to interpret by X-ray diffraction. In order to be subjected to X-ray diffraction, the analysed cell was treated with hydrofluoric acid for 1-3 minutes, because above it is the SiO_2 layer, after which it was ultrasonicated in ionized water and finally dried with a flow of Azote. We identified with Si and the presence of silicon oxide. On one side of the platelet, the silicon oxide was intentionally created. On the other hand, the amount of oxide is small and is due to an accumulation of oxide time on the surface of the single crystalline platelets. From the X-ray diffraction spectra for the solar cell, we observed a

shift of the peaks corresponding to the monocrystalline silicon. I noticed not only the additional peaks corresponding to the dopants but also the peaks corresponding to the metal impurities from the metal contacts.

2.1. Data Acquisition of Technological Parameters. The determination of functional parameters of photovoltaic solar cells is essential for the subsequent usage of these semiconductor devices. This is of major interest to manufacturers of such devices, because the parameter's improvement has as an effect on the growth of

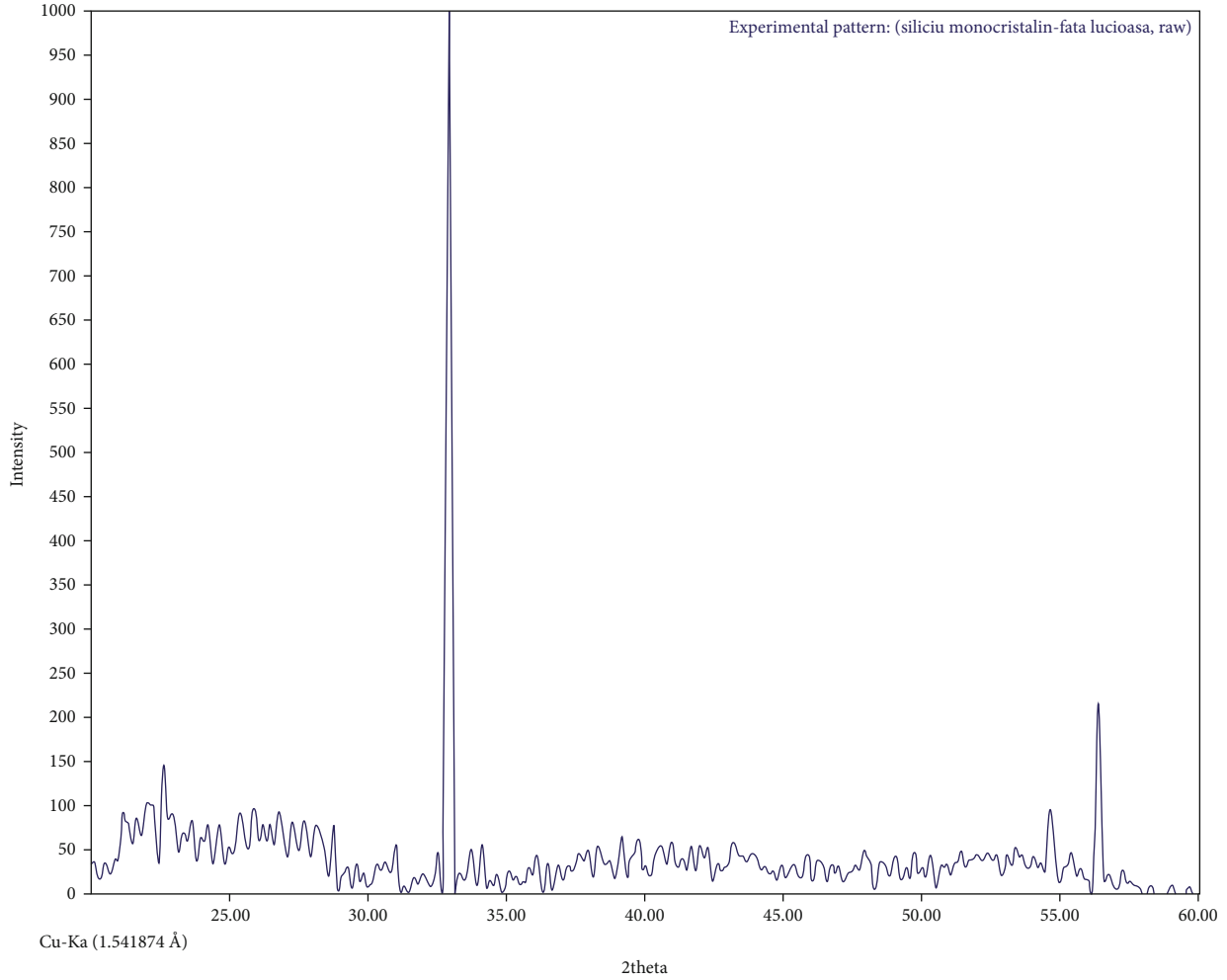


FIGURE 5: Diffractometry spectrum realised using X-ray on smooth-faced of monocrystalline silicon solar cell.

photovoltaic cells' efficiency [13–21]. Measurements made on the photovoltaic solar cell were realised in laboratory conditions on the NI-ELVIS platform produced by National Instruments (see Figure 6) [26, 27].

I - V characteristics were determined by monitoring the current getting through the photovoltaic solar cell at various temperatures and illumination levels. The values obtained for short-short-circuit current I_{sc} and open circuit voltage V_{oc} were determined using NI-Elvis board and LabView software (see Figure 7).

2.2. Interpretation of I - V Characteristics of the Studied Photovoltaic Solar Cell. The I - V characteristics of the measured solar cell were represented and after that fitted using the theoretical model with two exponentials, according to the following relation [28, 29]:

$$I = I_{01} \cdot \exp\left(\frac{V - R_s \cdot I}{(kT/q) \cdot n_1}\right) + I_{02} \cdot \exp\left(\frac{V - R_s \cdot I}{(kT/q) \cdot n_2}\right) + \frac{V}{R_p}, \quad (1)$$

where I is the solar cell current, I_{01} is the saturation current of

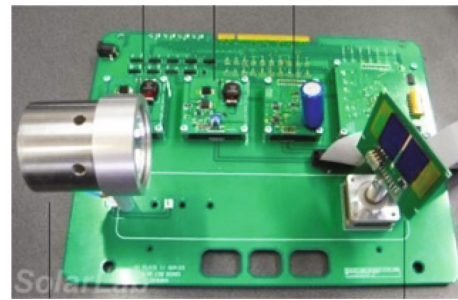


FIGURE 6: NI-ELVIS platform.

the diffusion component, I_{02} is the saturation current of the recombination component, R_s is the parasitic series resistance, R_p is the parasitic parallel (shunt) resistance, n_1 is the ideal factor of the diffusion current, and n_2 is the ideal factor of the recombination current.

The current in equation (1) contains two components:

- (i) A diffusion component representing the contribution of optic-generated carriers which move by diffusion

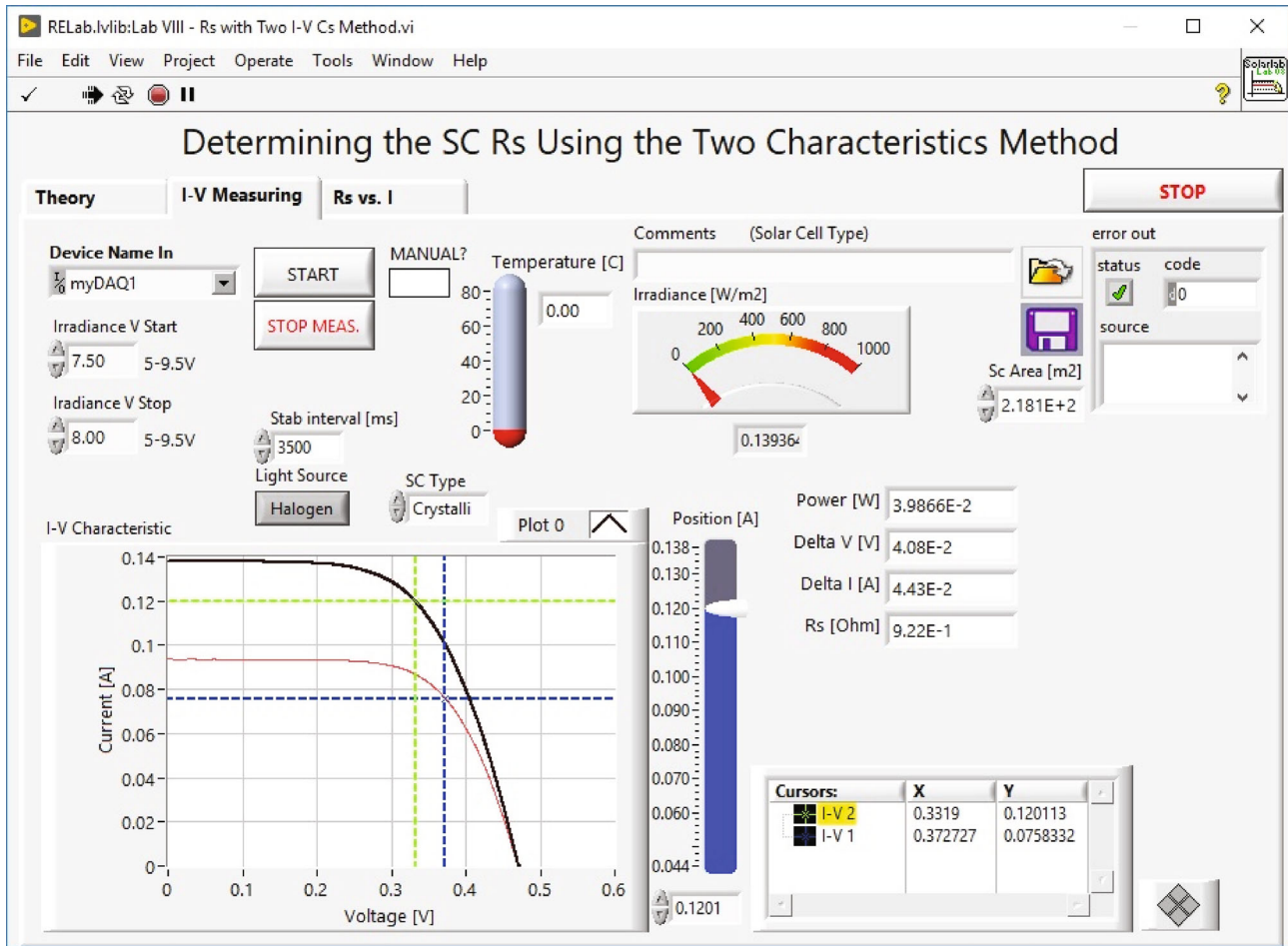


FIGURE 7: I_{sc} and V_{oc} study of the solar cell, as a function of temperature using the NI-ELVIS acquisition boards and LabView software.

in neutral regions of the p-n junction. For this component, it was considered that the ideal parameter n is the theoretical one, namely $n_1 = 1$

- (ii) The second exponential component of the solar cell's current is given by the recombination of carriers in the transition region of the p-n junction. It was considered that the recombination process is mainly controlled by the Shockley-Read-Hall recombination from the respective region, being produced by the existence of the contamination of metallic impurities in that area [30, 31]. Because the most profound metallic impurities, namely the ones that have the energetic level close to the forbidden bandwidth of silicon, are the ones that determine the recombination velocities, they were used as an ideal parameter for this current component, $n_2 = 2$

The values of parasitic resistances were determined by means of an experiment, and they have the following values: $R_s = 0.750 \Omega$ and $R_p = 379 \Omega$.

From measurement analysis, using the equation with 2 currents, considering $n_1 = 1$, $n_2 = 2$, $R_s = 0.75 \Omega$, and $R_p = 379 \Omega$ and using Mathematica soft for the determination of the parameters by overlapping the curves (see

Figures 8 and 9), the following values have been obtained (Table 1):

2.3. Analysis of Recombination Saturation Current I_{02} . Recombination saturation current of a photovoltaic solar cell with the p-n junction is given by the following relation:

$$I_{02} = qw \frac{n_i}{2\tau} A \tag{2}$$

where q is the electron's charge, w is the thickness of the transition region emitter base in direct polarization, n_i is the intrinsic concentration of carriers within silicon, A is the junction area emitter base, and τ is the lifetime of minority carriers from the silicon wafer volume.

The component of current I_{02} depends on the temperature by the medium of the intrinsic concentration n_i . In the range of the measured temperature $T = 32 - 37^\circ\text{C}$, this variation is very weak and can be neglected. Abnormal values, derived from measuring errors or errors of overlapping of the curves, were deleted.

From Table 1, the medium value of recombination saturation current, characteristic of a photovoltaic solar cell, is

$$I_{02} \approx 2 \times 10^{-9} \text{ A.} \tag{3}$$

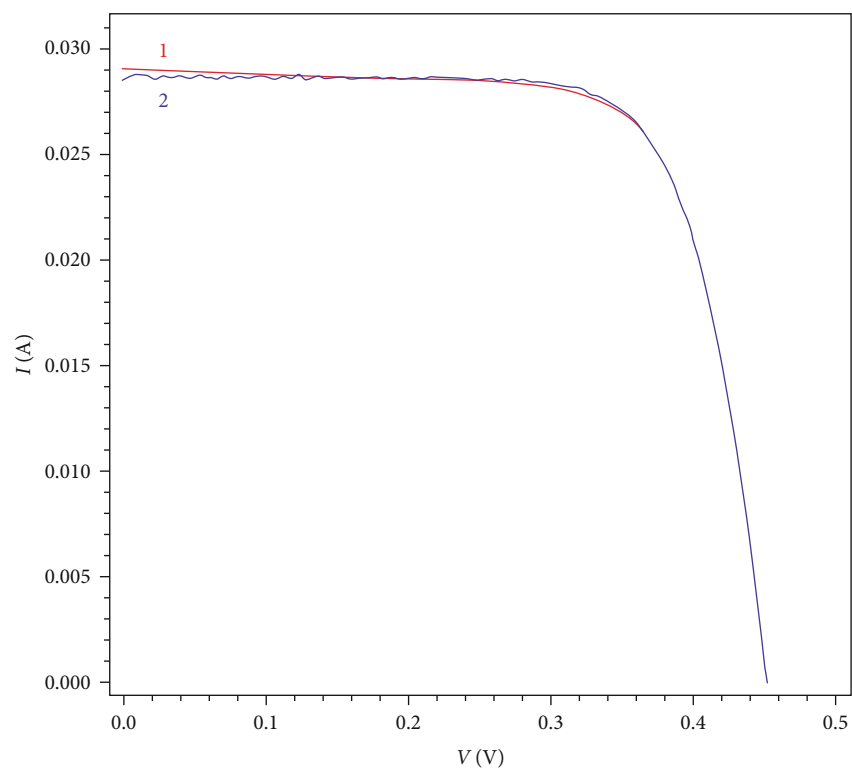


FIGURE 8: *I-V* diagram of solar cell 1 for $I_{ph} = 0.0291$ A (2) and overlapping of curves (1).

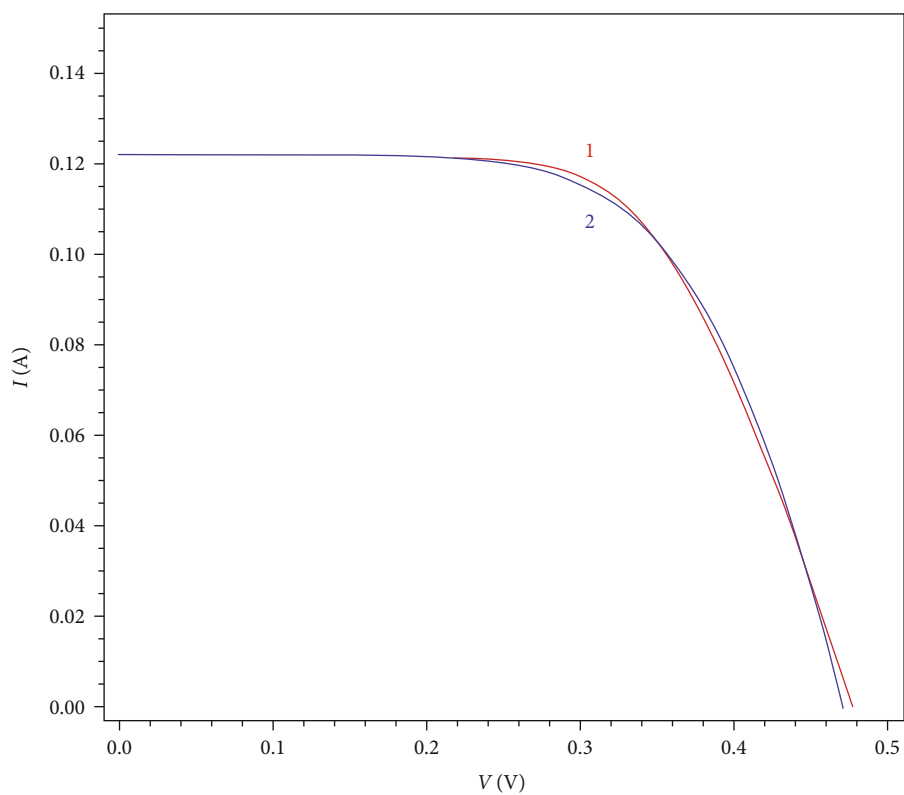


FIGURE 9: *I-V* diagram of solar cell 1 for $I_{ph} = 0.1225$ A (2) and overlapping of curves (1).

TABLE 1: Determination of the parameters of a photovoltaic solar cell.

I_{ph} (A)	I_{01} (A)	I_{02} (A)	T (°C)
0.0291	9.76×10^{-10}	4.37×10^{-9}	31.96
0.0357	1.38×10^{-9}	1.49×10^{-9}	32.50
0.0430	2.31×10^{-9}	2.05×10^{-9}	32.86
0.0512	2.1×10^{-9}	2.13×10^{-9}	33.17
0.0604	1.52×10^{-9}	1.58×10^{-9}	33.50
0.0705	1.71×10^{-9}	1.73×10^{-9}	33.85
0.0817	3.01×10^{-9}	3.09×10^{-9}	34.24
0.0941	1.62×10^{-9}	1.63×10^{-9}	34.64
0.1077	2.34×10^{-9}	2.35×10^{-9}	35.06
0.1225	1.98×10^{-9}	1.17×10^{-9}	35.54
0.1384	2.13×10^{-9}	1.61×10^{-9}	36.04

This value allows the estimation of a lifetime of the minority carriers within the single-crystal silicon wafers used for manufacturing of the photovoltaic solar cell.

From relation (2) we have

$$\tau_{\text{medium}} = \frac{qwn_i A}{2I_{02, \text{medium}}}. \quad (4)$$

The size of transition region w of the p-n junction is computed as follows [30, 31]:

$$w = \sqrt{\frac{2\epsilon}{q} \cdot \frac{N_A + N_D}{N_A \cdot N_D} \cdot (V_0 - V)}, \quad (5)$$

where V_0 is the internal voltage of the junction

$$V_0 = \frac{kT}{q} \cdot \ln \frac{N_A N_D}{n_i^2}, \quad (6)$$

and V is the direct voltage which drops on the solar cell in conditions of a maximum power output.

From the accomplished measurements are obtained,

$$V = 0.35 \text{ V}. \quad (7)$$

For the technological case,

$$\begin{aligned} N_D &= 10^{16} \text{ cm}^{-3}, \\ N_A &= 10^{17} \text{ cm}^{-3}, \end{aligned} \quad (8)$$

which obtains:

$$\begin{aligned} V_0 &= 26 \times 10^{-3} \text{ V} \times \ln \frac{10^{33} \text{ cm}^{-6}}{10^{20} \text{ cm}^{-6}} = 60 \times 13 \times 10^{-3} \text{ V} = 0.78 \text{ V}, \\ w &= \sqrt{\frac{2 \times 10^{-12} \text{ F/cm}}{1.6 \times 10^{-19} \text{ C}} \times \frac{1}{10^{16} \text{ cm}^{-3}}} \times 0.43 \text{ V} \\ &= 0.23 \times 10^{-4} \text{ cm} = 0.23 \text{ } \mu\text{m}. \end{aligned} \quad (9)$$

Finally, using relation (4), the lifetime results are

$$\begin{aligned} \tau_{\text{medium}} &= \frac{1.6 \times 10^{-19} \text{ C} \times 2.3 \times 10^{-5} \text{ cm} \times 10^{10} \text{ cm}^{-3} \times 4 \text{ cm}^2}{2 \times 2 \times 10^{-9} \text{ A}} \\ &= 3.7 \times 10^{-5} \text{ s} \cong 40 \text{ } \mu\text{s}. \end{aligned} \quad (10)$$

Because of the technological conditions of the manufacturing of photovoltaic solar cells, the following range of values is used:

$$\tau_{\text{SRH}} = 1 \div 100 \text{ } \mu\text{s}. \quad (11)$$

From the interpretation of the measurements for the I - V characteristics, a first important technological characteristic of photovoltaic solar cells is deduced, namely the value of a lifetime [17].

Hereafter, a qualitative analysis of diffusion saturation current in an ideal p-n junction were made.

For the ideal diode, I_{01} has the following form [20, 21]:

$$I_{01} = qA \left(\frac{D_p}{L_p} \cdot \frac{n_i^2}{N_D} + \frac{D_n}{L_n} \cdot \frac{n_i^2}{N_A} \right), \quad (12)$$

which becomes, in the case of abrupt junction P⁺N,

$$I_{01} = qA \cdot \frac{D_p}{L_p} \cdot \frac{n_i^2}{N_D}, \quad (13)$$

or

$$I_{01} = qA \cdot \sqrt{\frac{D_p}{\tau_p}} \cdot \frac{n_i^2}{N_D}, \quad (14)$$

where L_p and D_p are the length of diffusion and the diffusion coefficient of minority holes from base n doped with a concentration N_D of donor atoms.

By contrast with the recombination component I_{02} , the diffusion current I_{01} has a variation depending on the temperature which cannot be neglected anymore. It comes from the dependence of temperature of the following terms:

$$D = \frac{kT}{q} \cdot \mu \approx T^1, \quad (15)$$

TABLE 2: Values obtained for a photovoltaic solar cell measured in condition AM 1.5.

I_{sc} (A)	V_{oc} (V)	T (°C)	I_{01} (A)
0.122	0.48	35.5	2×10^{-9}

$$\tau = \frac{1}{c \cdot N_T} = \frac{1}{\sigma \cdot V \cdot N_T} \approx \frac{1}{V} \approx \frac{1}{T^{1/2}}, \quad (16)$$

$$n_i \approx T^{3/2} \cdot \exp\left(-\frac{E_G}{2kT}\right). \quad (17)$$

By solving equations (15), (16), and (17) then from (14), results

$$I_{01} \approx T^{1/2} \cdot T^{1/4} \cdot T^3 \cdot \exp\left(-\frac{E_G}{kT}\right), \quad (18)$$

where $qA \approx T^{1/2}$ and $(D_p/\tau_p) = T^{1/4}$. With a good approximation, the following can be written:

$$I_{01} \approx T^4 \cdot \exp\left(-\frac{E_G}{kT}\right). \quad (19)$$

From where

$$\frac{I_{01}(T_1)}{I_{02}(T_2)} = \left(\frac{T_1}{T_2}\right)^4 \cdot \exp\left[\frac{E_G}{k} \cdot \left(\frac{1}{T_2} - \frac{1}{T_1}\right)\right]. \quad (20)$$

The experimental values obtained for a light source that approach the condition AM 1.5 are presented in Table 2.

From this table, we have

$$I_{01} = 2 \times 10^{-9} \text{ A}, \quad (21)$$

$$\text{at } T = 309 \text{ K}.$$

Below formula (21), the value of the diffusion component at room temperature ($T = 300 \text{ K}$) was deduced. The following was obtained:

$$I_{01}(300 \text{ K}) = I_{01}(309 \text{ K}) \cdot \left(\frac{300}{309}\right)^4 \cdot \exp\left[\frac{1.1 \times 10^3}{26} \cdot \left(\frac{300}{309} - 1\right)\right]. \quad (22)$$

Then the numerical value is ((22)), we have

$$I_{01}(300 \text{ K}) = 5 \times 10^{-10} \text{ A}. \quad (23)$$

This value will represent the main checkout key of computer models.

3. Computing Programs for Correlation of Experimental Data with Theoretical Models Using Matlab Simulations

In order to compare the obtained experimental results, the theoretical model of direct current-voltage characteristic was used when $\tau_{\text{SRH}} = 5 \mu\text{s}$. To analyse in Matlab, we used the following material's features, constants, and calculus formulas, which are available for $T = 300 \text{ K}$ [17, 31]:

- (i) Intrinsic carrier concentration: $n_i = 10^{10} \text{ cm}^{-3}$
- (ii) Dielectric constant: $\epsilon = 10^{-12} \text{ F/cm}$
- (iii) Electron charge: $q = 1.6 \cdot 10^{-19} \text{ C}$
- (iv) Thermal potential and thermal energy: $T/q = 25.9 \text{ mV}$ and $kT/q = 25.9 \text{ mV}$
- (v) Coefficient of diffusion for load carriers:

$$D = \frac{D_0}{1 + (N/N_0)^d} D_1, \quad (24)$$

where electrons are $D_{0n} = 35 \text{ cm}^2/\text{s}$, $D_{1n} = 1.8 \text{ cm}^2/\text{s}$, $N_0 = 10^{17} \text{ cm}^{-3}$, $d = 0.6$ and the holes are $D_{0p} = 12.5 \text{ cm}^2/\text{s}$, $D_{1p} = 1 \text{ cm}^2/\text{s}$, $N_0 = 10^{17} \text{ cm}^{-3}$, and $d = 0.6$.

The following are the relationships between diffusion coefficient and electric mobility:

- (i) Einstein's relations are

$$D_n = \frac{kT}{q} \mu_n, \quad (25)$$

$$D_p = \frac{kT}{q} \mu_p.$$

- (ii) The Shockley-Read-Hall lifetime recombination is

$$\tau_{\text{SRH}} = \frac{\tau_0}{1 + (N/K)}, \quad K = 7 \times 10^{15} \text{ cm}^{-3} \quad (26)$$

- (iii) The lifetime of radiation recombination is

$$\tau_{\text{rad}} = \frac{1}{BN}, \quad B = 2 \times 10^{-14} \text{ cm}^3/\text{s} \quad (27)$$

- (iv) The Auger lifetime recombination is

$$\tau_{\text{Aug}} = \frac{1}{CN^2} \quad (28)$$

where silicon-n is $C_n = 10^{-31} \text{ cm}^6/\text{s}$ and silicon-p is $C_p = 2.8 \times 10^{-31} \text{ cm}^6/\text{s}$

(v) Total lifetime is

$$\frac{1}{\tau} = \frac{1}{\tau_{\text{SRH}}} + \frac{1}{\tau_{\text{rad}}} + \frac{1}{\tau_{\text{Aug}}} \quad (29)$$

(vi) The lengths of the diffusion of minority carriers are

$$\begin{aligned} \text{Electrons : } L_n &= (D_n \tau_n)^{1/2} \\ \text{Holes : } L_p &= (D_p \tau_p)^{1/2} \end{aligned} \quad (30)$$

(vii) The variation in bandwidth forbidden at high doping levels is

$$\Delta E_G = a \left[\left(\frac{N^*}{N} \right)^b + 1 \right]^{-c} \quad (31)$$

where $a = 0.231$ eV; $b = 3/4$; $c = 2/3$; and $N^* = 10^{20} \text{ cm}^{-3}$

(viii) The effective intrinsic concentration of carriers at high levels of doping is

$$n_{i,ef}^2 = n_i^2 \exp \frac{\Delta E_G}{kT} \quad (32)$$

(ix) The effective recombination speed at the P⁺P interface of the emitter is

$$s_{p,ef} = \frac{D_p^+ n_{i+}^2 N_D (s_p^+ L_p^+ / D_p^+) + th(w_B^+ / L_p^+)}{L_p^+ n_i^2 N_D^+ 1 + (s_p^+ L_p^+ / D_p^+) th(w_B^+ / L_p^+)} \quad (33)$$

(x) The density of saturation power at the P⁺P emitter is

$$J_{b0}^+ = \frac{q D_p n_i^2 (s_{p,ef} L_p / D_p) + th(w_B / L_p)}{L_p N_D 1 + (s_{p,ef} L_p / D_p) th(w_B / L_p)} \quad (34)$$

(xi) The effective recombination speed on the interface on the base N⁺N is

$$s_{n,ef} = \frac{D_n^+ n_{i+}^2 N_A (s_n^+ L_n^+ / D_n^+) + th(w_B^+ / L_n^+)}{L_n^+ n_i^2 N_A^+ 1 + (s_n^+ L_n^+ / D_n^+) th(w_B^+ / L_n^+)} \quad (35)$$

(xii) The density of saturation power on the base N⁺N is

$$J_{b0}^+ = \frac{q D_n n_i^2 (s_{n,ef} L_n / D_n) + th(w_B / L_n)}{L_n N_A 1 + (s_{n,ef} L_n / D_n) th(w_B / L_n)} \quad (36)$$

(xiii) Total saturation power is

$$\begin{aligned} I_0 &= J_{e0} A_E + J_{b0} A_{B,pas} + J_{b0}^+ A_{B,met} \\ A_{B,pas} + A_{B,met} &= A_{\text{cel}} \\ J_0 &= \frac{I_0}{A_{\text{cel}}} \end{aligned} \quad (37)$$

(xiv) The open circuit voltage is

$$V_{OC} = \frac{kT}{q} \cdot \ln \left(\frac{J_{SC}}{J_0} \right) \quad (38)$$

(xv) The efficient conversion of solar energy is

$$\eta = \frac{J_{SC} \cdot V_{OC} \cdot f}{P_{\text{solar } a}} \quad (39)$$

(xvi) The solar power in conditions AM 1.5 is

$$P_{\text{solar } a} = 100 \text{ mW/cm}^2 \quad (40)$$

(xvii) The average short-circuit current density value for an AM spectrum 1.5 is

$$J_{SC} = 35 \text{ mA/cm}^2 \quad (41)$$

3.1. The Effective Recombination Velocities from an Emitter's Interface P⁺/P Dependent on Recombination Velocities on the Region's P⁺ Surface of Emitter s_n^+ . From Figures 10–12, we observe that if at the emitter's surface, the recombination velocity is 10^5 cm/s for a doping concentration of the emitter of 10^{17} cm^{-3} , the recombination velocities decrease to a value of $s_{n,ef} = 10^3$ cm/s, $s_{n,ef} = 10^2$ cm/s, and $s_{n,ef} = 1$ cm/s, if an additional diffusion P⁺ is used with a concentration of 10^{17} cm^{-3} , 10^{18} cm^{-3} , and 10^{19} cm^{-3} , respectively. The minimal value for the effective recombination velocities on the interface P⁺/P of emitter $s_{n,ef}$ is obtained in the case of $N_A^+ = 10^{18} \text{ cm}^{-3}$, $w_E^+ = 0.5 \times 10^{-4} \text{ cm}$, and $\tau_{\text{SRH}} = 5 \mu\text{s}$ (see Figure 11), while using a doping concentration of the emitter of $N_A^+ = 10^{15} \text{ cm}^{-3}$, and its value becomes 0.2777 cm/s.

3.2. The Effective Recombination Velocities from Base's Interface N/N⁺ $s_{p,ef}$ Dependent on Base's Strongly Doped Concentration N_D^+ . A similar effect to the one of the effective recombination velocities from interface P⁺P is obtained at the contact surface of Al base where the recombination velocity is 10^6 cm/s (see Figures 13–14). If on the back of the wafer an additional layer of diffusion N⁺ is made with a thickness of $5 \mu\text{m}$ (see Figure 13) and a concentration of 10^{19} cm^{-3} , then the effective recombination velocities go down to the value of 10 cm/s for a base doped to 10^{15} cm^{-3} . The minimal value for the effective recombination value from base's interface N/N⁺ $s_{p,ef}$ is obtained in the case of $w_B^+ = 20$

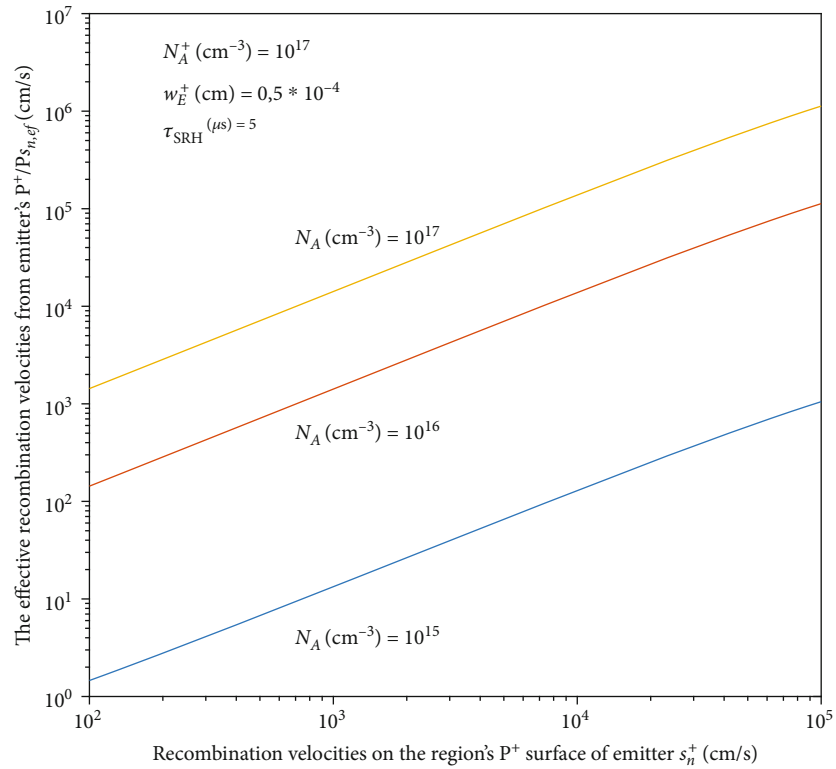


FIGURE 10: The effective recombination velocities from the emitter's interface P⁺/P $s_{n,ef}$ are dependent on recombination velocities on the region's P⁺ surface of emitter s_n^+ in the following conditions: $N_A^+ = 10^{17}$ cm⁻³, $w_E^+ = 0.5 \times 10^{-4}$ cm, and $\tau_{SRH} = 5$ μ s.

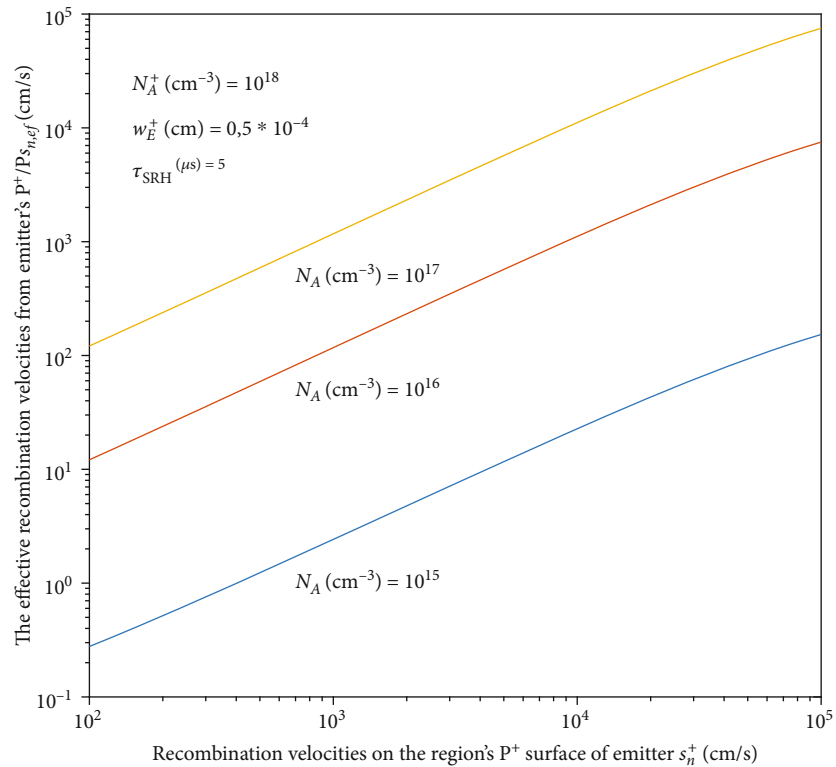


FIGURE 11: The effective recombination velocities from the emitter's interface P⁺/P $s_{n,ef}$ are dependent on recombination velocities on the region's P⁺ surface of emitter s_n^+ in the following conditions: $N_A^+ = 10^{18}$ cm⁻³, $w_E^+ = 0.5 \times 10^{-4}$ cm, and $\tau_{SRH} = 5$ μ s.

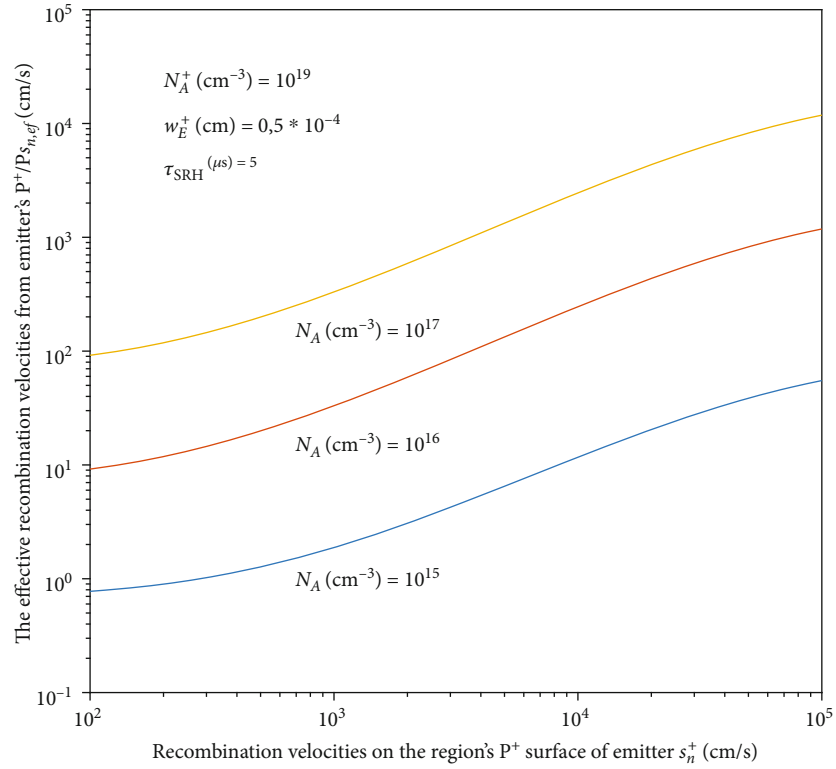


FIGURE 12: The effective recombination velocities from the emitter’s interface $P^+/P s_{n,ef}$ are dependent on recombination velocities on the region’s P^+ surface of emitter s_n^+ in the following conditions: $N_A^+ = 10^{19} \text{ cm}^{-3}$, $w_E^+ = 0.5 \times 10^{-4} \text{ cm}$, and $\tau_{SRH} = 5 \mu\text{s}$.

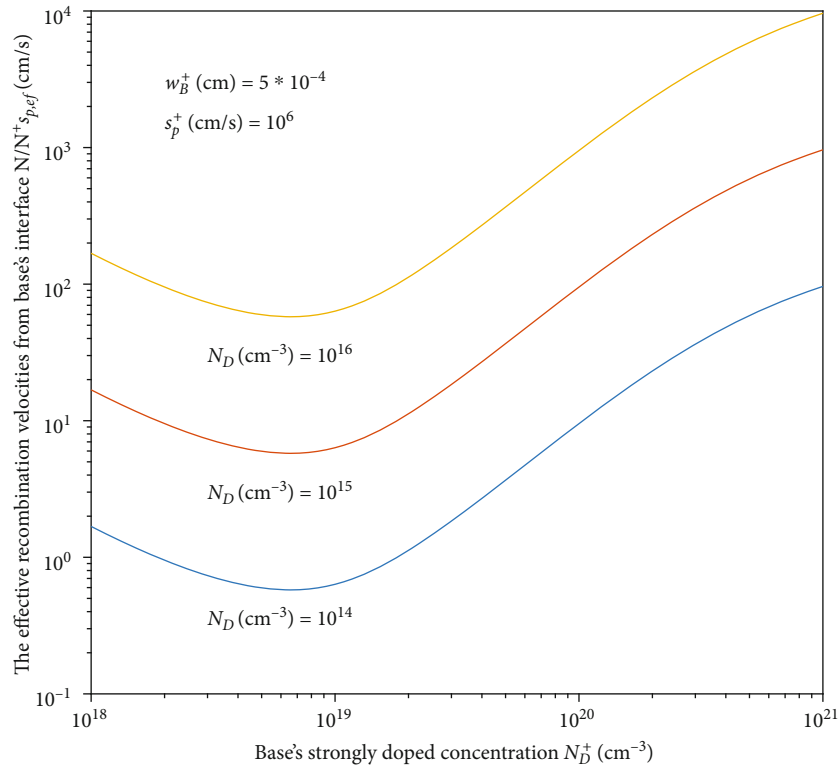


FIGURE 13: The effective recombination velocities from base’s interface $N/N^+ s_{p,ef}$ dependent on base’s strongly doped concentration N_D^+ in the case of $w_B^+ = 5 \times 10^{-4} \text{ cm}$ and $s_p^+ = 10^6 \text{ cm/s}$.

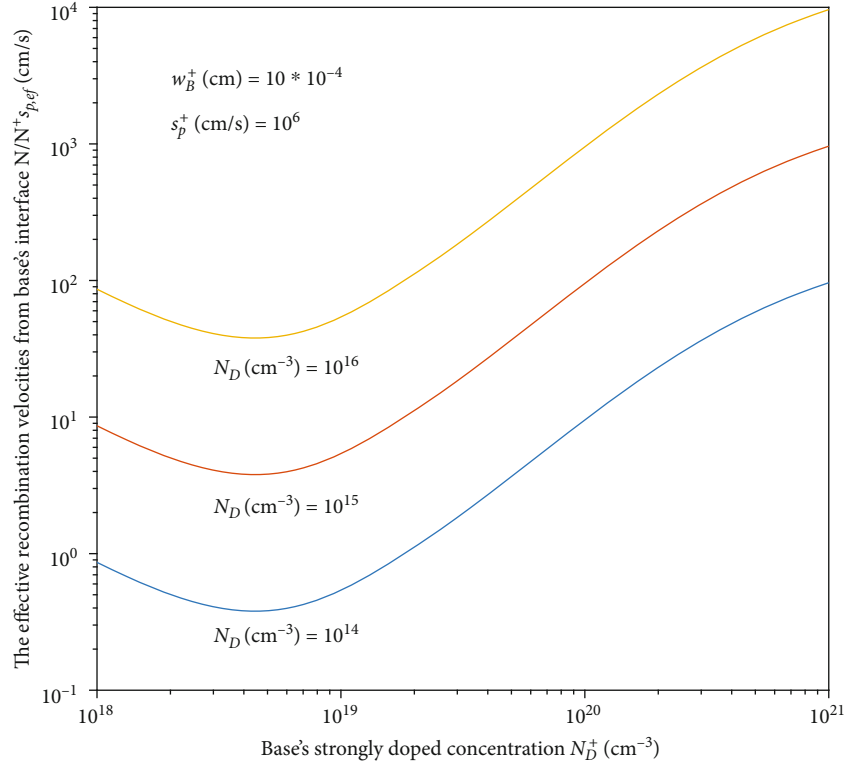


FIGURE 14: The effective recombination velocities from base's interface $N/N^+ s_{p,ef}$ dependent on base's strongly doped concentration N_D^+ in the case of $w_B^+ = 10 \times 10^{-4}$ cm and $s_p^+ = 10^6$ cm/s.

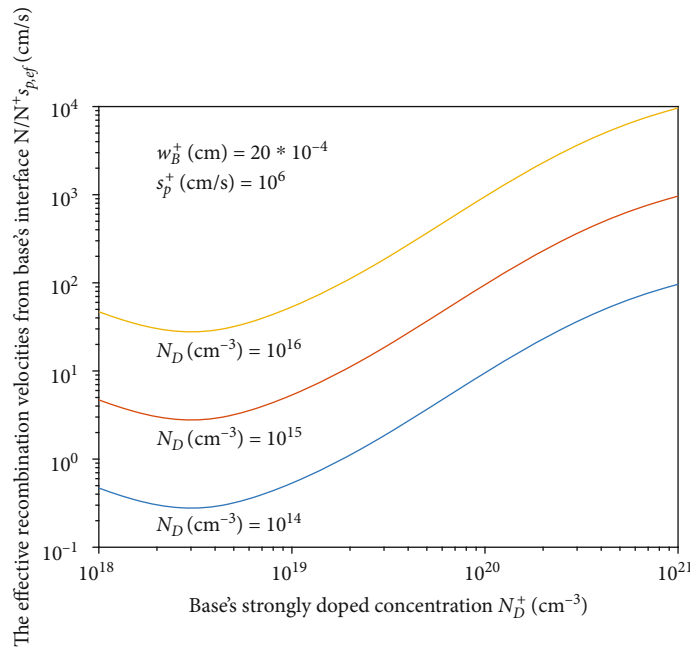


FIGURE 15: The effective recombination velocities from base's interface $N/N^+ s_{p,ef}$ dependent on base's strongly doped concentration N_D^+ in the case of $w_B^+ = 20 \times 10^{-4}$ cm and $s_p^+ = 10^6$ cm/s.

$\times 10^{-4}$ cm and $s_p^+ = 10^6$ cm/s (see Figure 15), using a doping concentration of $N_D = 10^{14}$ cm^{-3} , this value being of 0.5 cm/s.

The obtained values are available because they accomplish the following technological conditions:

- (i) The average value of phosphorus base doping: $N_D = 1.5 \cdot 10^{14}$ cm^{-3}
- (ii) The average value of emitter layer diffusion: $N_A = 10^{17}$ cm^{-3}

(iii) The depth of junction p-n emitter-base: $w_E = 5 \mu\text{m}$

4. Conclusions

In this study, current-voltage characteristics of a photovoltaic solar cell, measured in various conditions of illumination and temperature, are presented. Also, based on the analysis of these characteristics, the technological characteristics of the studied solar cell are determined.

A mathematical model of the physical processes which leads to the generation of electric currents in a complex photovoltaic solar cell type P⁺PNN⁺ with a finite recombination velocity on the surface is proposed.

Both recombination velocities of charge carriers on the surface and regions N⁺N and P⁺P are essential in photovoltaic solar cell type P⁺PNN⁺ functioning. In a photovoltaic solar cell with a p-n junction, the saturation current is given by the recombination on the two faces of the wafer.

The analysed case was accomplished for $\tau_{\text{SRH}} = 5 \mu\text{s}$ for the purpose of the correlation of the experimental data with theoretical models using Matlab.

The initial wafers of silicon are not competitive, but the application of the diffusion process of metallic contamination impurities by doping a phosphorus layer on the back of wafers led to a significant improvement of the lifetime in their volume.

Data Availability

The data used to support the findings of this study are available from the corresponding author upon request.

Conflicts of Interest

The authors declare that they have no conflicts of interest.

Acknowledgments

The authors would like to thank Dan Sachelarie for his helpful discussion and ICPE Bucharest for measurements of SEM and X-ray diffraction.

References

- [1] R. P. Smith, A. A.-C. Hwang, T. Beetz, and E. Helgren, "Introduction to semiconductor processing: fabrication and characterization of p-n junction silicon solar cells," *American Journal of Physics*, vol. 86, no. 10, pp. 740–746, 2018.
- [2] A. E. Becquerel, "Recherches sur les effets de la radiation chimique de la lumière solaire au moyen des courants électriques," *Comptes rendus de l'Académie des Sciences*, vol. 9, pp. 145–149, 1839.
- [3] W. G. Adams and R. E. Day, "V. The action of light on selenium," *Proceedings of the Royal Society of London*, vol. 25, no. 171–178, pp. 113–117, 1877.
- [4] C. Yu, S. Xu, J. Yao, and S. Han, "Recent advances in and new perspectives on crystalline silicon solar cells with carrier-selective passivation contacts," *Crystals*, vol. 8, no. 11, p. 430, 2018.
- [5] K. Yamamoto, K. Yoshikawa, H. Uzu, and D. Adachi, "High-efficiency heterojunction crystalline Si solar cells," *Japanese Journal of Applied Physics*, vol. 57, no. 8S3, article 08RB20, 2018.
- [6] J. Haschke, O. Dupré, M. Boccard, and C. Ballif, "Silicon heterojunction solar cells: Recent technological development and practical aspects - from lab to industry," *Solar Energy Materials and Solar Cells*, vol. 187, pp. 140–153, 2018.
- [7] W.-J. Ho, J.-J. Liu, Y.-C. Yang, and C.-H. Ho, "Enhancing output power of textured silicon solar cells by embedding indium plasmonic nanoparticles in layers within antireflective coating," *Nanomaterials*, vol. 8, no. 12, p. 1003, 2018.
- [8] M. Müller, G. Fischer, B. Bitnar et al., "Loss analysis of 22% efficient industrial PERC solar cells," *Energy Procedia*, vol. 124, pp. 131–137, 2017.
- [9] C.-L. Cheng, C.-C. Liu, and C.-T. Yeh, "Photovoltaic and physical characteristics of screen-printed monocrystalline silicon solar cells with laser doping and electroplated copper," *International Journal of Photoenergy*, vol. 2019, Article ID 5372904, 9 pages, 2019.
- [10] S. Chander, A. Purohit, A. Sharma, Arvind, S. P. Nehra, and M. S. Dhaka, "A study on photovoltaic parameters of monocrystalline silicon solar cell with cell temperature," *Energy Reports*, vol. 1, pp. 104–109, 2015.
- [11] E. Cuce, P. M. Cuce, and T. Bali, "An experimental analysis of illumination intensity and temperature dependency of photovoltaic cell parameters," *Applied Energy*, vol. 111, pp. 374–382, 2013.
- [12] A. K. Biswas, S. Biswas, and A. Sinha, "The photocurrent and spectral response of proposed P⁺PNN⁺ silicon solar cells," *International Journal of Renewable Energy Research*, vol. 8, no. 1, pp. 82–89, 2018.
- [13] H. Sun, J. Wei, Y. Jia, X. Cui, K. Wang, and D. Wu, "Flexible carbon nanotube/mono-crystalline Si thin-film solar cells," *Nanoscale Research Letters*, vol. 9, no. 1, p. 514, 2014.
- [14] T. Saga, "Advances in crystalline silicon solar cell technology for industrial mass production," *NPG Asia Materials*, vol. 2, no. 3, pp. 96–102, 2010.
- [15] A. M. Bagher, M. M. A. Vahid, and M. Mohsen, "Types of solar cells and application," *American Journal of Optics and Photonics*, vol. 3, no. 5, p. 94, 2015.
- [16] A. Goodrich, P. Hacke, Q. Wang et al., "A wafer-based monocrystalline silicon photovoltaics road map: utilizing known technology improvement opportunities for further reductions in manufacturing costs," *Solar Energy Materials and Solar Cells*, vol. 114, pp. 110–135, 2013.
- [17] C. P. Fluieraru, *Studies and research on the using monocrystalline silicon solar cells manufacturing*, [Ph.D. thesis], Valahia Univeristy Press, Târgoviște, Romania, 2013.
- [18] A. M. Green, *Third Generation Photovoltaics, Advanced Solar Energy Conversion*, Springer, 2003.
- [19] H. Andrei, T. Ivanovici, G. Predușcă, E. Diaconu, and P. C. Andrei, "Curve fitting method for modeling and analysis of photovoltaic cells characteristics," in *Proceedings of 2012 IEEE International Conference on Automation, Quality and Testing, Robotics*, pp. 307–312, Cluj-Napoca, Romania, 2012.
- [20] N. Jenny, *The Physics of Solar Cells*, Imperial College Press, 2003.
- [21] W. Shockley and H. J. Queisser, "Detailed Balance Limit of Efficiency of p-n Junction Solar Cells," *Journal of Applied Physics*, vol. 32, no. 3, pp. 510–519, 1961.

- [22] A. S. Brown and M. A. Green, "Limiting efficiency for current-constrained two-terminal tandem cell stacks," *Progress in Photovoltaics: Research and Applications*, vol. 10, no. 5, pp. 299–307, 2002.
- [23] E. V. Stoian, C. P. Fluieraru, and M. C. Enescu, "Determining electromagnetic attenuation for material composites polymer," *Scientific Bulletin of the Electrical Engineering Faculty*, vol. 12, no. 3, pp. 49–53, 2012.
- [24] C. Z. Rizescu, E. V. Stoian, D. N. Ungureanu, Z. Bacinshi, and F. C. Petre, "Study on powdered samples and particle size determinations by scanning electronic microscopy (SEM), diffraction of X-rays," *International Journal of Mechanics*, vol. 5, no. 3, pp. 138–147, 2011.
- [25] D. K. Schroder, *Semiconductor Material and Device Characterization*, John Willey & Sons Inc., 3rd edition, 2006.
- [26] P. A. Cotfas and D. T. Cotfas, "Design and implementation of RELab system to study the solar and wind energy," *Measurement*, vol. 93, pp. 94–101, 2016.
- [27] D. T. Cotfas, P. A. Cotfas, and O. M. Machidon, "Study of temperature coefficients for parameters of photovoltaic cells," *International Journal of Photoenergy*, vol. 2018, Article ID 5945602, 12 pages, 2018.
- [28] D. Sachelarie, *Semiconductoare si Heterostructuri*, Matrix Rom, 2000.
- [29] D. Sachelarie, *Bazele Dispozitivelor Semiconductoare*, Matrix Rom, 2003.
- [30] D. Sachelarie, G. Preduşcă, and H. G. Coandă, *Probleme Fundamentale de Microelectronică*, MatrixRom, Bucureşti, Romania, 2004.
- [31] G. Preduşcă and D. Sachelarie, *Matlab Pentru Microelectronică*, MatrixRom, Bucureşti, Romania, 2011.

Research Article

Experimental Study of Thermal Effect of Lacquer Coating for PV-Trombe Wall System Combined with Phase Change Material in Summer

Chenglong Luo ¹, Wu Zou,¹ Dan Sun,¹ Lijie Xu ², Jie Ji ² and Mengyin Liao¹

¹Institute of Energy Research, Jiangxi Academy of Sciences, Nanchang 330096, China

²Department of Thermal Science and Energy Engineering, University of Science and Technology of China, Hefei 230027, China

Correspondence should be addressed to Chenglong Luo; xxlong@ustc.edu

Received 4 April 2019; Revised 22 August 2019; Accepted 19 September 2019; Published 30 October 2019

Guest Editor: Alireza Rezaniakolaei

Copyright © 2019 Chenglong Luo et al. This is an open access article distributed under the Creative Commons Attribution License, which permits unrestricted use, distribution, and reproduction in any medium, provided the original work is properly cited.

This paper proposes a novel PV-Trombe wall system combined with phase-change material, which is named as PV-PCM-Trombe system. The work mainly experimentally studies the effectiveness and characteristics of using phase change materials to improve the overheating problem of PV-Trombe wall in summer. Through experiments, the photoelectric performance of the system using phase-change board surfaces with and without a matte black paint lacquer are compared; moreover, the influence on thermal environment of building is evaluated. The results indicate the PV-PCM-Trombe wall system shows an effective cooling effect on PV cell in both experiments and that the surface lacquer coating treatment of PCM plates affects little the photoelectric performance of the system and can reduce the working temperature of PV cell.

1. Introduction

Building-integrated photovoltaic/thermal technology (BIPV/T) is an important technology for using solar energy that generates solar energy photovoltaic power while improving the thermal environment of buildings to efficiently use solar energy. This can be considered as a significant contribution to the implementation of sustainable development of the energy.

Recently, focusing on BIPV/T technology, many numerical and experimental studies have been carried out from various perspectives. Yang and Jie [1] established a heat transfer model for photovoltaic-wall integrated (PV-WALL) structure and concluded that the heat gain of PV-WALL structures could be significantly reduced in summer. Jie et al. [2, 3] presented a novel Trombe wall with PV cells (PV-Trombe), which theoretically and experimentally studied the effect of the PV-Trombe system on indoor temperature and electrical efficiency and found that the aesthetic value was much more than that of normal Trombe wall. Hu et al. [4] compared and analyzed the annual thermal performance and electric performance of three types of BIPV system, and the result showed that a PV blind-integrated

Trombe wall system (BIPVBTW) is superior to the other two systems in the total electricity saving and CO₂ emissions reduction. Dupeyrat et al. [5] studied the electric performance and thermal performance of PV/T solar collectors with different laminates and the results indicated that PV/T solar collectors could provide advantages over separated solar thermal and PV technologies in configuration of limited available space for solar collector area. Herrando et al. [6] established a system performance evaluation model and mainly analyzed the effects of cover ratio of cells and coolant flow rate on system performance. Koyunbaba and Yilmaz [7] researched energy performance comparison of single glass, double glass, and a-Si semitransparent PV module integrated on the Trombe wall facade of a model test room. The change in electrical efficiency by surface temperature of the PV module had been interpreted and the electrical power rate of the PV module had been designated. Zogou and Stapountzis [8] studied the flow and heat transfer of a BIPV/air wall system for building application. In this work, the results from flow visualization and hot wire anemometry measurements performed on the basic structural module of a double-skin photovoltaic (PV/T) facade were discussed. Jiang et al. [9]

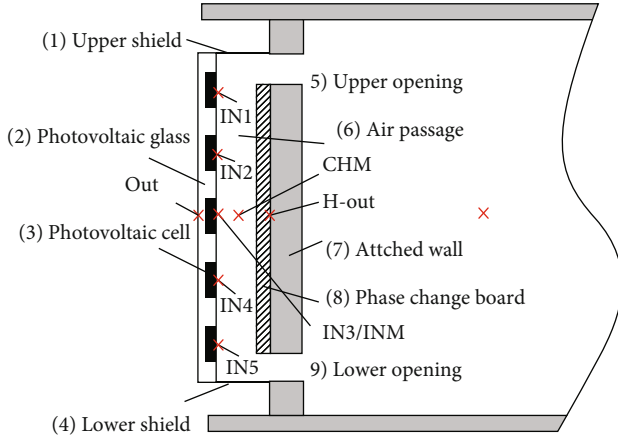


FIGURE 1: Schematic of structural principle of PV-PCM-Trombe wall system and the arrangement diagram of thermocouples.

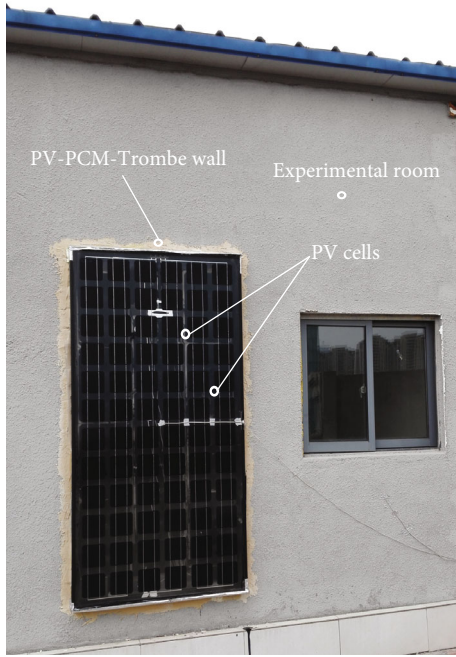


FIGURE 2: The test PV-PCM-Trombe wall system.

TABLE 1: Dimensions of the experimental setup.

Experimental setup	Length (m)	Height (m)	Width/thickness (m)
Hot box room	3.0	2.6	3.0
Door	0.6	1.6	—
Window	1.0	1.0	—
Upper/lower opening	0.3	0.2	—
Upper/lower shield	1.0	—	0.15
Photovoltaic glass board	1.0	2.0	0.004
Phase change board	0.3	0.5	0.02
Air passage	—	—	0.15
South wall	—	—	0.24

TABLE 2: Main properties of PCM.

Properties	Unit	Number
Melting point	$^{\circ}\text{C}$	29-31 (standard 29)
Solid point	$^{\circ}\text{C}$	26-28 (standard 26)
Latent heat (18-33 $^{\circ}\text{C}$)	kJ/kg	160
Solid density(20 $^{\circ}\text{C}$)	kg/L	1.43
Liquid density (40 $^{\circ}\text{C}$)	kg/L	1.23
Volume expansion rate	%	13.98
Thermal conductivity	W/(m·K)	0.6
Viscosity (50 $^{\circ}\text{C}$)	m^2/s	16.88

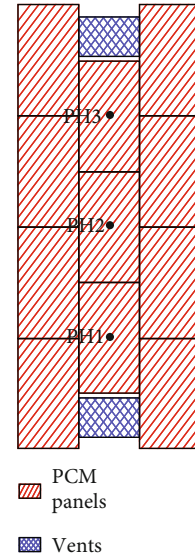


FIGURE 3: Distribution of phase change board and the thermocouples.

TABLE 3: Uncertainty of sensors at test conditions.

Copper-constantan thermocouples: temperature	$\pm 0.5^{\circ}\text{C}$
Pyranometer	Secondary standard (global irradiance on the south wall surface)
Output voltage: V_{oc}	1% of $V_{oc} \pm 0.1\text{ V}$
Output current: I_{sc}	1% of $I_{sc} \pm 9\text{ mA}$

presented a novel photovoltaic-Trombe wall (PV-TW). The electrical and thermal performance of the PV-TW are investigated experimentally and theoretically. Ahmed et al. [10] attempted to enhance the performance of a hybrid photovoltaic/Trombe wall (PV/TW) system through employing a porous medium. The results revealed that incorporating the porous medium and DC fan offered favorable features of the system performance, while the glass cover has a conflicting effect.

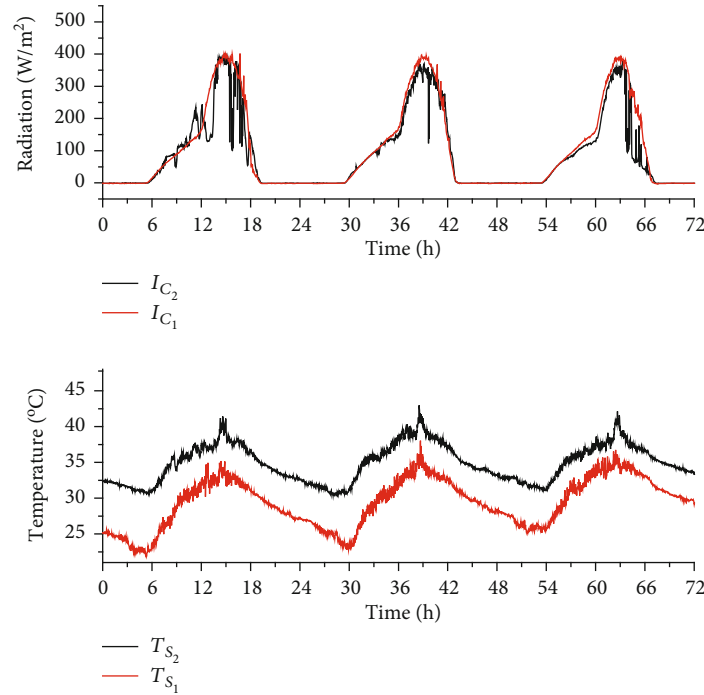


FIGURE 4: Solar irradiation intensity and ambient temperature.

Combining PCM (phase change material) and PV (photovoltaic) technologies to cool PV board or store heat by PCM has attracted scholars' attention. Huang [11–13] applied PCM to PV board and carried out many studies on the effect of PCM on the thermal regulation performance of BIPV systems. Lin et al. [14] floored all the internal walls of a room with PCM to study the influence of PV/T solar collector and PCM on indoor thermal environment. Through experiments and transient energy balance approach, Hachem et al. [15] and Kibria et al. [16] studied the effect of PCM on the performance of PV board and concluded that PCM could decrease the temperature of PV board and increase the electrical efficiency. Curpek and Hraska [17] compared and studied the PV board with and without PCM as well as the flow passage with and without ventilation, the results showed that natural ventilation of PV façade with added PCM could reduce the temperature of PV board better. Aelenei et al. [18, 19] developed a simplified thermal network model for BIPV-PCM and studied the thermal behavior of the system. Ma et al. [20] conducted a detailed review of the literature focusing on the use of PCM for PV module thermal regulation and electrical efficiency improvement and found that the PV-ST-PCM system, i.e., PV-PCM integrated with a solar thermal (ST) system, had an obvious scope for practical applications but met challenges.

Focusing on the inclination of solar heating wall of regular PV-Trombe wall system being overheated in summer working conditions, based on the feature that the temperature cannot rise during phase-change heating process of PCM, the present work proposes a novel PV-Trombe wall system combined with PCM, i.e., the PV-PCM-Trombe. The proposed system uses the thermal feature of PCM by combining the PCM and conventional PV-Trombe wall

TABLE 4: Test results of ambient temperature and solar irradiation intensity.

Date	Max. T_s (°C)	Mean T_s (°C)	Max. I_c (W/m ²)	Mean I_c (W/m ²)
2017.05.27	33.3	28.3	392.8	178.8
2017.05.28	34.8	29.3	388.5	181.2
2017.05.29	34.9	30.5	388.2	175.5
2017.07.14	39.7	34.5	379.5	155.2
2017.07.15	40.6	35.1	345.0	163.5
2017.07.16	40.3	35.0	364.5	126.6

system to reduce the temperature of solar heating wall in summer working conditions to avoid overheating issue of the wall resulted by solar radiation. This work mainly studies the effectiveness and characteristics of using phase change materials to improve the overheating problem of PV-Trombe wall in summer. Under summer working conditions, experimental investigations are carried out on a test system including the comparison of photoelectric performance of the novel system with and without matte black paint lacquer coating on phase-change board, and the analysis of their effects on thermal environment of the building.

2. Principle of PV-PCM-Trombe Wall System and the Experiment

The PV-PCM-Trombe wall system is composed of photovoltaic glass units, upper and lower openings, upper and lower shields, phase-change heat-storage wall, air passage, and a frame (Figure 1). The system is installed on the south

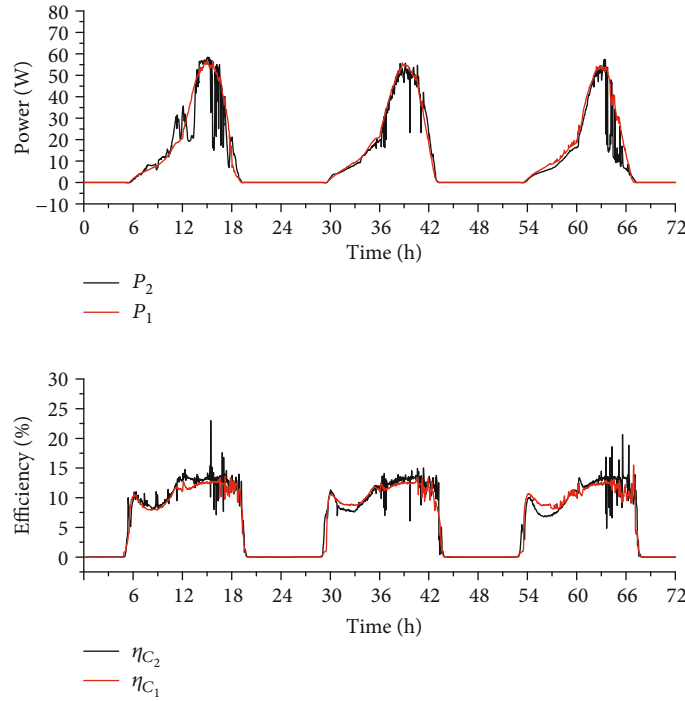


FIGURE 5: Electric power and efficiency of photovoltaic cells.

elevation (Figure 2), where the PCM board is attached to the external side of the south wall of building to form the PCM wall; the photovoltaic glass units cover the PCM wall and a certain gap is kept to form an air passage. By upper and lower openings and upper and lower shields, the system achieves passive heating in room in winter and heat dissipation to outdoor ambient to cool the room down in summer. Therefore, photoelectric conversion efficiency increases and indoor thermal environment improves. The design purpose of phase-change heat-storage wall is to use the characteristics of great phase-change energy storage, no increase in temperature during phase change process and phase-change temperature selected near the human comfort temperature; reduce the temperature of the passage where photovoltaic cells work especially in high-temperature summer while ensuring sufficient hot air supply in winter to meet the demand of building heating corresponding to human comfort temperature requirement; and achieve the overall effects of the system that the photovoltaic cells are cooled better and the photoelectric efficiency is higher, and the indoor thermal environment better meets the requirement of human comfort.

The working principle of the system is as follows.

1. Photovoltaic Part: the DC current generated by photovoltaic glass is converted into AC current
2. Solar Thermal Part

In summer, the upper opening (5) and the lower opening (9) are closed while the upper shield (1) and the lower shield (4) are opened so that the air passage (6) and the outdoor air forms a loop; thermal siphoning causes the air flowing

TABLE 5: Photovoltaic performance.

Date	Max. P (W)	Mean P (W)	Daily power generation (kW·h)	Mean η_c (%)
2017.05.27	55.4	23.5	0.322	10.7
2017.05.28	54.6	23.7	0.325	10.8
2017.05.29	54.1	22.3	0.299	10.5
2017.07.14	56.2	21.4	0.306	11.0
2017.07.15	51.8	22.2	0.318	10.6
2017.07.16	53.1	16.6	0.239	10.2

upwards from bottom in the passage, bringing away the heat absorbed by the phase-change heat-storage wall (7, 8) and the photovoltaic glass (2), and thereby the photovoltaic cells can be cooled down to some extent and overheating of the room in summer can be prevented. In addition, when the air temperature in the passage rises to the phase transition temperature of PCM, the PCM undertakes phase change process; the temperature can hardly rise as the PCM absorbs a significant amount of heat in the phase change process, and thus the rise of air temperature in the passage is inhibited and meanwhile, the photovoltaic cells and the building walls can be cooled down to some extent.

In winter, the upper opening (5) and the lower opening (9) are opened while the upper shield (1) and the lower shield (4) are closed so that the air passage (6) and the indoor room form a loop, bringing the heat absorbed by the phase change heat-storage wall (7, 8) and photovoltaic glass (2) into the room.

To investigate the system, a test system is established on a comparable hot box test platform. The experimental setup

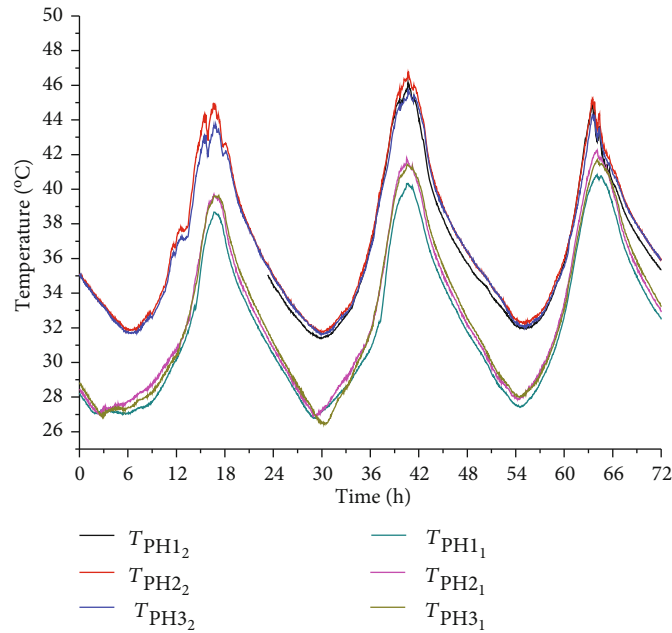


FIGURE 6: Temperature distribution of PCM plates.

TABLE 6: Characteristic data of mean temperature of external side temperature of phase change board 1, 2, and 3.

Temperature	Experiment 1			Experiment 2		
	Day 1	Day 2	Day 3	Day 1	Day 2	Day 3
Max. temperature (°C)	39.3	41.1	41.6	44.4	46.2	44.8
Mean temperature (°C)	31.3	32.6	33.5	36.4	37.1	36.6

consists of one hot box room, photovoltaic collector wall combined with PCM, openings, and a measurement system. Among them, the hot box room installed with photovoltaic collector wall combined with PCM is the experimental room. The south wall of both hot box rooms are brick structure, while other walls are lightweight insulating material. The dimensions of the experimental setup are shown in Table 1. The area of photovoltaic cells A_C is 1.125 m^2 , and the coverage ratio of photovoltaic cells on the photovoltaic glass board is 56.25%. The package material of PCM plate is aluminum, the surface is plated with a light color anticorrosion material, and the inner portion is crystalline hydrate and organic PCM; thus, the advantages of both PCMs, hydrate and organic matter, are met. The phase transition temperature of the PCM plates is 29°C ; its surface can be treated by matte black paint or kept as it is to perform comparable experimental analyses. The material properties of the PCM are listed in Table 2. The array configuration of the phase-change board is shown in Figure 3.

Measured parameters of the system include voltage, current, temperature, and solar irradiation intensity. Table 3 summarizes the ranges of parameters' accuracies. The temperature is measured using a conventional copper-constantan thermocouple (accuracy of $\pm 0.5^\circ\text{C}$). The main measuring points for temperature measurement are shown in Figures 1 and 3. Figure 1 represents a structural section

view of the system to show the locations of temperature measuring points marked by "x," i.e., external surface of photovoltaic glass board (1 point), back side of photovoltaic cells (5 points along height), air passage (1 point), external surface of the wall attached by phase change board (1 point), and indoor air temperature (1 point). Figure 3 presents the locations of the thermocouples distributed on the external surface of phase change heat storage board marked by "●." In addition, one thermocouple is placed on external surface of the south wall of experimental room. For the control room, there are two temperature measuring points which are indoor air temperature (1 point) and external surface of the south wall (1 point). The measurement system also includes the measurement of ambient temperature, output voltage and current of photovoltaic cells, and the total solar irradiation intensity on the south-faced vertical surface measured by a TBQ-2 pyranometer. DC voltage isolation sensor and AC-DC current isolation sensor are used, respectively, to detect the output voltage V_{oc} and current I_{sc} . The real-time acquisition of all data are done by an Agilent 34970A data acquisition instrument.

3. Experimental Results and Analysis

Experiments were carried out in Nanchang city in 2017, in three consecutive days on 27–29 May (experiment 1) and

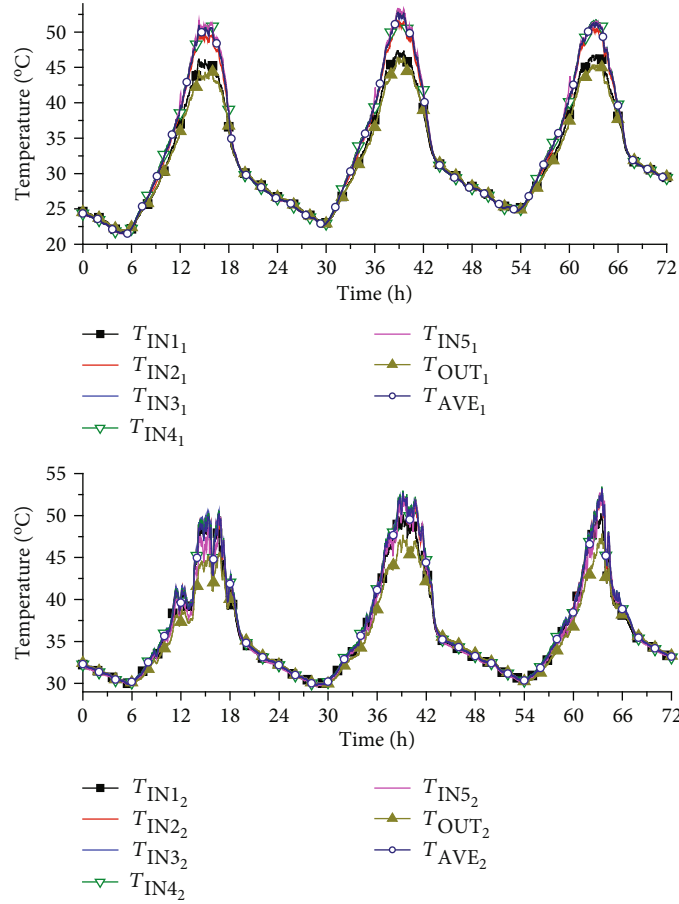


FIGURE 7: Inner and outer temperature distributions of PV cells.

TABLE 7: Test results of inner and outer temperatures of PV cells.

Date	T_{AVE} (°C)		T_{OUT} (°C)		Maximum difference between T_{AVE} and T_{OUT} (°C)
	Max. temperature	Mean temperature	Max. temperature	Mean temperature	
2017.05.27	50.5	32.1	44.0	30.6	6.5
2017.05.28	52.1	33.5	45.8	32.0	6.3
2017.05.29	51.1	34.2	45.1	32.7	6.0
2017.07.14	48.4	36.2	44.1	35.2	4.3
2017.07.15	51.4	37.3	46.7	36.1	4.7
2017.07.16	50.8	36.4	46.2	35.5	4.7

14-16 July (experiment 2). During the tests, the outdoor openings were kept open and the indoor openings closed, while room doors of the experimental room and the control room were kept open all the time. Matte black paint lacquer covered the external surface of the phase change board during the tests in July, like the treatment for the surface of the heating wall of a regular passive Trombe wall system. For the tests in May, the surface of the phase change board was not coated.

Figure 4 presents the distribution of solar irradiation intensity and ambient temperature during the three days of tests, and the detailed data is listed in Table 3 (mean ambient temperature is the average over a whole day; solar radiation is

the irradiation on the south-faced vertical wall, and its mean value is the average in the period from sunrise to sunset). I_c is the solar irradiation intensity and T_s is the ambient temperature. Their subscripts 1 and 2, respectively, represent experiment 1 and experiment 2. Based on Figure 4 and Table 4, the solar irradiation intensity of experiment 2 is slightly lower than that of experiment 1 on each corresponding day in the three days, while the ambient temperature is higher. The mean ambient temperature of experiment 1 is 29.4°C while that of experiment 2 is 34.9°C.

3.1. Power and Efficiency of Photovoltaic Cells. Electric power and photoelectric conversion efficiency are two important

parameters measuring the performance of photovoltaic cells. Through the definition of electric power $P = U \times I$, being U the voltage and I the current, electric power of photovoltaic cells can be calculated once voltage and current are measured. The photoelectric conversion efficiency can be obtained by Eq. (1).

Electric power of photovoltaic cells is given by

$$P = \eta_c I_c A_c, \quad (1)$$

where A_c is the area of photovoltaic cells, m^2 ; I_c is the solar irradiation intensity, W/m^2 ; and η_c is the photoelectric conversion efficiency.

Figure 5 presents the trends of electric power and efficiency of photovoltaic cells with time for experiments 1 and 2. P and η_c are the electric power and efficiency of photovoltaic cells, respectively. The electric powers and efficiencies of photovoltaic cells are similar between each pair of corresponding days in both experiments, and the efficiency varies in the range of 7%~13.5%. Table 5 lists the daily measured data from sunrise to sunset, i.e., at around 5:30~19:00 in experiment 1 and 5:15~19:30 in experiment 2. From the table, regarding experiment 1, the mean efficiency of power generation is about 10.7%, the daily mean power output is 23.1 W, and the daily power generation is 0.315 kW-h; for experiment 2, the mean efficiency of power generation is about 10.6%, the daily mean power output is 20.0 W, and the daily power generation is 0.287 kW-h. The difference in photovoltaic performance of photovoltaic cells is small between the two experiments, and the overall change characteristics are almost consistent. Thus, the matte black coating treatment slightly impacts on both electric power and efficiency of photovoltaic cells.

3.2. Temperature of PCM Plate. Figure 6 presents the external side temperatures of phase change boards 1, 2, and 3 (see Figure 3) in experiments 1 and 2. T_{PH} is the temperature of the external side of the PCM plate, and subscripts 1, 2, 3, respectively, represent PCM plates 1, 2, and 3. From the curves, all the external side temperatures of PCM plates 1, 2, and 3 in the two experiments are almost identical, and those in experiment 2 are higher than those in experiment 1. The external side temperatures of PCM plates 1, 2, and 3 are averaged, and the compared results of both experiments are listed in Table 5. According to Table 6, the highest temperature of the PCM plates in experiment 1 was 41.6°C and in experiment 2 46.2°C. On the one hand, the coating on the surface of the PCM plates in experiment 2 increases the absorption of solar heat. On the other hand, experiment 2 has a higher ambient temperature.

3.3. Cooling Effect on PV Cell. Figure 7 presents the temperatures at different height locations on the inner side and at the middle of the outer side of PV cells in experiments 1 and 2. T_{IN} is the temperature of each node along the high direction on the inner side of PV cells, and the subscript numbers 1-5 from small to large represents the high direction from low to high. T_{OUT} is the temperature at the middle of the outer side of PV cell. T_{AVE} is the mean temperature of the four locations

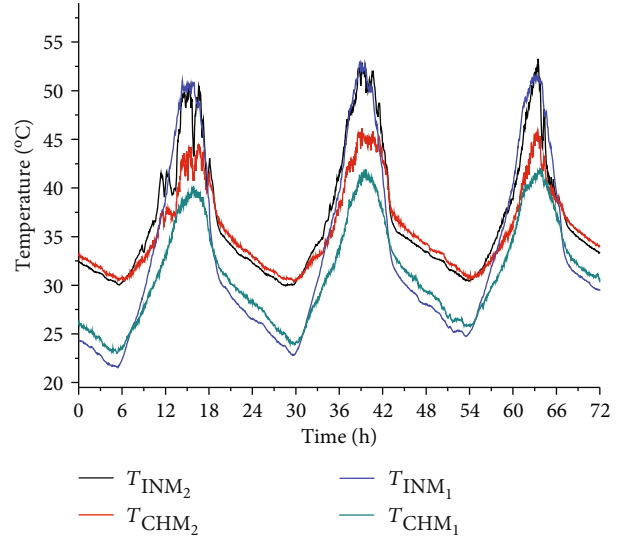


FIGURE 8: Inner side temperatures of PV cell and of the passage in the middle position.

in the upper part of the inner side of PV cell. As shown in the figure, during daytime, the internal temperatures are all higher than the outer temperature of PV cell; during nighttime, the internal temperatures at different height locations are close to the outer temperature of PV cell; the temperature distribution laws of PV cells are similar in both experiments. The specific data for T_{AVE} and T_{OUT} are listed in Table 7. As shown in the table, although the ambient temperature is higher in Experiment 2 and the maximum outer temperature of PV cells in experiment 2 is slightly higher than that of experiment 1, the internal maximum temperature of the PV cells in experiment 2 is slightly lower than that of experiment 1. The result shows that the absorption coating treatment on the surface of the PCM plates will increase the temperature of the PCM plates; however, there is a reduction in the working temperature of the PV cells.

Figure 8 shows the temperature in the middle of the inner side of PV cell and that of passage varying with time in experiments 1 and 2. T_{INM} is the temperature in the middle of the inner side of PV cell, and T_{CHM} is the temperature in the middle of passage. From the comparison between experiment 1 and experiment 2, the value of T_{INM} in experiment 2 is close to that in experiment 1, even slightly lower, but T_{CHM} in experiment 2 is higher than that in experiment 1. The results also indicate that the absorption coating treatment on the surface of the PCM plates can reduce the working temperature of PV cell. Table 8 lists the specific test results of the two experiments. The maximum value of T_{INM} is 52.3°C in experiment 1 and it is 51.7°C in experiment 2. The maximum values of T_{CHM} are 41.4°C and 45.3°C in experiments 1 and 2, respectively. The temperature difference between the inner side of PV cell and the passage reaches 11.6°C in experiment 1 and 6.7°C in experiment 2. According to [21], without a ventilation passage on the PV wall, the working temperature of PV cell reaches up to 70°C in summer. From the comparison,

TABLE 8: Test results of the inner side temperatures of PV cell and passage temperatures in the middle position.

Date	T_{INM} (°C)		T_{CHM} (°C)		Maximum difference between T_{INM} and T_{CHM} (°C)
	Max. Temperature	Mean temperature	Max. Temperature	Mean temperature	
2017.05.27	50.6	32.2	39.6	30.2	11.6
2017.05.28	52.3	33.6	41.3	31.4	11.4
2017.05.29	51.4	34.3	41.4	32.3	10.3
2017.07.14	49.2	36.5	43.1	35.3	6.5
2017.07.15	51.7	37.5	45.3	36.2	6.5
2017.07.16	51.2	36.6	44.6	35.6	6.7

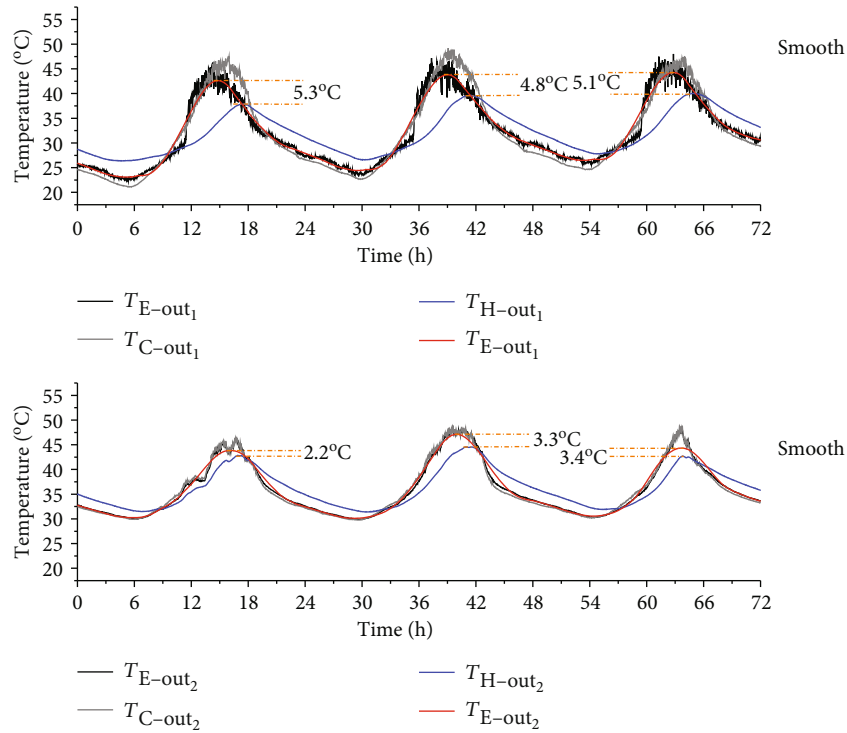


FIGURE 9: External side temperatures of the south wall and the Trombe wall.

the PV-PCM-Trombe wall system shows the effective cooling effect on PV cell both in experiments 1 and 2.

3.4. Thermal Effect on the Indoor Room. As is shown in Figure 9, $T_{\text{E-out}}$, $T_{\text{C-out}}$, and $T_{\text{H-out}}$ are, respectively, the temperatures of the external side of the south wall of experimental room, south wall of the control room, and Trombe wall in experiments 1 and 2. $T_{\text{E-out smooth}}$ is the smoothed curve of $T_{\text{E-out}}$. For each of experiments 1 and 2, the two temperature curves of the external side of the south wall of the experimental room and control room are almost coincident with each other; in daytime, the temperatures of the external side of the south wall of the experimental room and control room are higher than that of the Trombe wall which means that the passive solar building will not result in summer overheating problem of the wall, and the peak of temperature occurs earlier; in nighttime, the temperature of the external side of

the Trombe wall is higher than the that of others. From the comparison between the two experiments, the main characteristic is that the peak temperature difference between the south wall and the Trombe wall for the experimental room are lower in experiment 2. Take day 2 as an example, as is given by Table 9, the delay is 2 hours in experiment 1 and 40 minutes in experiment 2. In addition, the maximum value of $T_{\text{C-out}}$ in experiment 1 is almost the same as that of experiment 2, but the maximum values of $T_{\text{E-out}}$ and $T_{\text{H-out}}$ in experiment 2 are slightly greater than those in experiment 1; in each experiment, the daily mean values of $T_{\text{E-out}}$, $T_{\text{C-out}}$, and $T_{\text{H-out}}$ are substantially identical. Overall, though the coating on the external side of phase change board increases the solar heat absorption and the temperature of the Trombe wall slightly, the effect of preventing the wall from overheating in summer is still available for the passive solar system.

TABLE 9: Summarized results of the external side temperatures of the south wall and the Trombe wall.

Temperature and time	Experiment 1			Experiment 2		
	T_{E-out}	T_{C-out}	T_{H-out}	T_{E-out}	T_{C-out}	T_{H-out}
Max. temperature (°C)	44.4	47.7	39.6	47.8	47.8	44.5
Daily mean temperature (°C)	33.2	32.4	32.1	36.5	36.4	36.5
Day time to reach max.	14:11	15:17	17:21	16:19	16:17	17:01

4. Conclusions

Aiming at the summer overheating problem existing in regular PV-Trombe wall system, the present work proposes a novel PV-Trombe wall system combined with PCM, i.e., the PV-PCM-Trombe wall system. This work mainly experimentally studies the effectiveness and characteristics of using phase change materials to improve the overheating problem of PV-Trombe wall in summer. Through hot box experiments, two experiments were carried out in summer for comparing the proposed PV-Trombe wall system combined with phase change material (PV-PCM-Trombe system). Experiment 1 was carried out without coating the external surface of PCM plates, whereas in experiment 2, the external surface of the PCM plates was coated; in experiment 2, the solar irradiation intensity is slightly lower and the ambient temperature is higher. The following conclusions are addressed:

1. From the two experiments, electric power and the efficiency of photovoltaic cells are similar, so the coating treatment on the external surface of phase change board impacts a little on both electric power and efficiency of photovoltaic cells
2. The lacquer coating on the surface of the PCM plates can increase the absorption of solar heat. Therefore, it can increase the temperature of the PCM plates
3. The PV-PCM-Trombe wall system shows the effective cooling effect on PV cell compared with the regular PV-Trombe wall system, even the absorption coating treatment on the surface of the PCM plates can reduce the working temperature of PV cells
4. Though the coating on the external side of phase change board increases the solar heat absorption, the novel phase change heat storage-type PV-Trombe wall system will not induce room overheating whether the external surface of the phase change board is coated or not

The improvement of the PV-PCM-Trombe wall system is the use of phase change material layer. The above experimental results show that this improvement can help to avoid the summer overheating problem of the regular PV-Trombe wall system. In the future, this system will be further studied and optimized mainly from the aspects of theoretical modeling analysis and economic analysis.

Data Availability

All data used to support the findings of this study are included within the article.

Conflicts of Interest

The authors declare that they have no conflicts of interest.

Acknowledgments

This study was sponsored by the National Science Foundation of China (NSFC), (1) Project No. 51408278 and (2) No. 21663013.

References

- [1] H. Yang and J. Jie, "Study on the heat gain of a PV wall," *Acta Energiac Solaris Sinica*, vol. 20, no. 3, pp. 270–273, 1999.
- [2] J. Jie, Y. Hua, H. Wei, P. Gang, L. Jianping, and J. Bin, "Modeling of a novel Trombe wall with PV cells," *Building and Environment*, vol. 42, no. 3, pp. 1544–1552, 2007.
- [3] J. Ji, H. Yi, G. Pei, B. Jiang, and W. He, "Study of PV-Trombe wall assisted with DC fan," *Building & Environment*, vol. 42, no. 10, pp. 3529–3539, 2007.
- [4] Z. Hu, W. He, J. Ji et al., "Comparative study on the annual performance of three types of building integrated photovoltaic (BIPV) Trombe wall system," *Applied Energy*, vol. 194, pp. 81–93, 2017.
- [5] P. Dupeyrat, C. Ménézo, and S. Fortuin, "Study of the thermal and electrical performances of PVT solar hot water system," *Energy & Buildings*, vol. 68, pp. 751–755, 2014.
- [6] M. Herrando, C. N. Markides, and K. Hellgardt, "A UK-based assessment of hybrid PV and solar-thermal systems for domestic heating and power: system performance," *Applied Energy*, vol. 122, no. 122, pp. 288–309, 2014.
- [7] B. K. Koyunbaba and Z. Yilmaz, "The comparison of Trombe wall systems with single glass, double glass and PV panels," *Renewable Energy*, vol. 45, pp. 111–118, 2012.
- [8] O. Zogou and H. Stapountzis, "Flow and heat transfer inside a PVT collector for building application," *Applied Energy*, vol. 91, no. 1, pp. 103–115, 2012.
- [9] B. Jiang, J. Ji, and H. Yi, "The influence of PV coverage ratio on thermal and electrical performance of photovoltaic-Trombe wall," *Renewable Energy*, vol. 33, no. 11, pp. 2491–2498, 2008.
- [10] O. K. Ahmed, K. I. Hamada, and A. M. Salih, "Enhancement of the performance of photovoltaic/Trombe wall system using the porous medium: experimental and theoretical study," *Energy*, vol. 171, pp. 14–26, 2019.

- [11] M. J. Huang, "The effect of using two PCMs on the thermal regulation performance of BIPV systems," *Solar Energy Materials & Solar Cells*, vol. 95, no. 3, pp. 957–963, 2011.
- [12] M. J. Huang, P. C. Eames, and B. Norton, "Thermal regulation of building-integrated photovoltaics using phase change materials," *International Journal of Heat & Mass Transfer*, vol. 47, no. 12–13, pp. 2715–2733, 2004.
- [13] A. Hasan, S. J. McCormack, M. J. Huang, and B. Norton, "Evaluation of phase change materials for thermal regulation enhancement of building integrated photovoltaics," *Solar Energy*, vol. 84, no. 9, pp. 1601–1612, 2010.
- [14] W. Lin, Z. Ma, P. Cooper, M. I. Sohel, and L. Yang, "Thermal performance investigation and optimization of buildings with integrated phase change materials and solar photovoltaic thermal collectors," *Energy & Buildings*, vol. 116, pp. 562–573, 2016.
- [15] F. Hachem, B. Abdulhay, M. Ramadan, H. el Hage, M. G. el Rab, and M. Khaled, "Improving the performance of photovoltaic cells using pure and combined phase change materials - experiments and transient energy balance," *Renewable Energy*, vol. 107, pp. 567–575, 2017.
- [16] M. A. Kibria, R. Saidur, F. A. Al-Sulaiman, and M. M. A. Aziz, "Development of a thermal model for a hybrid photovoltaic module and phase change materials storage integrated in buildings," *Solar Energy*, vol. 124, pp. 114–123, 2016.
- [17] J. Curpek and J. Hraska, "Simulation study on thermal performance of a ventilated PV Façade coupled with PCM," *Applied Mechanics & Materials*, vol. 861, pp. 167–174, 2017.
- [18] L. Aelenei, R. Pereira, A. Ferreira, H. Gonçalves, and A. Joyce, "Building integrated photovoltaic system with integral thermal storage: a case study," *Energy Procedia*, vol. 58, pp. 172–178, 2014.
- [19] L. Aelenei, R. Pereira, H. Gonçalves, and A. Athienitis, "Thermal performance of a hybrid BIPV-PCM: modeling, design and experimental investigation," *Energy Procedia*, vol. 48, pp. 474–483, 2014.
- [20] T. Ma, H. Yang, Y. Zhang, L. Lu, and X. Wang, "Using phase change materials in photovoltaic systems for thermal regulation and electrical efficiency improvement: a review and outlook," *Renewable & Sustainable Energy Reviews*, vol. 43, pp. 1273–1284, 2015.
- [21] H. Hulin, H. Dong, and L. Kong, "Theoretical and experimental research on the natural convection cooling for solar cell," *Acta Energiac Solaris Sinica*, vol. 27, no. 3, pp. 309–313, 2006.

Research Article

Assessment of the Use of PV Panels with Energy Accumulation Option for Riga City Office Building

Kristina Berzina, Inga Zicmane , and Konstantins Kasperuks

Faculty of Power and Electrical Engineering, Riga Technical University, Azenes Street 12/1, Riga, Latvia

Correspondence should be addressed to Inga Zicmane; inga.zicmane@rtu.lv

Received 21 March 2019; Revised 10 July 2019; Accepted 18 July 2019; Published 8 October 2019

Guest Editor: Daniel T. Cotfas

Copyright © 2019 Kristina Berzina et al. This is an open access article distributed under the Creative Commons Attribution License, which permits unrestricted use, distribution, and reproduction in any medium, provided the original work is properly cited.

Currently, demand-side management (DSM) covers a whole range of technological and policy measures aimed at reducing electricity consumption connected with economic activities. Thus, the development of wind PV and other renewable energy technologies, combined with microgrid technology, offers the remote consumers and prosumers ample opportunities to stabilize long-term costs and increase local energy system security. Apart from that, DSM from microgrid based on renewable sources also has certain social benefits, such as protection of the environment and conservation of natural resources. Due to the advances in photovoltaic material research and solar panel price reduction over the last years, the usage of this alternative energy source in Baltic region countries seems more attractive. The usage of energy storage devices can help use the solar power more efficiently and smarter. This paper deals with the optimization of a proposed solar panel array of a renovated office building's communal lighting in Riga, using storage devices and demand-side management of the produced power, looking into a way to calculate the needed storage capacity on the basis of potential PV system and existing power consumption for communal space lighting system. The proposed approach will become one of the first basic steps in applying DSM to help reduce the communal space's illumination power consumption, in turn helping to reduce the needed PV generating power and energy storage.

1. Introduction

Today, the use of renewable energy is one of the most promising forms of electricity consumption that can be considered as a virtually inexhaustible source of energy. This future perspective is determined by the ecological aspects, low operating costs, and projected deficit of nonrenewable natural resources. According to the forecasts of the European Commission, the renewable energy industry will account for 1.1% of the total product in 2020.

Many large corporations contribute to the use of renewable energy. For example, Apple Inc., as the leading solar power station owner, provided the operation of two data centres with alternative energy [1]. Tesla, for its part, is investing in solar power plants with the aim to reduce CO₂ emissions in regions with high levels of atmospheric pollution [1].

In northern countries, where the sun's radiance is not that high throughout the year, the introduction of solar energy as a viable renewable energy source has been hard.

But in recent years, the efficiency of the photovoltaic (PV) panels has been improved greatly [2] and this has caused the prices to drop [3] significantly. These advances should be considered, when thinking of ways to reduce on-grid power consumption and solving the problem of demand-side management.

The air temperature affects the work ratio of the solar panels. The majority of solar cells demonstrate a drop of work ratio (up to 30%) as the temperature rises, but while it is exceeding the operating temperature value, the equipment can be damaged. For almost all types of solar cells, the operating temperature is in the range of -40°C to +85°C. Taking into account the average air temperature in Latvia (-5.9°C) (LEGMC data, Figure 1) [4], the operating temperature of the cells would not be exceeded and there would not be an additional need for the installation of cooling equipment. But during hot summer days, the air temperature can exceed +30°C, when the panel surface is heated to 60°C-70°C, reducing its work ratio. This problem can be solved

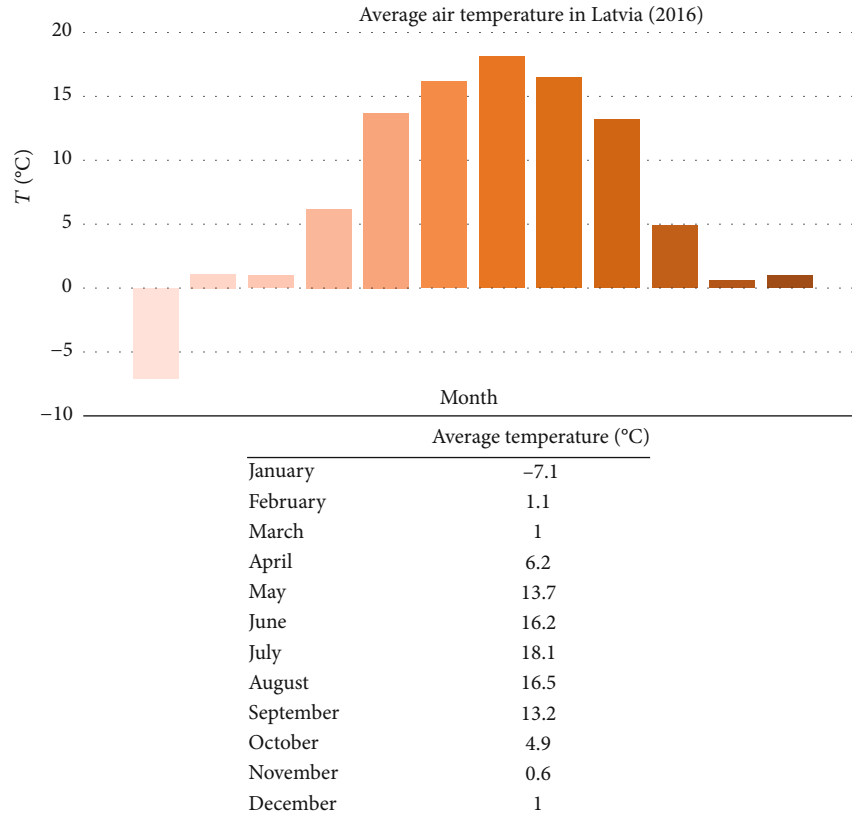


FIGURE 1: Average air temperature in Latvia (in 2016).

by installing solar panels on the metal structures of a roof, thus creating a gap of few centimetres in order to ensure air flow between the roof and solar panels.

Germany is the EU's leading country in the extraction of electric energy by means of solar cells. In 2015, nearly 40 GWh of solar energy was generated in Germany [5]. As shown in the map (Figure 1), in Latvia, there is approximately the same solar activity as in Germany (1000 kWh/m² and 1200 kWh/m², respectively), which suggests that the production of electric energy from solar cells would be as successful as in neighbouring countries.

The map (Figure 2) visually shows that greater solar activity is in coastal areas, in the vicinity of Riga and in Zemgale. So, the installation of solar panels for Riga buildings (including the office ones) shall be considered useful. The average annual solar activity is 1000 kWh/m². According to the data of the Latvian Environment, Geology and Meteorology Centre (LEGMC) [6] collected since 1950, the longest duration of sunshine per year is observed on the Baltic Sea coast (Kolka, Ventspils, and Liepaja): 1840-1940 hours per year. The sun shines in Zemgale about 1850 hours a year. In the eastern regions, the duration of sunshine is less: 1670-1720 hours per year; but in the Vidzeme Highland, it is only 1580 hours per year. In general, in coastal areas in summer, there are the biggest number of clear days and fewer fall-outs than in region areas, located further away from the sea. The duration of sunshine is also largely determined by the amount of clouds, not only by astronomical factors. The sun is shining slightly less than half the probable duration

of sunshine in the territory of Latvia as a result of great cloudiness. During the winter months in the territory of Latvia, the sun shines only 10-25% of the possible shining time. In the summer months, in general, the average the sun shines is only 50-60% of the possible duration of sunshine. In the territory of Latvia, without the sun, there is an average of 90-110 days per year; in the Vidzeme and Latgale Highlands, 110-120 days. In the winter months, on average, more than half of the days of the month the sun does not shine. As can be seen from the above data, the maximum sunny hours in Riga are 2110 hours per year, but the minimum is -1519 hours per year. When installing solar cells in Riga, their average working time will be about 22% of the total time.

This paper considers ways to ensure the illumination of a renovated office building's staircase and communal space, using solar power as much as possible.

Due to the increase in the tariff for electricity, there is interest in switching office loads to renewable energy sources.

This article considers the possibility of switching the load of communal lighting to renewable sources; in particular, the use of solar batteries (PV) is planned. The choice was made based on the aspects and limitations of the urban environment.

The consumption of communal lighting has partly probabilistic nature. When considered in detail, like any other load curve, the load curve of the lighting system can be divided into a stationary and probabilistic component.

The office building itself is newly renovated. Its common space is equipped with LED lights. Nevertheless, the total

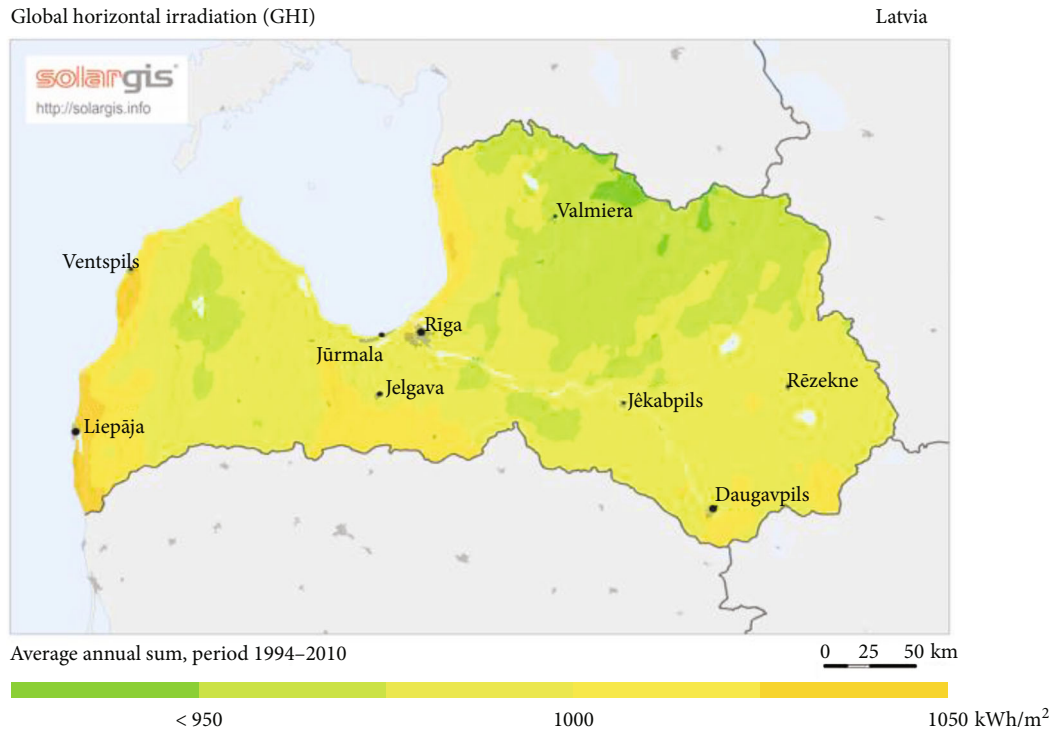


FIGURE 2: Solar activity in Latvia [6].

daily energy consumption for the communal space lighting system is more than

$$E_{cl} = 380 \text{ kWh}, \quad (1)$$

where E_{cl} is the communal space light system energy consumption.

2. The PV Generation and Sun Insulation Analysis

2.1. Types of the Solar Panel

- (i) Monocrystalline solar panels
- (ii) Polycrystalline solar panels

Thin film solar panels:

- (i) Amorphous silicon solar panels
- (ii) Cadmium telluride solar panels (CdTe)
- (iii) Copper indium gallium solar panels (CIGS or CIS), (Table 1) [7]

2.2. Optimal Position of the Solar Panel. The efficiency of solar panels is determined not only by the intensity of the received solar radiation but also from the angle at which the panel is directed towards the direction of the solar radiation. Therefore, for the panel to get maximum solar radiation, this angle should be 90° . In order to find out the angle

of a stream of the sun and the sun's height in solstice, you need to know the geographic latitude and geographic longitude of the particular place (Figures 2 and 3); Riga: latitude $56^\circ 56' 56''$ N, longitude $24^\circ 6' 23''$ E (56.948889, 24.106389) (Figures 4 and 5) [4].

Using the Photovoltaic Geographic Information System, it is possible to determine the optimal angle of inclination of the position of the solar panels (Figure 5) [8], where H_h is the solar radiation on a horizontal surface ($\text{Wh}/\text{m}^2/\text{per day}$), H_{opt} is the radiation to the optimal angle of inclination ($\text{Wh}/\text{m}^2/\text{per day}$), $H(39)$ is the radiation at the inclination of 39° ($\text{Wh}/\text{m}^2/\text{per day}$), I_{opt} is the optimal angle of inclination ($^\circ$); PP is the repayment factor of the investment project, I_0 is the amount of initial investment, and CF is the cash flow from project implementation.

Based on the results (Table 2) obtained, the optimal angle of inclination of the installation of solar panels for the mapping point is 38° . Positioning solar panels at this angle will reduce reflected solar energy and thus increase the efficiency of the solar plant.

3. The Load Analysis in Office Building's Staircases and Communal Space

Five recorders "Circutor CIR-e3" were installed to record the overall energy consumption and load character of the office building, as well as to carry out audit and further analysis of the data obtained. Two analyzers were connected to the input cable for fixing the data of the total electricity consumed in the building (Figure 6) [9].

TABLE 1: Types of solar panel.




Name			
Type	Monocrystalline	Polycrystalline	Thin film (CIS)
Product name	Sharp NU-RD280	Trina Solar TSM-270 PD05	Solar Frontier SF170S
Nominal power P_{max} (W)	280	270	170
No-load voltage U_{oc} (V)	39.2	38.4	112
Short-circuit current I_{sc} (A)	9.67	9.18	2.2
Voltage at maximum power U_{mpp} (V)	31.2	30.9	87.5
Current at maximum power I_{mpp} (A)	8.97	8.73	1.95
η (%)	17	16.5	13.8
Panel area S (m ²)	1.643	1.553	1.228
Occupied area of solar panels per 1 kWp S_{kWp}	5.87	5.75	7.22
The cost of solar panels per 1 kWp C_{kWp}	996.4	959.3	923.5
Temperature factor k_t (%/°C)	-0.31	-0.41	-0.30
Power losses P_{zud} , % at $T = 70^\circ\text{C}$	13.95	18.45	13.5
Price per piece (EUR)	279	259	157



FIGURE 3: Visualization of solar panel design.

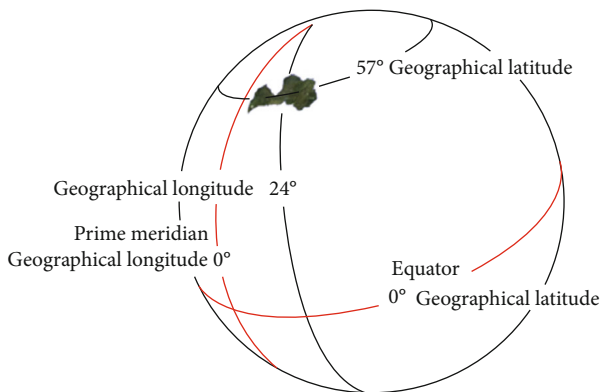


FIGURE 4: Geographic latitude and longitude in Latvia [4].

The solar panels are intended to be used only for utility lighting; internal installation was reorganized, and the lift equipment (the peaks indicated by the arrows at Figure 6)

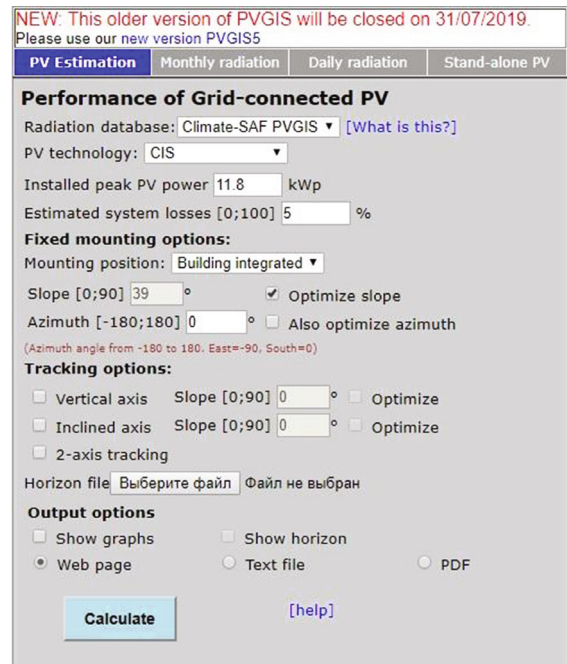


FIGURE 5: Calculation of the optimal angle of inclination [8].

was connected to another entry. After the pump was disconnected, measurements were made again and graphs were obtained (Figure 7).

As a basic model of the lighting load, the load schedule of communal lighting of office space was adopted. The schedule is presented in 10x relative units, because the typical lighting load is minor than the typical whole office building load curve.

TABLE 2: Monthly solar activity on the roof of an office building.

Month	H_h	H_{opt}	$H(39)$	I_{opt}	T_{24h}
January	450	847	847	71	-5.5
February	1060	1730	1730	64	-4.3
March	2570	3730	3730	55	0.1
April	4210	5150	5150	41	6.2
May	5540	5870	5870	27	12.5
June	5860	5810	5810	18	16.1
July	5550	5630	5630	22	19.6
August	4400	5010	5010	35	17.9
September	2860	3770	3770	48	13
October	1380	2110	2110	60	6.8
November	513	895	895	68	3.8
December	297	558	558	72	-1.1
Per year	2900	3430	3430	39	7.1

On the basis of lighting schedule data for mathematical model, the common consumed power of building's communal space lighting (Figure 8) is built.

4. The Mathematical Model of Sun Insulation and PV Generation

A load analysis was performed, using a mathematical model [10]. The result data are represented in Figure 8. The communal space lighting system's consumption in our case is constant through the season in summer and winter months, because the communal space is without windows and there is no daylight component.

To model the electrical load of the lighting system, we use the probability and statistical model:

$$P_{pi} = \bar{P}_l + \beta\sigma \cdot (P_i), \quad (2)$$

where P_i is the wattage rating on the i th hour of the daily schedule; \bar{P}_l is the mathematical expectation on the i th hour of the daily schedule; β is the reliability factor of the calculation, which determines the probability with which the random load values will remain lower than the assumed estimated value P_{pi} , and $\sigma(P_i)$ is the average square deviation for the i th stage of the daily schedule.

Under the normal probability distribution law of the load values under $\beta = 2$, $\sigma(P_i) = 0.025$.

$$P_{pi} = \bar{P}_l P_{max} \cdot (1 \pm \beta\sigma(P_i)) K_s, \quad (3)$$

where K_s is the seasonal factor, the value of which in our case is equal to 1 [11].

The intensity of solar radiation depends on a variety of factors, geographical latitude, the angle of inclination of the receiving surface towards the sun, climate, air pollution, sea level elevation, and season. The study assumes the installation of PV on a roof of the existing building in Riga. Arising

from these, all the above-mentioned parameters were taken into account.

The direct solar radiation Q_1 is found by Kostrov's formula:

$$Q_1 = \frac{Q_0 \sin \alpha}{\sin \alpha + c}, \quad (4)$$

where Q_0 is the solar constant of 1370 W/m² and c is the value characterized by the degree of transparency of the atmosphere (in our case $c = 0.81$).

Calculation of the sun's altitude α , geographical latitude, and inclination towards the horizon is calculated using the Kupa approximation formula.

Diffuse solar radiation is calculated by the formula

$$Q_2 = Q_{2h} [0.55 + 0.434 \cos \theta + 0.313(\cos \theta)^2], \quad (5)$$

where Q_{2h} is the flow of diffuse solar energy falling on the horizontal plane (according to Berlage's expression) [12].

Thus, the orientation angles of the site were set using the above-mentioned expressions to determine the given energy falling on the inclined platform (at an angle of 38°). After the data analysis, it was decided to place 72 photovoltaic panels on the building's roof; the generation is represented in Figure 9 [11].

5. Calculation of Power Balance and Optimal Battery Storage

Assuming the transfer of the power of communal lighting to alternative sources of generation, potential balance of capacities is shown in Figure 10.

The main condition for the working capacity of the planned closed-loop system is the ability to provide the consumer with sufficient power.

$$P_{GPV} + P_a \geq P_c K_s, \quad (6)$$

where P_{GPV} is the generated PV power, P_a is the accumulated power, P_c is the consumed power, and K_s is the safety factor.

The amount of energy possible to save at the current time (t) is determined by two parameters of "free" capacity of the accumulation system (D_a) and the maximal charge current value (I_c).

If the battery capacity is equal to C_a , then

$$0.8 \cdot C_a \geq D_a. \quad (7)$$

Coefficient 0.8 is taken from the equation $(1 - K_p)$, where K_p is the coefficient of allowable battery charge ($K_p \sim 0.8$) [10].

Thus, the mathematical expression for the required accumulation when calculating the power balances of the system of communal lighting in the charging mode of accumulating devices will be equal to

$$P_a = P_{GPV} - \frac{P_c}{E_i} \geq 0, \quad (8)$$

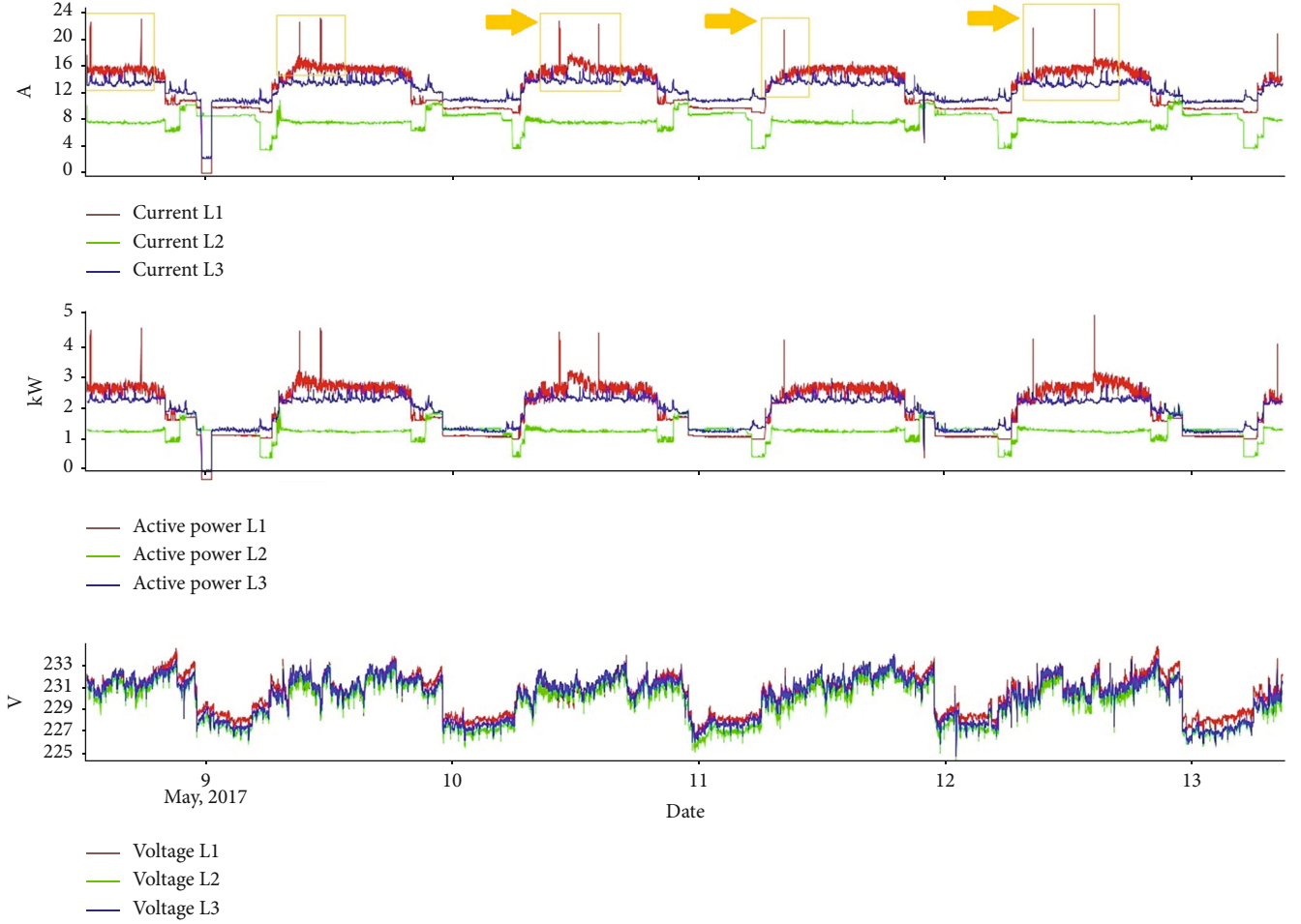


FIGURE 6: Utility schedule before adjustment.

where P_{GPV} is the generated PV power, P_c is the power consumed by the system, and E_i is the efficiency of the inverter.

Correspondingly, in the battery discharge mode

$$P_a = P_{\text{GPV}} - \frac{P_c}{E_i} < 0. \quad (9)$$

The mathematical expression for calculating the power balance in the charging mode of the accumulating unit will be equal to

$$\begin{cases} P_a t \leq D_a U_a K_a, \\ I_a = \frac{P_a}{n_a U_a} \leq I_C, \\ P_a t > D_a U_a K_a, \\ I_a = \frac{P_a}{n_a U_a} \leq I_C, \end{cases} \quad (10)$$

where n_a is the number of battery units, U_a and I_a are the voltage and the charge current of one battery, and $K_a < 1$ is the efficiency of the battery [10].

Optimizing the expression will look like

$$\begin{cases} \bar{D}_a = D_a - I_a t K_a, \\ P_C = P_a - I_a U_a, \\ \bar{D}_a = D_a - I_a t K_a, \\ P_C = [(P)]_a - I_a U_a. \end{cases} \quad (11)$$

Mathematical expressions for calculating the power balance in the discharge mode of the accumulating unit will be equal to [10]

$$\begin{cases} |P_a| t \leq [(1 - K_p) C_a - D_a] U_a, \\ I_a = \frac{|P_a|}{n_a U_a} \leq I_p. \end{cases} \quad (12)$$

The C_a and I_a values determine the working capacity of an autonomous electrical power supply system using renewable energy sources.

By adding battery storage, it is possible to use the solar power more efficiently, but there is the unknown variable, how much exactly has to be stored.

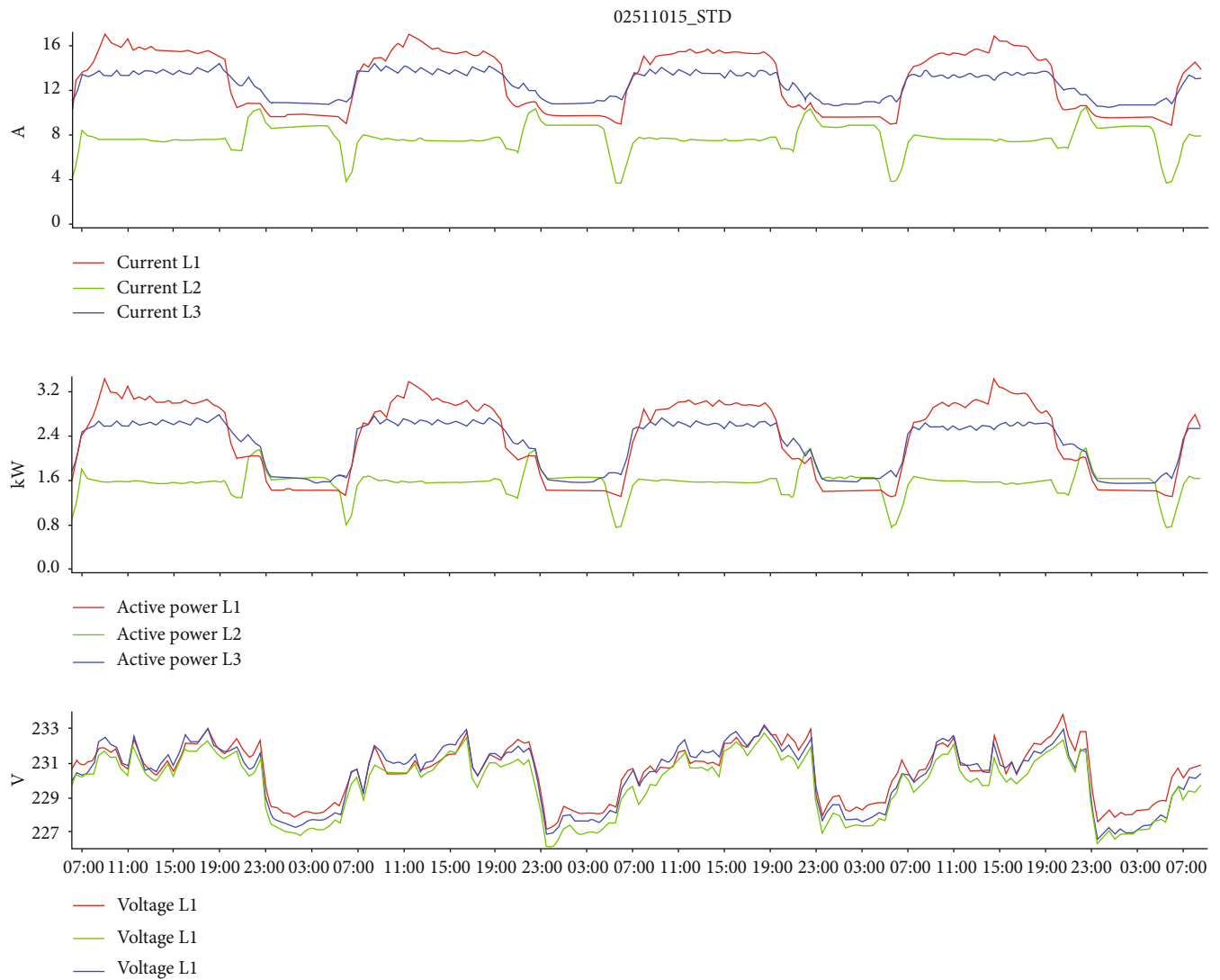


FIGURE 7: Utility lighting schedule after adjustment.

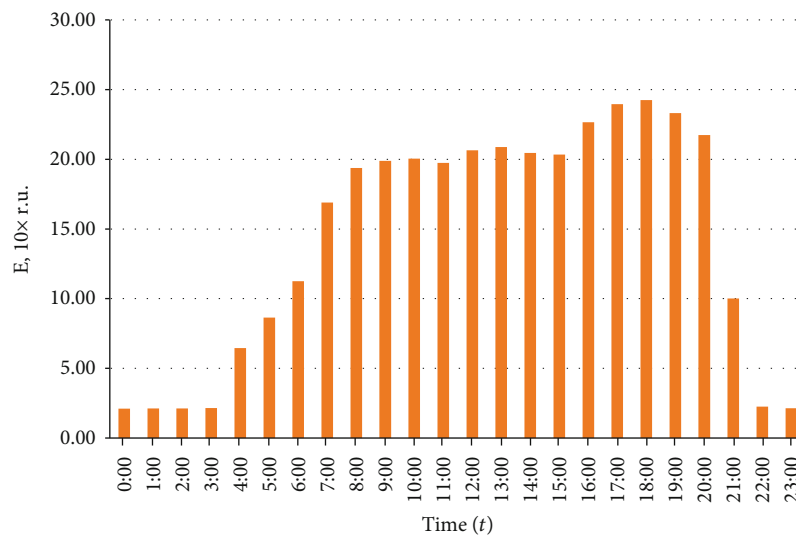


FIGURE 8: Consumed power of building's communal space lighting.

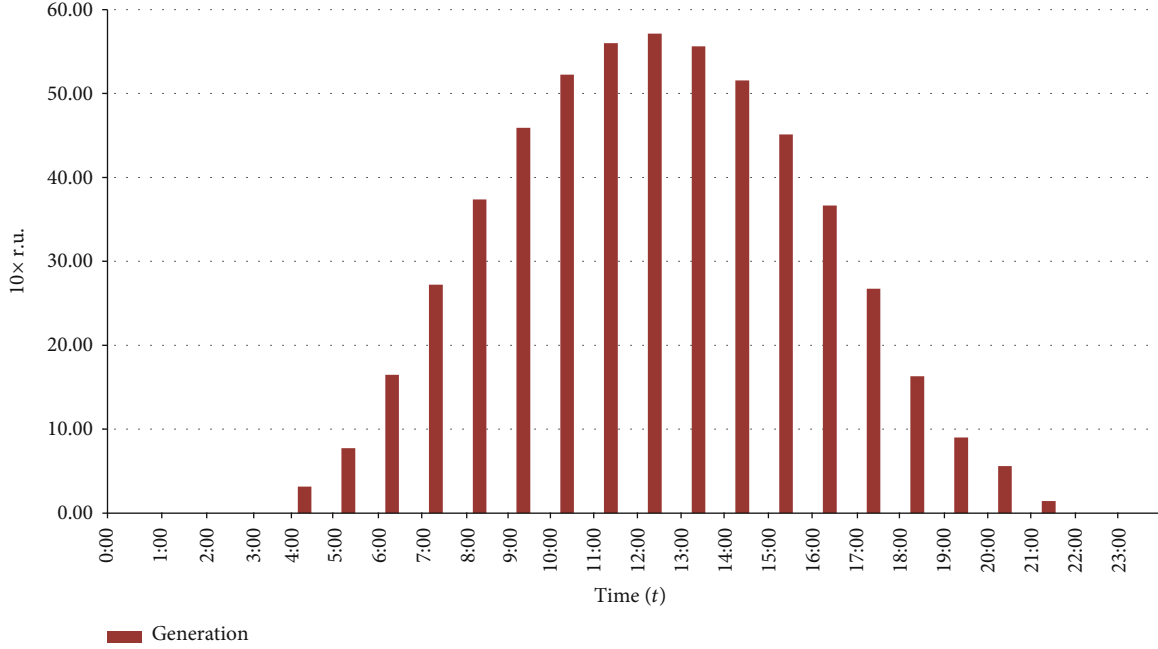


FIGURE 9: Generated power of PV at the building's roof.

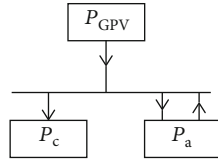


FIGURE 10: Power balance.

By looking back to Figure 9 and adding the energy produced by photovoltaic elements, it can be seen that in summer months there is potentially a lot of wasted energy, which can be stored. And for the time of the year when there is not enough solar energy to cover the whole daily consumption, it can be used to shave off the demand peaks.

The minimum storage capacity can be calculated, using the following procedures:

- (i) For consumption and generation graph, both producing functions $P_{pV} = f(t)$ and $P_c = f(t)$ can be found, see Figure 11
- (ii) Two intersections can be found
- (iii) Three regions P_{st1} , P_{st2} , and P_{st3} can be separated for integration operations
- (iv) The sum of these areas (13) is the minimum storage capacity of the needed battery storage

$$P_{st.sum} = P_{st1} + P_{st2} + P_{st3}. \quad (13)$$

Individual areas of the graph can be found using equations (13) to (14).

$$P_{st1} = \int_a^b P_C(t)dt - \int_a^b P_{pV}(t)dt, \quad (14)$$

$$P_{st2} = \int_c^d P_C(t)dt - \int_c^d P_{pV}(t)dt, \quad (15)$$

$$P_{st3} = \int_d^a P(t)dt, \quad (16)$$

where a is the sunrise time $t = t_{sunrise}$, b is the first intersection of functions P_C and P_{pV} , c is the second intersection of functions P_C and P_{pV} , and d is the sunset time $t = t_{sunset}$ (Figure 12).

The calculation should be done for summer months to fully consider the maximum generating potential of the solar panels. At the same time, equation (17) must be considered:

$$P_{st.summ} \cdot k_{loses} \leq P_{OG}, \quad (17)$$

where

$$P_{OG} = \int_b^c P_{pV}(t)dt - \int_b^c P_C(t)dt \quad (18)$$

is denoted as the maximum overgenerated power.

The k_{loses} coefficient considers conversion and other loses.

The building in question has already taken steps to decrease the usage of electrical energy for communal space lighting, but further improvements are possible. The usage of direct current (DC) and wireless dimming sensors can bring great benefits.

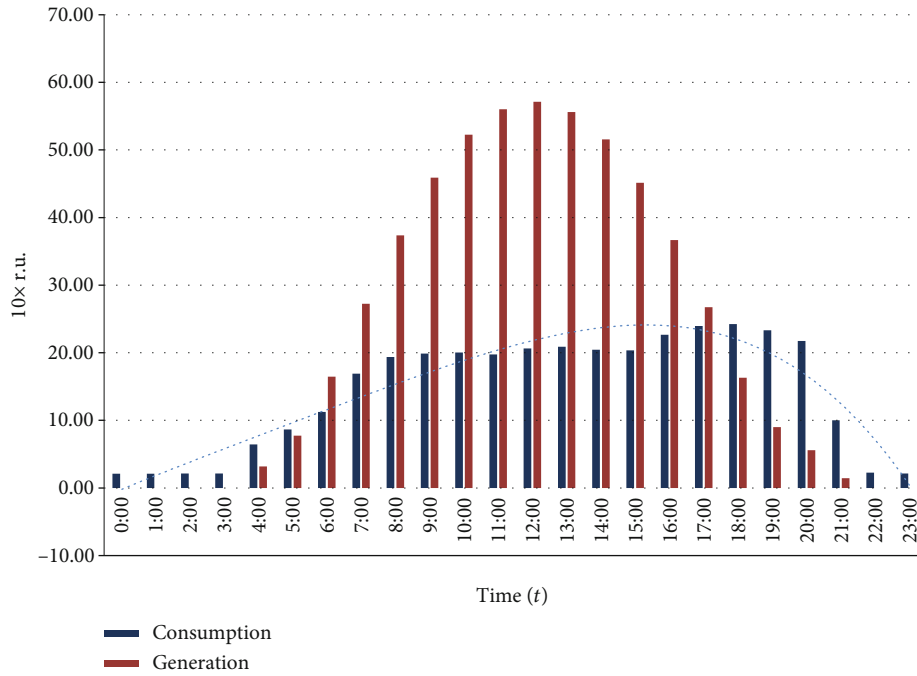


FIGURE 11: Consumption and average square value of power generated in summer months.

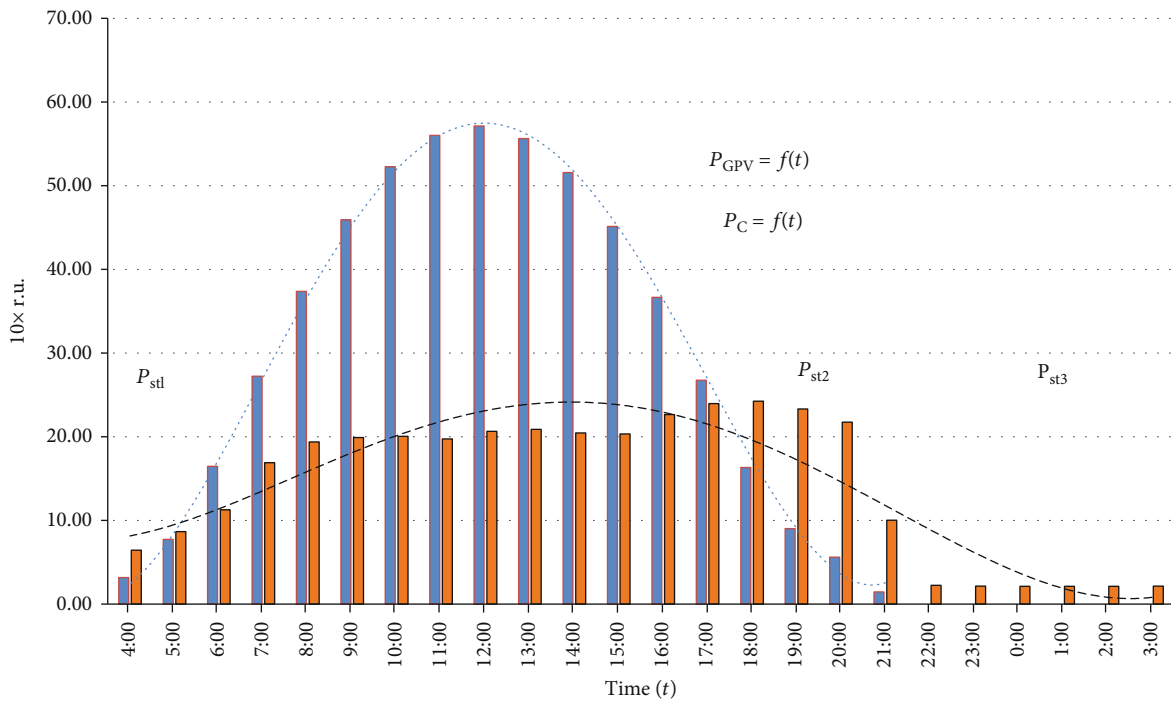


FIGURE 12: Representation of areas to be calculated.

6. Repayment Calculation

Such a repayment calculation is not permissible, as the annual profit will be different, because the amount of electricity produced will vary from year to year, as well as the

price of electricity will be different. At the same time, the manufacturer of solar panels indicates a decrease in the panel's work ratio over time (no more than 10% after 10 years of operation and no more than 20% after 25 years of operation).

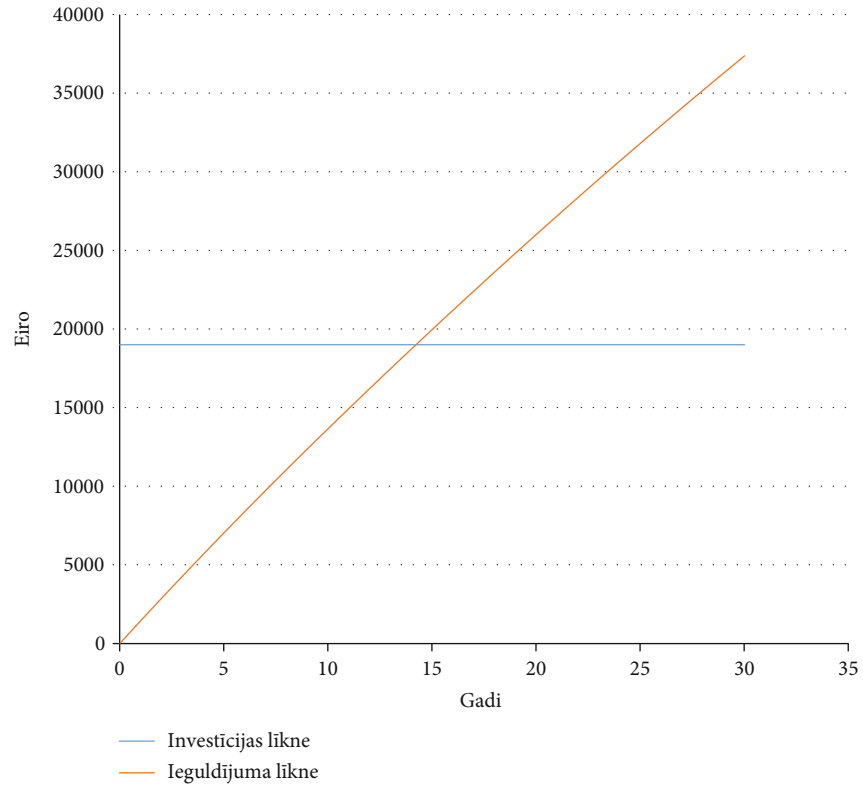


FIGURE 13: Repayment schedule.

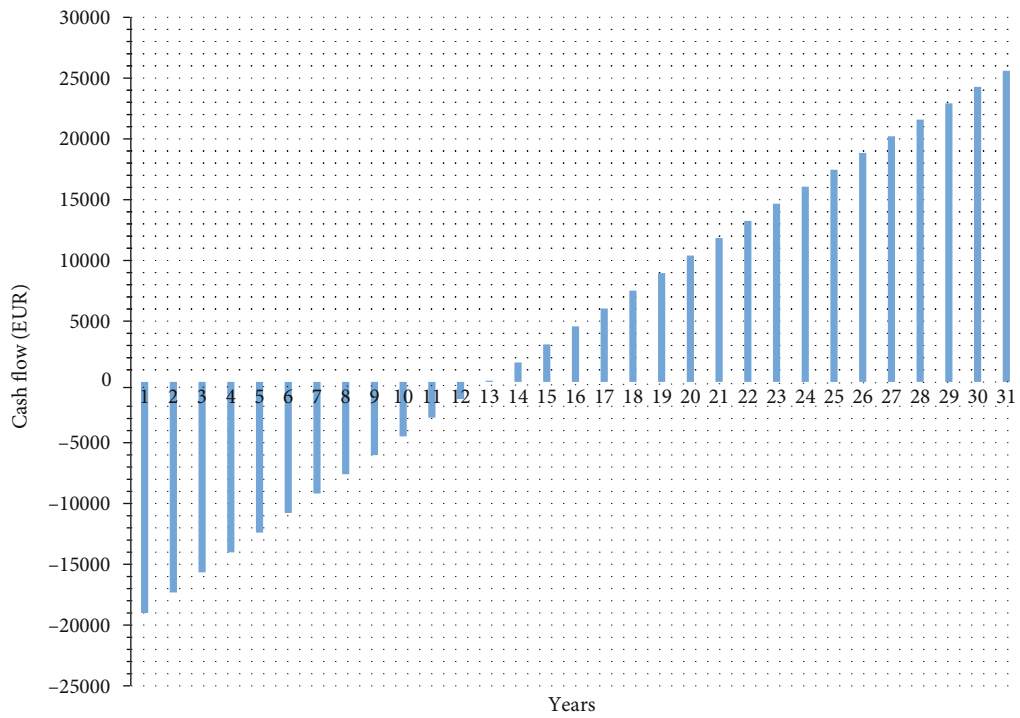


FIGURE 14: Cash flow schedule.

Therefore, a formula that takes into account discount rates will be applied:

$$NPV = \sum_{t=0}^n \frac{CF_t}{(1+i)^t}, \quad (19)$$

where NPV is the current net value, i is the discount rate, CF_t is the incoming cash flow during the period t , n is the repayment deadline, and t is the period of time [10].

During the year, the solar panel produces a maximum of 11970 kWh at a constant electricity tariff (€ 0.14/kWh), which means annual profits will be approximately € 1600 with a decrease every year thereafter. In light of this, we will construct the investment repayment schedule (Figure 13).

As the schedule shows, the investments will be paid back in 12-13 years, which is to be considered an acceptable indicator. Given the constant rise in electricity prices, investments can be paid even more quickly (Figure 14).

The calculation of the total payment amount is based on the following formula [13]:

$$Y = \frac{D(i/m)}{1 - 1/((1 + (i/m))^n \cdot m)}, \quad (20)$$

where Y is the monthly payment amount, D is the amount of a loan, i is the interest rate, m is the number of interest accruals during the year, and n is the loan maturity in years.

7. Conclusion

Choosing the right size for PV panel quality, quantity, angle, and energy storage in the photovoltaic system can prove itself to be difficult, especially in Baltic region countries, where the initial investment can be expensive and should be considered.

In this paper, the authors have looked into a way to calculate the needed storage capacity on the basis of potential PV system and existing power consumption for communal space lighting system.

Future work will incorporate other factors, such as the usage of DC power supply to help reduce the communal space's illumination power consumption, in turn helping to reduce the needed PV generating power and energy storage.

The usage of direct current (DC) and wireless dimming sensors can bring great benefits. The next optimization step is the possibility to combine local DC lighting distribution, avoiding the voltage conversion losses in LED luminaires.

Data Availability

Unfortunately, the PV measurement data used to support the findings of this study will not ever be made available because all those are confidential information which we have no right to disclose. We can present only a link to the site <https://www.csb.gov.lv/en> from which the statistical data was obtained.

Conflicts of Interest

The authors declare that they have no conflicts of interest.

References

- [1] <http://www.datacenterdynamics.com/content-tracks/design-build/apple-reaches-100-renewable-energy-across-all-data-centers/74708.fullarticle>.
- [2] A. Polman, M. Knight, E. C. Garnett, B. Ehrler, and W. C. Sinke, "Photovoltaic materials: present efficiencies and future challenges," *Science*, vol. 352, no. 6283, article aad4424, 2016.
- [3] R. Fares, *The price of solar is declining to unprecedented lows*, Scientific America, 2017, <https://blogs.scientificamerican.com/plugged-in/the-price-of-solar-is-declining-to-unprecedented-lows/>.
- [4] <http://www.ingdep.lv/lv/Saules-lenkis-virs-horizonta-Latvija>.
- [5] https://www.energy-charts.de/energy_pie.htm.
- [6] <http://solargis.com/products/maps-and-gis-data/free/download/europe>.
- [7] O. Yehezkeili, R. Tel-Vered, J. Wasserman et al., "Integrated photosystem II-based photo-bioelectrochemical cells," *Nature Communications*, vol. 3, no. 1, 2012.
- [8] <http://re.jrc.ec.europa.eu/pvgis/apps4/pvest.php>.
- [9] http://circuitor.com/docs/FT_CIR-e3_EN.pdf.
- [10] B. V. Lukutin, S. G. Obukhov, and E. B. Shandarova, *Autonomous Power Supply from the Micro Hydro Power Station*, STT, Tomsk, Russia, 2001, <http://window.edu.ru/catalog/pdf2txt/252/75252/55909>.
- [11] T. Huld and E. D. Dunlop, *PVGIS*, European Commission, Joint Research Centre Institute for Energy and Transport, Renewable Energy Unit, 2012.
- [12] I. O. Muravlev, M. A. Surkov, E. V. Tarasov, and N. F. Uvarov, "Fuse selection for the two-stage explosive type switches," *IOP Conference Series: Materials Science and Engineering*, vol. 189, article 12004, 2017.
- [13] <https://www.citadele.lv/>.

Research Article

Investigation of Repurposed Material Utilization for Environmental Protection and Reduction of Overheat Power Losses in PV Panels

Ammar Alkhalidi , Mohamad K. Khawaja, and Abdel Ghaffar Al Kelany

Energy Engineering Department, Germany Jordanian University, Amman, Jordan

Correspondence should be addressed to Ammar Alkhalidi; ammar.alkhalidi@gnu.edu.jo

Received 26 February 2019; Revised 10 May 2019; Accepted 28 June 2019; Published 14 August 2019

Guest Editor: Daniel T. Cofas

Copyright © 2019 Ammar Alkhalidi et al. This is an open access article distributed under the Creative Commons Attribution License, which permits unrestricted use, distribution, and reproduction in any medium, provided the original work is properly cited.

Constant exposure of a photovoltaic (PV) panel to sunlight causes it to overheat and, consequently, its rated efficiency decreases leading to a drop in its generated power. In this study, a PV panel was tested under standard test conditions in a halogen lamp solar simulator at different solar irradiance values. The PV panel was then fitted with heat dissipating fins and measured under identical test parameters; thereafter, repurposed materials such as high-density polyethylene (HDPE) and plastic bags were, separately, added to the PV panel with fitted heat-extraction fins and the performance was evaluated again. Passively cooling the PV panel with fins and repurposed materials resulted in a 22.7% drop in the PV panel's temperature, while an 11.6% increase in power output occurred at 1000 W m^{-2} . Utilizing repurposed waste materials in PV cooling improves a panel's efficiency and saves the environment from the ecological effects of dumping these materials.

1. Introduction

Photovoltaic (PV) cells' efficiency for converting sunlight into electricity is low, and it drops even more as the cells are heated when exposed to a great deal of solar irradiance. There is an approximately 0.25% and 0.5% drop in efficiency for amorphous and crystalline silicon cells, respectively, for every 1°C increase in the cells' temperature [1]. Hence, cooling PV panels is essential in utilizing the maximum conversion efficiency. The two currently used PV panel cooling systems are active cooling and passive cooling. Active cooling is a system based on expending energy to cool the PV panel down, while passive cooling is a system that does not use any energy to cool off a PV panel.

PV cooling has been widely researched [2, 3]. Hybrid integrated PV/thermal systems are classified as (i) water based, (ii) air based, (iii) refrigerant based, (iv) heat pipe based, and (v) phase change material (PCM) based [4], while passive cooling systems are divided into air (heat sink), liquid

(liquid immersion), and PCM [5]. Heat sinks, or fins, were also effective cooling additives to various applications [6–8]; PV panels can benefit from these properties to reduce their temperature and to increase their relative efficiencies, as was confirmed by multiple studies. There are plenty of uses for fins, such as in electronic equipment, heat exchangers, and turbine cooling. Increases of up to 0.3~1.8% and 1.8~11.8% in average electrical efficiency and average output power, respectively, were reported after the addition of passive cooling fins to a PV panel [9]. Installing aluminium fins to the backside of PV panels increased the electrical conversion efficiency by 1.75% [10] and the output power by 2% [11]. A study investigated a hybrid solar photovoltaic/wind system to maintain the cell's surface temperature, and according to the results, the system not only enhanced the PV cell's performance but also helped the wind turbine generate more electrical power [12].

PCMs have been extensively investigated as heat-extraction additive components to PV panels yielding favorable outcomes

in increasing the relative efficiency by reducing the PV panels' surface temperatures [13–16]. The advantages of adding PCMs to PV panels are their high heat transfer rate, passive heat exchange, no maintenance cost, among others, while some of the disadvantages are high cost, toxicity, fire safety, and corrosion issues [17]. Additional investigations of passive methods of PV panel cooling include the use of cotton wicks [18], rainwater [19], and radiative cooling [20].

State-of-the-art PV passive cooling reviews [21, 22] show a plethora of research on the subject but none look into the utilization of materials that would otherwise be discarded as passive cooling additives to PV panels. This work focuses on passive cooling and the repurposing of different materials to aid in reducing a PV panel's temperature. Repurposing of a material is defined as the utilization of a material, which was originally manufactured to serve a primary function, to serve a secondary purpose instead of being disposed of after its primary function is spent. An alternative to the disposal of particular materials or products is repurposing them to cool down a PV panel. Polyethylene is made from petroleum and considered as a thermoplastic (a plastic material that solidifies when it is cooled down and is easy to shape and bend when it is heated). High-density polyethylene (HDPE) is used for manufacturing plastic bags, plastic bottles, geomembranes, lumber plastic, and anticorrosion pipes. This work introduces a new hybrid passive cooling classification that combines air cooling using heat sinks (fins) under natural ventilation and no wind speed with repurposed materials. The repurposed materials that will be explored in this work are ground HDPE and plastic bags.

The disposal of plastic creates plenty of negative environmental impacts. Despite the fact that plastic is a durable material, it poses a considerable threat to the environment as it decomposes slowly and its incineration could lead to the emission of poisonous gases into the atmosphere. In addition to that, producing plastic proved to have a harmful effect on the environment as a large number of pollutants, together with enormous amounts of fossil fuels, are needed during the production process. Recycling is not always a viable option in many parts of the world; therefore, reducing the nonbiodegradable waste and using it for PV cooling can be beneficial to both the environment and to the efficiency and output power of PV panels. Renewable energy generation combined with environmental protection support the new trend of sustainable cities' design [23].

2. Methodology

The overheating problem in PV panels will be experimentally investigated. A PV panel will be prepared according to the test requirements; it will be tested under laboratory conditions. Halogen lights will be set to the required intensity, and the PV panel's front and back temperatures will be monitored. The temperature will be recorded after ensuring that a steady state was reached.

Heat loss from the PV panel is important for the fins' design. To estimate the heat loss from the PV panel, a math-

ematical model will be proposed and solved analytically. The following assumptions were considered:

- (i) Steady state, one-dimensional problem in the direction of flow. Thus, the temperatures of the glass cover, solar cells, and plates vary only in the direction of working fluid flow
- (ii) The capacity effects of the glass cover, solar cells, and back plate have been neglected

2.1. Heat Dissipation Rate by Convection, Q_{conv} . Q_{conv} is the degree at which heat dissipates through convection from the top and bottom surfaces of the PV panel and is assigned a function of convection coefficient and the temperature gradient between the surface and ambient temperature [24].

$$\begin{aligned} Q_{\text{conv}} &= Q_{\text{conv,front}} + Q_{\text{conv,back}}, \\ Q_{\text{conv,front}} &= A \times h_{\text{front}} \times (T_{\text{pv}} - T_{\text{amb}}), \\ Q_{\text{conv,back}} &= A \times h_{\text{back}} \times (T_{\text{pv}} - T_{\text{amb}}), \end{aligned} \quad (1)$$

where A is the surface area of the PV panel, h_{front} and h_{back} are the heat convection coefficients for the front and back surfaces of the PV panel in $\text{W m}^{-2} \text{K}^{-1}$, and T_{pv} and T_{amb} are the PV panel and the ambient temperatures, respectively.

The convection coefficients are a mixture of both forced and free convections. They differ in velocity, air temperature, and geometry of the PV panel. In this research, not much attention was paid to forced convection. On the contrary, free convection is the main focus of attention. Free convection coefficients are derived from the base of a heated inclined plate for the entire range of Rayleigh numbers that were assigned to the Nusselt number (Nu). All equations were provided by [24].

2.2. Heat Dissipation Rate by Radiation, Q_{rad} . Q_{rad} is the degree to which the PV panel gives off heat. It relies on the emissivity of the PV panel as well as the temperature gradient between the PV panel and the environment. As for horizontal surfaces, the radiation heat transfer between the front and back surfaces of the panel and the surroundings was represented by the following:

$$\begin{aligned} Q_{\text{rad,front}} &= A \times \sigma \times \varepsilon_{\text{pv}} \times \left((T_{\text{pv}} + 273.15)^4 - (T_{\text{sky}} + 273.15)^4 \right), \\ Q_{\text{rad,back}} &= \frac{A \times \sigma \times \left((T_{\text{pv}} + 273.15)^4 - (T_{\text{ground}} + 273.15)^4 \right)}{1/\varepsilon_{\text{pv}} + 1/\varepsilon_{\text{ground}} - 1}. \end{aligned} \quad (2)$$

As for the tilted panels, the net heat, which is dissipated through radiation, was among the panel, the sky, and the ground and was given by the following:

$$\begin{aligned}
Q_{\text{rad,front}} &= A * \sigma * \left\{ \left(\epsilon_{\text{pv}} * (T_{\text{pv}} + 273.15)^4 \right) \right. \\
&\quad - \left(\frac{(1 + \cos\varnothing)}{2} * \epsilon_{\text{sky}} * (T_{\text{sky}} + 273.15)^4 \right) \\
&\quad \left. - \left(\frac{(1 - \cos\varnothing)}{2} * \epsilon_{\text{ground}} * (T_{\text{ground}} + 273.15)^4 \right) \right\}, \\
Q_{\text{rad,back}} &= A * \sigma * \left(\epsilon_{\text{pv}} * (T_{\text{pv}} + 273.15)^4 \right) \\
&\quad - \left(\frac{(1 + \cos\varnothing)}{2} * \epsilon_{\text{ground}} * (T_{\text{ground}} + 273.15)^4 \right) \\
&\quad - \left(\frac{(1 - \cos\varnothing)}{2} * \epsilon_{\text{sky}} * (T_{\text{sky}} + 273.15)^4 \right), \tag{3}
\end{aligned}$$

where σ is the Stefan-Boltzmann constant at $5.67 \times 10^{-8} \text{ W m}^{-2} \text{ K}^{-4}$, PV is the panel's emissivity, and ϵ_{pv} is considered to be 0.9. Here, the sky's temperature of 15 K is lower than the ambient temperature and the ground temperature is presumed to be 10°C warmer than the ambient temperature.

2.3. Fin Design. The degree of heat transfer could be escalated through expanding the surface where convection takes place. This can be achieved through the application of fins, which stretch from end to end on the backside of the PV panel. The fin material's thermal conductivity could have a considerable impact on the circulation of temperature across the fin. Ideally, the fin material should possess a high level of thermal conductivity in order to diminish the variations in temperatures from top to bottom.

2.4. Selection of Fins' Shape. The fins' configurations were selected based on a few parameters such as weight, space, and cost. On one hand, fins can have simple designs such as rectangular, triangular, parabolic, annular, and pin shapes. On the other hand, fins' design can be complicated such as spiral shapes. In this study, rectangular fins were selected from three known and easy-to-install configurations. These configurations were (i) rectangular fins, (ii) parabolic fins, and (iii) pin fins. Table 1 shows the results of that calculation where each fin design produced a different efficiency; based on these results, the rectangular fin shape was selected.

The rectangular fin shape allows airflow in one direction only; if the air blows from a transverse direction, the fin will create high drag on the panel and will negatively affect the heat transfer. To overcome the flow direction problem, a perforated fin was used. Perforations in the rectangular fin allow the air to flow in all directions and reduce the amount of material used in the fin, thus making it lighter in weight. Perforated, lighter-weight fins are cheaper and exert less stress on the panel.

The perforated fin is shown in Figure 1. Under natural convection conditions, a perforated fin dissipated more heat than an identical solid fin. Perforated fins achieve better heat transfer than solid fins. In addition, light permeable fins reduce the cost of the fin material compared to solid fins. Furthermore, using a large number of permeable fins leads

TABLE 1: Fin efficiency based on design type.

Design	Efficiency (η)
Rectangular fin	84%
Parabolic fin	78.4%
Pin fin	81.5%

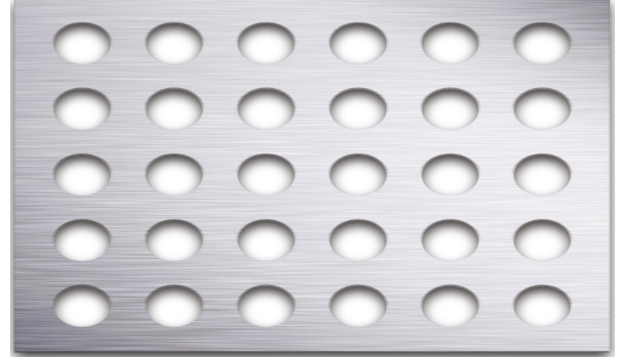


FIGURE 1: A perforated fin that was attached to the backside of a PV panel to act as a heat sink and to reduce the PV panel's temperature.

to an increase in the Nusselt number [25]. The permeable nature of perforated fins leads to a larger heat loss and a drop in the PV panel's temperature due to air passing through the fins freely. The fin's area, pores' area, and fin's weight were all calculated.

The fin's heat transfer rate was assessed using the q_{fin} rule on the fin's base as shown in equations (4)–(6) [24].

$$q_{\text{fin}} = M \frac{\sinh(mL) + (h/mk) * \cosh(mL)}{\cosh(mL) + (h/mk) * \sinh(mL)}, \tag{4}$$

$$M = \sqrt{hPkA_c} \theta_b, \tag{5}$$

$$m = \sqrt{\frac{hP}{kA_c}}, \tag{6}$$

$$\theta_b = T_{\text{base}} - T_{\infty}. \tag{7}$$

Fins were utilized to boost the heat transfer from a particular surface by expanding the surface area. Nevertheless, the fins installed were resistant to heat transfer through conduction from the designated surface. Therefore, any increase in the heat transfer rate could not be guaranteed. To address this issue, fin efficacy, ϵ_f , had to be evaluated. Accordingly, fins' effectiveness can be defined as the proportion of the heat transfer rate with fins to the heat transfer rate without the use of fins [24].

$$\epsilon_f = \frac{q_{\text{fin}}}{hA_{c,b} \theta_b}, \tag{8}$$

where $A_{c,b}$ is the fin's cross-sectional area at the base. The results of the fins' effective calculations are shown in Table 2.

TABLE 2: Calculations of the fins' effectiveness.

Area of PV panel	0.156 m ²
Ambient temperature	25°C
Heat convection coefficient (h_{lower})	3.06 W m ⁻² K ⁻¹
Length of the fin (l)	0.15 m
Width of the fin (w)	0.31 m
Thickness of fin (t)	0.001 m
Material's thermal conductivity (k)	237 W m ⁻¹ K ⁻¹
Number of fins	21
Finned area	1.56 m ²
Unfined area	0.15 m ²
Heat rate from the finned area (q)	110.8 W
Heat rate from the unfined area (q)	10.117 W
Backside temperature of PV panel	47°C
Fin's cross-sectional area (A_{cs})	0.00031 m ²
The effectiveness of fin (ϵ_f)	11.455
The efficiency of the fin (η)	84.2%

2.5. Selection of Fins' Material. There were many factors considered when selecting the fins' material to guarantee maximum heat conduction through the fins. Those factors involved weight, thermal conductivity, and cost. Table 3 shows the benefits and drawbacks of three main and available materials: iron, aluminium, and copper; based on the table, aluminium was preferred to the other materials because of its good thermal conductivity, light weight, and medium cost. Therefore, a rectangular aluminium fin was designed.

3. Experimental Setup

The experimental investigation aimed at evaluating the PV panel after having been fitted with heat-extraction fins and later with fins and repurposed materials, as illustrated in Figure 2. The new PV cooling system's effects on the electrical performance of a PV panel and its efficiency were assessed. The PV panel's electrical performance is commonly determined according to the standard test conditions (STC) that correspond to 1000 W m⁻² and 25°C cell temperature, with a reference solar spectral irradiance called Air Mass 1.5, as defined in IEC 60904-3 [26]. The testing conditions, including the nominal operating cell temperature (NOCT), STC, high-temperature condition, and low irradiance condition, together with irradiance and temperature measurement procedures are determined by this standard. Controlled indoor test conditions were preferred to fluctuations in temperature and to enable the repeatability of tests. A solar simulator was used to mimic solar irradiance for the indoor testing.

3.1. Solar Simulator. A locally designed solar simulator, shown in Figure 3(a), was utilized covering an area of 2 × 2 m² using thirty-six 1000 W tungsten halogen lamps with a colour temperature of 3000 K.

3.2. PV Panel. A 30 W PV panel, shown in Figure 3(b), was first tested as is in the solar simulator. Then, it was fitted with aluminium perforated fins, as illustrated in Figure 3(c) (before attaching the fins) and in Figure 3(d) (after attaching the fins). Later, repurposed materials were added to the fin-fitted PV panel. The thermal behaviour was evaluated at the three stages to determine the fins' effects on the PV panel's temperature and efficiency, first without and then with repurposed materials. The data collected was used as a reference to compare the thermal and electrical behaviour of the PV panel at the different stages.

3.3. PV Analyser. The PVA-1000 PV Analyser Kit is a 1000-volt I - V curve tracer designed by Solmetric Corp., as shown in Figure 3(e). It has integral performance modelling and excellent wireless irradiance, and it detects tilt and temperature. This device can achieve measurement throughput along with accuracy. Both the I - V curve (current vs. voltage) and P - V curve (power vs. voltage) were measured using this device, and then a comparison was made between the measured results and the anticipated performance in terms of irradiance and PV panel temperature when carrying out the I - V measurement. The I - V unit communicated with the data acquisition computer wirelessly.

3.4. Measuring and Monitoring Devices. The ambient temperature, as well as the PV panel's temperature, was measured through the application of a Type K thermocouple (SE029) exposed junction and a 0.2 mm PTFE insulated twisted pair conductor. The thermocouples were positioned on the item's surface to measure its temperature. Consequently, the measured temperature was a mixture of the surface and the ambient temperatures. The measurements of the thermocouples were automatically recorded via a Pico Technology Environment Quad Temperature Converter together with a Pico Technology Environment DataLogger. The distribution of thermocouples is shown in Table 4. The device used to measure radiation was a silicon cell pyranometer (SP-212) with ±5% accuracy. The measurements of the pyranometer were automatically recorded by a Pico Technology Environment DataLogger.

4. Results and Discussion

All measurements were conducted in a laboratory setting to mimic the behaviour of the sun on a typical day; when the sun rises, its irradiance is low and when it is at its hottest, its irradiance reaches its peak and then starts to decrease until it diminishes. Hence, the PV panel was placed under the solar simulator with 500 W m⁻² irradiance to simulate solar radiation in the morning (8 a.m.). The solar simulator's temperature started to rise gradually, and as it became stable, the irradiance of the solar simulator was adjusted to 750 W m⁻², late morning (10 a.m.). Similarly, when the temperature was stable once again, the irradiance was adjusted to 1000 W m⁻², noon (12 p.m.). Once the temperature reached a steady state, the irradiance was adjusted back to 750 W m⁻², afternoon (2 p.m.). Finally, irradiance was dropped to 500 W m⁻², late afternoon (4 p.m.). All

TABLE 3: Merits and demerits of common fins' materials.

	Advantages	Disadvantages
Aluminium	Relatively lightweight material (density = 2702 kg m^{-3}) Corrosion-resistant material Relatively high thermal conductivity Flexible and easy-to-install material	Relatively high cost
Copper	A high thermal conductivity of $401 \text{ W m}^{-1} \text{ K}^{-1}$ Corrosion-resistant material	Relatively heavyweight material (density = 8933 kg m^{-3}) High cost
Iron	Low cost	Relatively low thermal conductivity Corrosive material Heavyweight material (density = 7870 kg m^{-3})

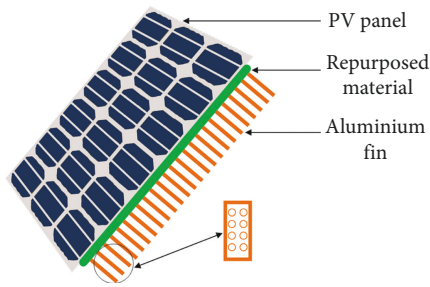


FIGURE 2: Schematic of a PV panel fitted with repurposed materials and fins.

tests were conducted under identical conditions and no wind speed.

4.1. As-Is PV Panel. The surface temperature and the output power of the PV panel measurements were recorded at different trials and consistently resulted in similar outcomes. The PV panel's surface temperature increased with the rise in solar irradiance until it reached a steady maximum of 106°C at 1000 W m^{-2} . As expected, the PV panel's output power increased with the increase in solar irradiance. Figure 4(a) shows the PV panel's temperature consistency over three trials, and Figure 4(b) shows the average surface temperature and the average output that were used for comparison.

4.2. Modified PV Panel. The PV panel was fitted with perforated aluminium fins as illustrated in Figure 3(d), and the thermal and electrical properties were measured. 19 cylindrical shaped wraps of ground HDPE grains weighing 70 mg each with an average diameter and height of 4.07 mm and 3.24 mm , respectively, were stuffed between the backside of the PV panel and the fins; two wraps are shown in Figure 5(a) before attachment to the PV panel. Plastic bags (PBs), as shown in Figure 5(b), were folded in a way that closely resembles the HDPE wraps and replaced HDPE wraps to evaluate their thermal and electrical effects on the PV panel.

The results in Figure 6 show that a significant drop in temperature occurred when the PV panel was modified. The as-is PV panel's surface temperature dropped by 23%, 22.7%, and 22% for the PV panel modified with fins, fins+HDPE, and fins+PBs, respectively, at a solar irradiance of 1000 W m^{-2} . Inversely, the as-is PV panel's output power

increased with the cooling modifications by 11.5%, 12.1%, and 11.6% for the PV panel modified with fins, fins+HDPE, and fins+PBs, respectively, at a solar irradiance of 1000 W m^{-2} . For the other solar irradiance values, the trend was similar for the PV panel's surface temperature. As for the output power, the highest increase was recorded at 1000 W m^{-2} and was maintained, albeit at lower percentages, as the solar irradiance values dropped. As expected, less heat was received at lower solar irradiance values reducing the increase in output power compared to that observed at the maximum irradiance of 1000 W m^{-2} .

The certainty and reproducibility analyses were considered. The maximal difference in temperature measurements between the tests was 1.7°C , and the relative error between them was 1.6%. As a result, no corrections were required to determine the fins' effects on temperature. The maximum error for the measured PV panel was 2.4% with a maximum relative uncertainty of 0.32.

4.3. The Efficiency of As-Is and Modified PV Panels. The efficiency was calculated according to equation (9). The three different modifications that were applied to the PV panel all yielded higher efficiency than the unmodified one. The highest increase in efficiency was recorded at a solar irradiance of 1000 W m^{-2} where the as-is PV panel's measured efficiency was 8.67%, while the efficiency of the cooled PV panel with fins+PBs was 9.67% as shown in Figure 7. The highest overall efficiency, 10.15%, was measured at the morning solar irradiance of 500 W m^{-2} for the PV panel cooled with fins+HDPE. The efficiencies of the modified PV panels dropped as time went by, and solar irradiance values changed because the additives had retained some of the heat from the PV panel itself, essentially rendering them as thermal storage additives. Yet with that aforementioned decrease in efficiency, the modification aided in the reduction of the PV panel's surface temperature and resulted in higher efficiencies for all cooling cases.

$$\eta_{\max} = \frac{P_{\max}}{GA_c} \quad (9)$$

5. Conclusions

The PV panels' conversion of solar radiation into electricity decreases with the rise in the panels' temperature. Therefore,

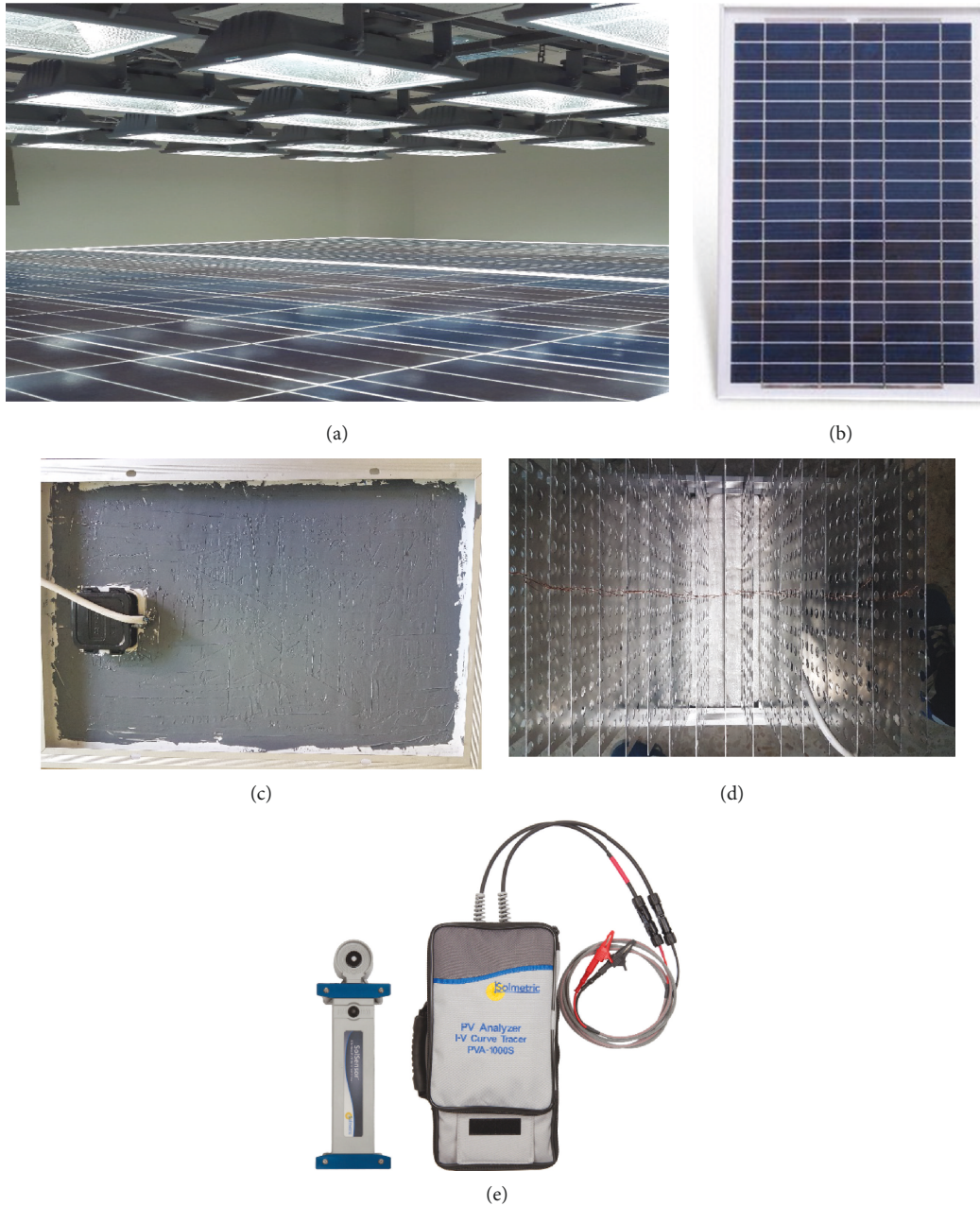


FIGURE 3: (a) Solar simulator, (b) PV panel used, (c) backside of the PV panel with paste for fin installation, (d) installed perforated aluminium fins, and (e) PV analyser.

TABLE 4: Distribution of thermocouples.

Thermocouple	Location
A	Ambient temperature
B, C	Backside temperature
D, E	Surface temperature
F	Frame temperature
J	Fin temperature
K	Repurposed materials temperature

it is important to cool PV panels to maintain their rated conversion efficiencies. In this study, a hybrid passive cooling system was proposed that consisted of aluminium heat-extraction fins along with repurposed materials, i.e., HDPE and plastic bags. Recycling is not always an option, so repurposing certain materials can reduce nonbiodegradable waste and cool down PV panels.

The results obtained showed that modifying a PV panel with fins and repurposed materials reduced the temperature of the panel and increased its efficiency. Different solar irradiance values using a solar simulator, in a controlled laboratory setting, were utilized to mimic the sun's behaviour on a typical day. The highest temperature drop of 23.7°C at

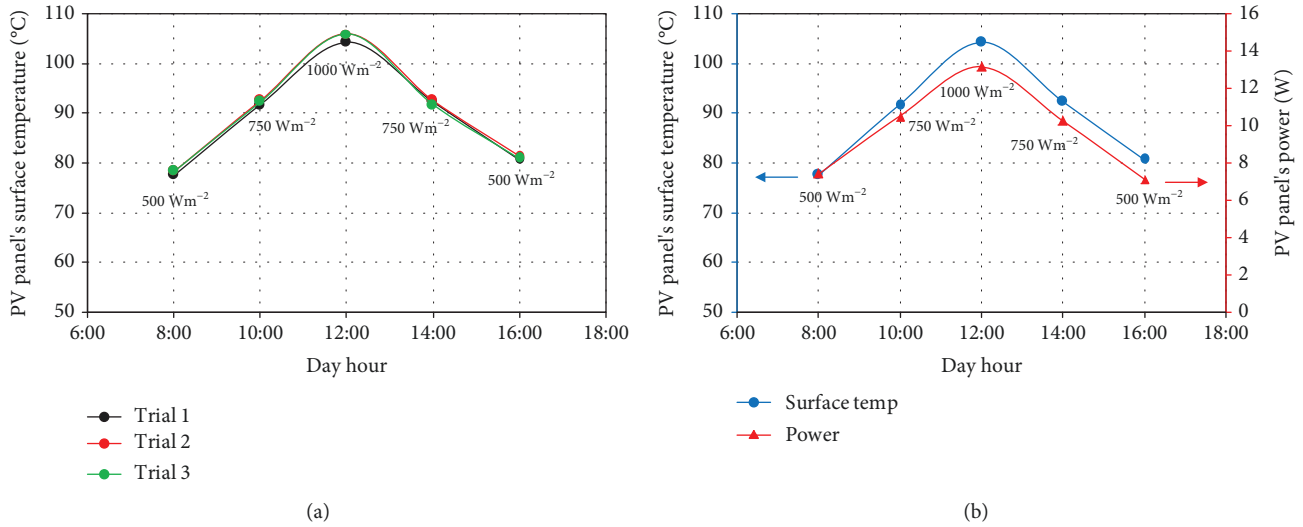


FIGURE 4: Measurement of the PV panel at three different solar irradiances to simulate morning, late morning, noon, afternoon, and late afternoon (a) surface temperatures of three trials and (b) average surface temperature and average output power.



FIGURE 5: Additives to the PV panel between its backside and the installed fins: (a) HDPE grain wraps and (b) folded plastic bags.

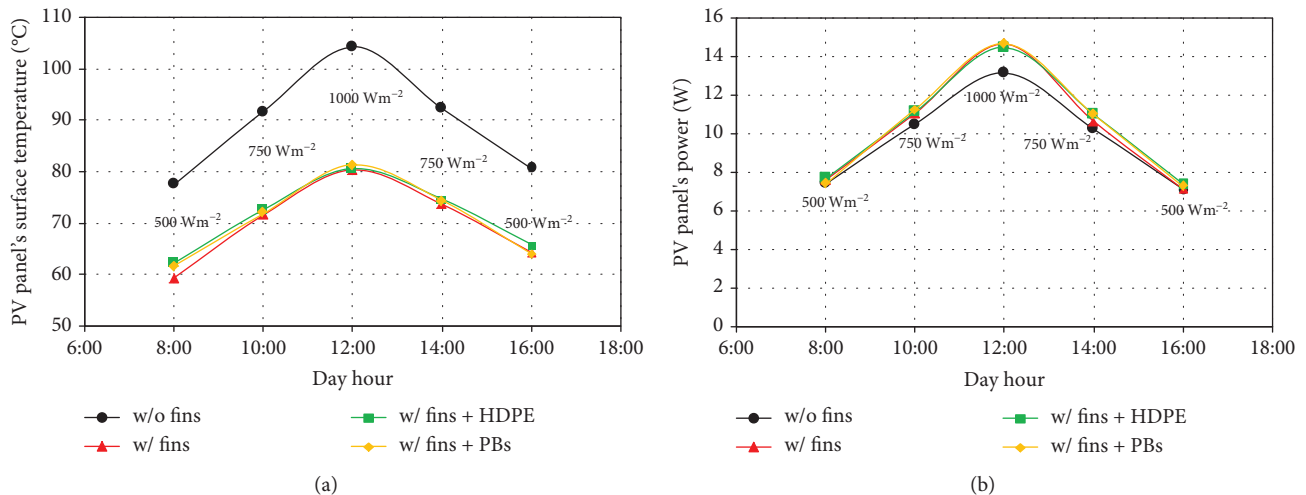


FIGURE 6: Comparison of results for the as-is PV panel and the PV panel modified using fins, fins+HDPE, and fins+PBs for (a) a PV panel's surface temperature and (b) a PV panel's output power.

1000 W m⁻² was observed when the PV panel was cooled with fitted fins and HDPE grain wraps. The highest output power was attained at 1000 W m⁻² when the PV panel was cooled with fitted fins and folded plastic bags showing a rise of 11.6%. Lastly, the highest efficiency increase was recorded at 1000 W m⁻² when fitted fins and folded plastic bags were used to cool down the PV panel; all those values were com-

pared to the PV panel's measurements prior to making cooling modifications.

Passively cooling PV panels can effectively reduce their temperatures and enhance their thermal and electrical performance. Using repurposed materials that can otherwise be harmful to the environment if thrown away reduces the cost of raw cooling materials; at the same time passive

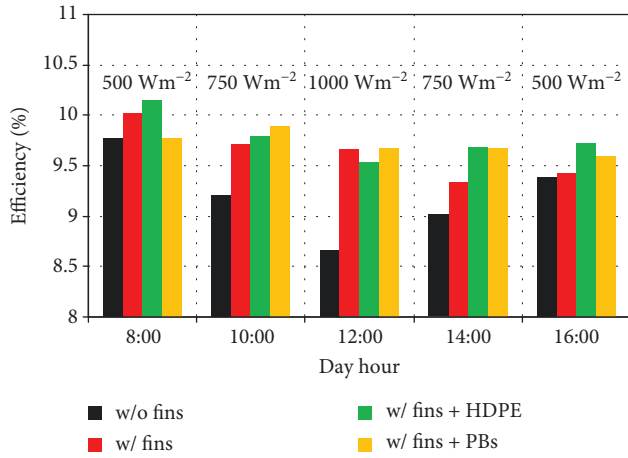


FIGURE 7: Measure efficiencies of the PV panel with no fins, fins, fins +HDPE, and fins+PBs.

cooling requires no energy input for the cooling process. The main drawbacks to the utilization of this repurposed material-based system are the collection of those materials before disposal and the possible labour cost of installation. However, if those disadvantages are addressed, the new PV panel cooling system could prove to be an important step in maintaining the rated efficiency and reducing negative environmental impact.

Nomenclature

A :	Surface area of PV panel (m ²)
A_c :	Cross-sectional area of fin (m ²)
$A_{c,b}$:	Cross-sectional area of the fin at the base (m ²)
η_{\max} :	PV panel's maximum efficiency
ε_f :	Fin's effectiveness
$\varepsilon_{\text{ground}}$:	PV panel emissivity
ε_{pv} :	Ground emissivity
G :	Incident solar irradiance (W m ⁻²)
h :	Conventional heat transfer coefficient around the fin (W m ⁻² K ⁻¹)
h_{front} :	Heat convection coefficient of the front of the PV panel (W m ⁻² K ⁻¹)
h_{back} :	Heat convection coefficient of the back of the PV panel (W m ⁻² K ⁻¹)
HDPE:	High-density polyethylene
k :	Fin material's thermal conductivity (W m ⁻² K ⁻¹)
L :	Fin's length (m)
P :	Fin parameter (m)
P_{\max} :	PV panel's maximum power output (W)
PV:	Photovoltaic
PCM:	Phase change material
\varnothing :	PV panel's tilt angle (°)
Q_{conv} :	Heat dissipation through convection (W)
$Q_{\text{conv,front}}$:	Q_{conv} of the front of the PV panel (W)
$Q_{\text{conv,back}}$:	Q_{conv} of the back of the PV panel (W)
q_{fin} :	Fin's heat transfer rate rule
Q_{rad} :	Heat dissipation through radiation (W)
$Q_{\text{rad,front}}$:	Q_{rad} of the front of the PV panel (W)

$Q_{\text{rad,back}}$:	Q_{rad} of the back of the PV panel (W)
T_{amb} :	Ambient temperature (K)
T_{base} :	Fin's base temperature (K)
T_{ground} :	Ground temperature (K)
T_{co} :	Room temperature (K)
T_{pv} :	PV panel temperature (K)
T_{sky} :	Effective sky temperature (K)
σ :	Stefan-Boltzmann's constant ($5.67 \times 10^{-8} \text{ W m}^{-2} \text{ K}^{-4}$).

Data Availability

The measured data used to support the findings of this study are included within the article.

Conflicts of Interest

The authors declare that there is no conflict of interest regarding the publication of this paper.

References

- [1] X. Yang, L. Sun, Y. Yuan, X. Zhao, and X. Cao, "Experimental investigation on performance comparison of PV/T-PCM system and PV/T system," *Renewable Energy*, vol. 119, pp. 152–159, 2018.
- [2] M. Hasanuzzaman, A. B. M. A. Malek, M. M. Islam, A. K. Pandey, and N. A. Rahim, "Global advancement of cooling technologies for PV systems: a review," *Solar Energy*, vol. 137, pp. 25–45, 2016.
- [3] F. M. Montagnino, "Solar cooling technologies. Design, application and performance of existing projects," *Solar Energy*, vol. 154, pp. 144–157, 2017.
- [4] S. Preet, "Water and phase change material based photovoltaic thermal management systems: a review," *Renewable and Sustainable Energy Reviews*, vol. 82, pp. 791–807, 2018.
- [5] M. C. Browne, B. Norton, and S. J. McCormack, "Phase change materials for photovoltaic thermal management," *Renewable and Sustainable Energy Reviews*, vol. 47, pp. 762–782, 2015.
- [6] B. Sunden and Z. Wu, "On heat transfer issues for wind energy systems," *Journal of Energy Resources Technology*, vol. 139, no. 5, pp. 51201–51201–5, 2017.
- [7] R. Masci and E. Scubba, "A lumped thermodynamic model of gas turbine blade cooling: prediction of first-stage blades temperature and cooling flow rates," *Journal of Energy Resources Technology*, vol. 140, no. 2, p. 20901, 2018.
- [8] K. Vincent Wong, "Anthropogenic heat generation and heat exhaust to the ultimate sink," *Journal of Energy Resources Technology*, vol. 139, no. 3, article 34701, 2017.
- [9] H. Chen, X. Chen, S. Li, and H. Ding, "Comparative study on the performance improvement of photovoltaic panel with passive cooling under natural ventilation," *International Journal of Smart Grid and Clean Energy*, vol. 3, pp. 375–379, 2014.
- [10] A. El Mays, R. Ammar, M. Hawa et al., "Improving photovoltaic panel using finned plate of aluminum," *Energy Procedia*, vol. 119, pp. 812–817, 2017.
- [11] F. Grubišić-Čabo, S. Nižetić, D. Čoko, I. Marinić Kragić, and A. Papadopoulos, "Experimental investigation of the passive cooled free-standing photovoltaic panel with fixed aluminum

- fins on the backside surface,” *Journal of Cleaner Production*, vol. 176, pp. 119–129, 2018.
- [12] M. A. Al-Nimr, S. Kiwan, and H. Sharadga, “Simulation of a novel hybrid solar photovoltaic/wind system to maintain the cell surface temperature and to generate electricity,” *International Journal of Energy Research*, vol. 42, no. 3, pp. 985–998, 2018.
- [13] R. Stropnik and U. Stritih, “Increasing the efficiency of PV panel with the use of PCM,” *Renewable Energy*, vol. 97, pp. 671–679, 2016.
- [14] S. Sharma, A. Tahir, K. S. Reddy, and T. K. Mallick, “Performance enhancement of a building-integrated concentrating photovoltaic system using phase change material,” *Solar Energy Materials & Solar Cells*, vol. 149, pp. 29–39, 2016.
- [15] A. Hasan, S. J. McCormack, M. J. Huang, J. Sarwar, and B. Norton, “Increased photovoltaic performance through temperature regulation by phase change materials: materials comparison in different climates,” *Solar Energy*, vol. 115, pp. 264–276, 2015.
- [16] M. J. Huang, P. C. Eames, B. Norton, and N. J. Hewitt, “Natural convection in an internally finned phase change material heat sink for the thermal management of photovoltaics,” *Solar Energy Materials & Solar Cells*, vol. 95, no. 7, pp. 1598–1603, 2011.
- [17] A. Hasan, J. Sarwar, H. Alnoman, and S. Abdelbaqi, “Yearly energy performance of a photovoltaic-phase change material (PV-PCM) system in hot climate,” *Solar Energy*, vol. 146, pp. 417–429, 2017.
- [18] M. Chandrasekar, S. Suresh, T. Senthilkumar, and M. Ganesh karthikeyan, “Passive cooling of standalone flat PV module with cotton wick structures,” *Energy Conversion and Management*, vol. 71, pp. 43–50, 2013.
- [19] S. Wu and C. Xiong, “Passive cooling technology for photovoltaic panels for domestic houses,” *International Journal of Low-Carbon Technologies*, vol. 9, no. 2, pp. 118–126, 2015.
- [20] T. S. Safi and J. N. Munday, “Improving photovoltaic performance through radiative cooling in both terrestrial and extra-terrestrial environments,” *Optics Express*, vol. 23, no. 19, article A1120, 2015.
- [21] D. Sato and N. Yamada, “Review of photovoltaic module cooling methods and performance evaluation of the radiative cooling method,” *Renewable and Sustainable Energy Reviews*, vol. 104, pp. 151–166, 2019.
- [22] B. Zhao, M. Hu, X. Ao, N. Chen, and G. Pei, “Radiative cooling: a review of fundamentals, materials, applications, and prospects,” *Applied Energy*, vol. 236, pp. 489–513, 2019.
- [23] A. Alkhalidi, L. Qoaidar, A. Khashman, A. R. Al-Alami, and S. Jiryas, “Energy and water as indicators for sustainable city site selection and design in Jordan using smart grid,” *Sustainable Cities and Society*, vol. 37, pp. 125–132, 2018.
- [24] T. L. Bergman, A. S. Lavine, F. P. Incropera, and D. P. DeWitt, *Fundamentals of Heat and Mass Transfer*, John Wiley & Sons, 2011, <http://books.google.com/books?id=vvyIoXEywMoC&pgis=1>.
- [25] B. A/K Abu-Hijleh, “Enhanced forced convection heat transfer from a cylinder using permeable fins,” *Journal of Heat Transfer*, vol. 125, no. 5, p. 804, 2003.
- [26] R. Arndt and R. Puto, “Basic understanding of IEC standard testing for photovoltaic panels. TUV SUD America Inc.,” 2015, <http://www.tuvamerica.com/services/photovoltaics/articlebasicunderstandingpv.pdf>.

Research Article

Preparation of Nano-Ag-TiO₂ Composites by Co-60 Gamma Irradiation to Enhance the Photocurrent of Dye-Sensitized Solar Cells

Le Thanh Nguyen Huynh ^{1,2}, Viet Hai Le,³ Thanh Long Vo,¹ Thi Kim Lan Nguyen,⁴ Quoc Hien Nguyen ⁴ and Thai Hoang Nguyen ^{1,2}

¹Department of Physical Chemistry, Faculty of Chemistry, VNUHCM-University of Science, Ho Chi Minh City, Vietnam

²Applied Physical Chemistry Laboratory, VNUHCM-University of Science, Ho Chi Minh City, Vietnam

³Faculty of Materials Science and Technology, VNUHCM-University of Science, Ho Chi Minh City, Vietnam

⁴Research and Development Center for Radiation Technology, Vietnam Atomic Energy Institute (VAEI), Ho Chi Minh City, Vietnam

Correspondence should be addressed to Thai Hoang Nguyen; nthoang@hcmus.edu.vn

Received 19 February 2019; Revised 21 April 2019; Accepted 16 May 2019; Published 12 June 2019

Guest Editor: Petru A. Cotfas

Copyright © 2019 Le Thanh Nguyen Huynh et al. This is an open access article distributed under the Creative Commons Attribution License, which permits unrestricted use, distribution, and reproduction in any medium, provided the original work is properly cited.

Nano-silver-titanium dioxide (Ag-TiO₂) composites were prepared from commercial TiO₂ (P25, Degussa) and silver nitrate (AgNO₃) by gamma Co-60 irradiation method with various initial concentrations of AgNO₃. The nano-AgTiO₂ composites are utilized as the photoanode for dye-sensitized solar cells (DSCs). Under full sunlight illumination (1000 W/m², AM 1.5), the efficiency of DSCs has improved significantly despite the Ag content of below 1%. The DSC— assembled with 0.75 Ag-TiO₂ (0.75% Ag) photoanode— showed that the photocurrent was significantly enhanced from 8.1 mA.cm⁻² to 9.5 mA.cm⁻² compared to the DSCs using bared TiO₂ photoanode. The unchanged open-circuit voltage resulted in the overall energy conversion efficiency to be increased by 25% from 3.75% to 4.86%. Electrochemical impedance spectroscopy (EIS) analysis showed that the charge transfer resistance is reduced when increasing Ag content, demonstrating that the charge transfer at TiO₂/dye interface was enhanced in the presence of silver nanoparticles.

1. Introduction

Research and application of new energy resources are essential approaches to reduce dependence on fossil fuels, and solar energy is considered one of the feasible solutions to solve the world's energy crisis. Dye-sensitized solar cells (DSCs) have promised to replace conventional silicon-based solar cells in the context of using clean solar energy due to their low cost, massive production, and facile process. Thus, DSC technology has been an attractive approach for the large-scale solar panel [1–5]. In DSCs, the cell architecture comprises nanostructured TiO₂ photoanode as an electron conductor, a dye Ru-complex as a light absorber, a redox shuttle for dye regeneration, and a counter electrode to collect electrons and reduce positive charges generated through the cell [1]. Commonly, the

DSCs showed efficient solar energy-to-electricity conversion of 10% [1, 6].

Many approaches have been studied to alternately improve the conversion efficiency of DSCs, including researching the novel counter electrode, electrolytes, dyes, and semiconductor photoanode materials. Among these, the photoanode plays a decisive part in determining the performance of cells [1, 7–9]. Many semiconductor materials have been studied to be used as photoanode in DSCs such as TiO₂, ZnO, SnO₂, Nb₂O₃, and SrTiO₃. In particular, TiO₂ has been universally used due to its chemical stability, excellent charge transport capability, low cost, and easy preparation [2, 10, 11]. In DSCs, TiO₂ plays three roles: (i) providing a substrate for dye adsorption, (ii) accepting electrons from the dye's excited state, and (iii) transporting the electrons from conduction band of TiO₂ to the conducting

substrate then to the external circuit [11, 12]. TiO_2 possesses a wide bandgap energy in both common structures: anatase at 3.2 eV and rutile at 3.0 eV. To improve the solar energy-to-electricity conversion efficiency, the surface of TiO_2 are modified with metallic ions such as Fe^{3+} and Zn^{2+} , alternatively, metallic nanoparticles such as Au, Ag, and Pt [3, 9, 10, 13, 14]. Study incorporation of Ag nanoparticles onto TiO_2 surface showed that the coupling of semiconductor and metal nanoparticles might yield a photoinduced electron transfer across the interface, which in turn may lead to the increased energy conversion efficiency of DSCs [11, 15–17]. Most of the previous reports showed the enhancement of efficiencies (4.86%) due to the plasmonic effect of Ag nanoparticles at high content (>2.5%) [8]. Many methods have been reported to prepare Ag- TiO_2 composite such as microwave-assisted sol-gel techniques [18], a microwave-hydrothermal technique [19], and UV irradiation [20]. Gamma irradiation has been well known as an effective method due to its simple preparation, massive produce, high efficiency, and eco-friendliness [14, 16, 21].

In this work, we prepared nano-Ag- TiO_2 composites at low Ag content (<1%) via Co-60 gamma irradiation. The nano-Ag- TiO_2 composites were used to prepare the photoanodes for DSCs. The role of Ag on the photoperformance of DSCs were investigated by the current-voltage method and the electrochemical impedance spectroscopy.

2. Experimental

2.1. Materials. TiO_2 (P25, Degussa), AgNO_3 (99.9%, Sigma-Aldrich), two types of ethyl cellulose (EC) powders (5–15 mPa·s and 30–50 mPa·s, Sigma-Aldrich), ethanol (95%, Sigma-Aldrich), and terpineol (anhydrous 99.9%, Sigma-Aldrich) were commercially available. Fluorine-doped tin oxide (FTO-TEX-8X, $15 \Omega/\text{cm}^2$) conductive glass substrates (Dyesol, Australia), electrolyte solution HPE (Dyesol, Australia), ruthenium complex dye N719 (Dyesol, Australia), and platinum paste PT1 (Dyesol, Australia) were used to fabricate the cathode of the DSCs.

2.2. Preparation of Nano-Ag- TiO_2 Composites. 4.00 g TiO_2 was dispersed in 20 mL solution of ethanol and distilled water (1/1, v/v) by magnetic stirring for 30 minutes; then, the solution was vibrated by ultrasound for 30 minutes. 10 mM AgNO_3 solution was added to the colloidal solution with the various weight ratios of Ag: TiO_2 . The mixtures were irradiated via the gamma-radiation from a Co-60 irradiator in the dose range of 10–30 kGy with a dose rate of 1.3 kGy per hour (VINAGAMMA Center, Ho Chi Minh City). Table 1 details the volume of AgNO_3 solution, the weight ratios of Ag: TiO_2 , and the dose of gamma-radiation. The irradiated colloidal solutions were centrifuged with speed up 10,000 rpm for 30 minutes to collect the powders; then, the final products were dried in air at 60°C overnight.

2.3. Fabrication of DSCs. DSCs (an active area of 0.2 cm^2) were assembled following our process in previous reports with four steps [22–24].

TABLE 1: Preparation of Ag- TiO_2 samples by gamma irradiation.

Sample	V_{AgNO_3} (mL)	m_{TiO_2} (g)	Ratio of Ag: TiO_2 (% weight)	Dose γ -irradiation (kGy)
0.25 Ag- TiO_2	9.3	4.0	0.25	13.7
0.50 Ag- TiO_2	18.5	4.0	0.50	20.4
0.75 Ag- TiO_2	27.8	4.0	0.75	27.3

2.3.1. Ag- TiO_2 Printing Paste Preparation. The Ag- TiO_2 printing paste is composed of Ag- TiO_2 (20% wt.), ethyl celluloses (10% wt.), and terpinol (70% wt.). 4.50 g EC (5–15 mPa·s) and 3.50 g EC (30–50 mPa·s) was dissolved in absolute ethanol to form 10% EC solution. 0.40 g nano-Ag- TiO_2 composites and 1.40 g terpineol were added to 2.00 g EC solution. The mixture was sonicated in three steps, each for 30 minutes. The final solution was heated in a vacuum oven at 40°C for 10 hours to remove the ethanol and water.

2.3.2. Photoanode Ag- TiO_2 Preparation. The FTO glass, as a current collector, was first cleaned in a detergent solution via ultrasonic for 15 minutes, and then rinsed with distilled water and ethanol. The FTO glass was soaked into a 40 mM TiCl_4 solution at 70°C for 30 minutes and re-washed with distilled water and ethanol. The Ag- TiO_2 paste with a thickness of 12–14 μm was coated on FTO substrate by using screen-printed method. After screen-printing, these coated electrodes were heated at 500°C under airflow for 30 minutes to form the Ag- TiO_2 photoanode.

2.3.3. Platinum Cathode Preparation. The FTO glass was treated in 0.1 M HCl in ethanol in an ultrasonic bath for 15 minutes and washed with acetone. The platinum cathode on the FTO substrate (Pt/FTO) was prepared by the screen-printing method using platinum paste PT1. The cathode Pt/FTO was annealed at 450°C for 30 minutes.

2.3.4. DSC Assembly. Both electrodes were arranged into sandwich-type cells by using a ply of melted surlyn at 190°C for 30 seconds. The dye solution (10 mM N719 in DMF) was injected successively into the cells through a hole in the back of platinum cathode, soaking in 4 hours and removing the DMF solvent. The cell was cleaned with acetonitrile for three times before being injected with electrolyte. The hole was then sealed using a quick-drying adhesive. The DSC assembly was performed in a nitrogen-filled glove-box to avoid oxygen and water.

2.4. Structural Characterization. The crystalline structures of nano-Ag- TiO_2 composites were characterized by X-ray diffractometer D8 Advanced (Bruker, Germany) with a copper anode ($\lambda K\alpha = 1.54 \text{ \AA}$). The XRD patterns were acquired in the 2θ range of 20°–80° (0.02° per second). The particle size of nano-Ag- TiO_2 was analyzed by transmission electron microscopy (TEM) images on a TEM 1400 (JEOL, Japan). The UV-vis spectra of nano-Ag- TiO_2 composites were recorded on a UV-vis spectrophotometer (Jasco-V630,

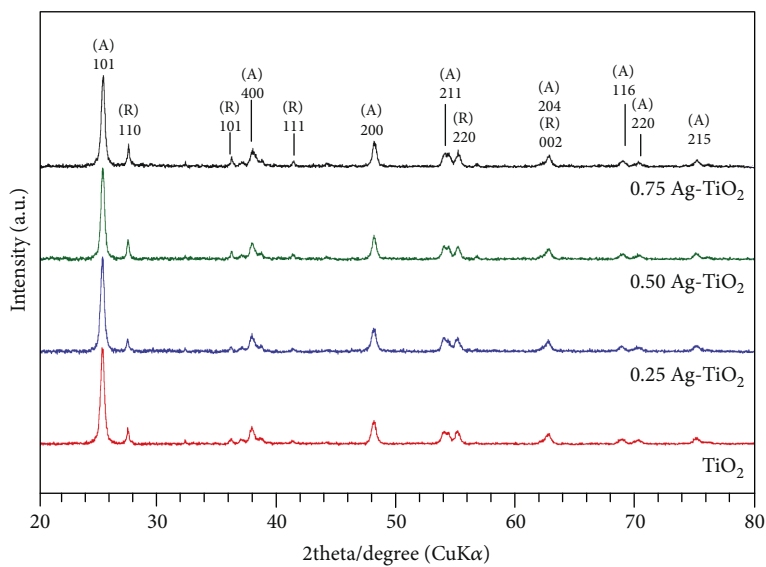


FIGURE 1: XRD patterns of nano-Ag-TiO₂ composites.

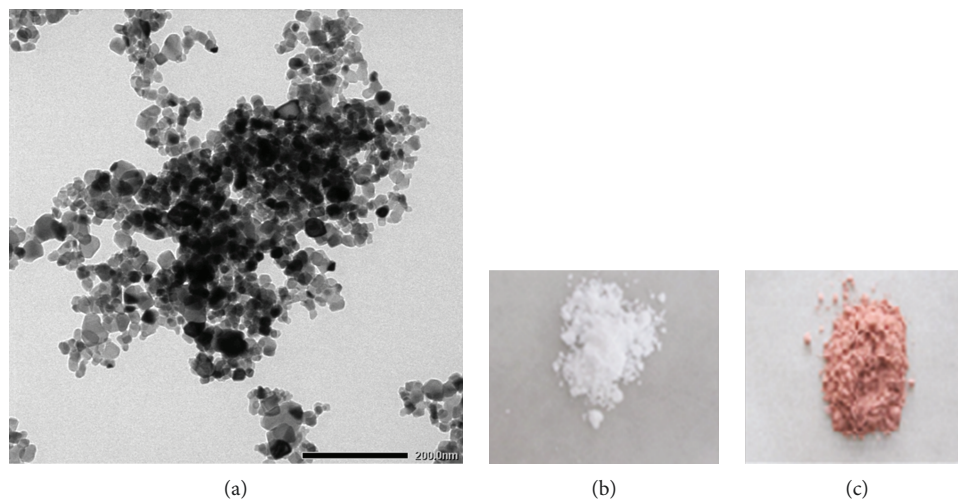


FIGURE 2: (a) TEM image of 0.75 Ag-TiO₂ composite. Digital photo of TiO₂ (b) and 0.75 Ag-TiO₂ composite (c).

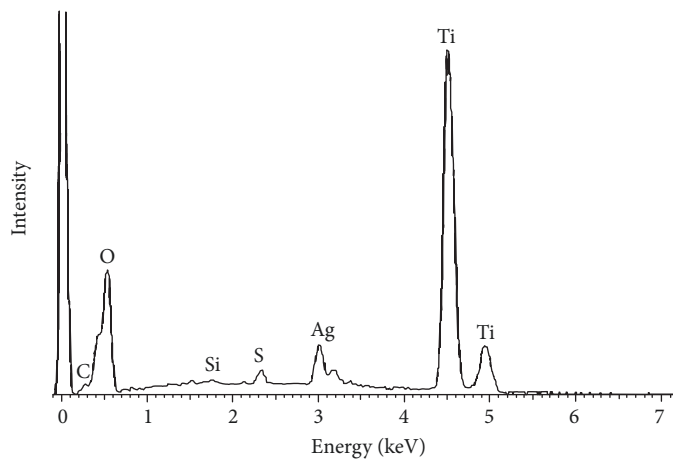
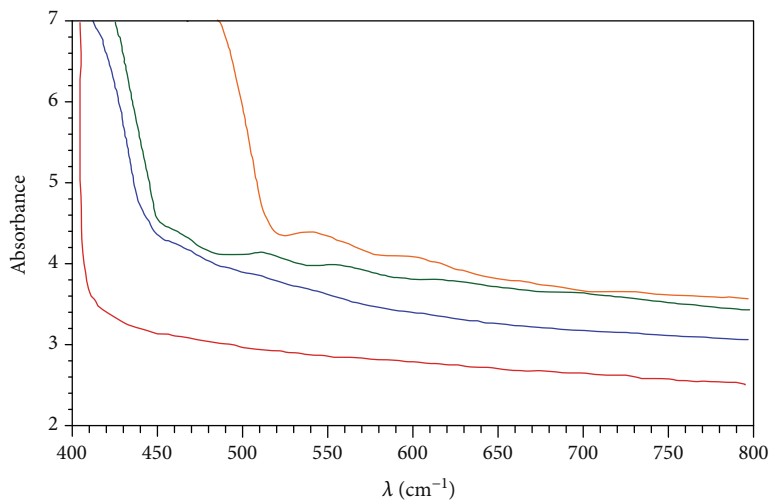
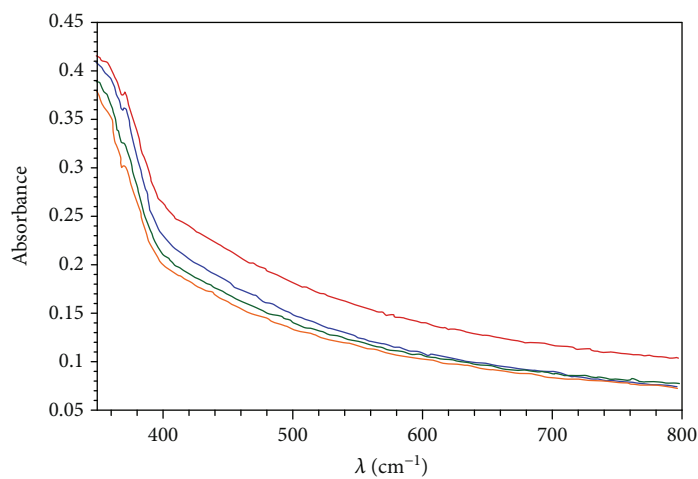


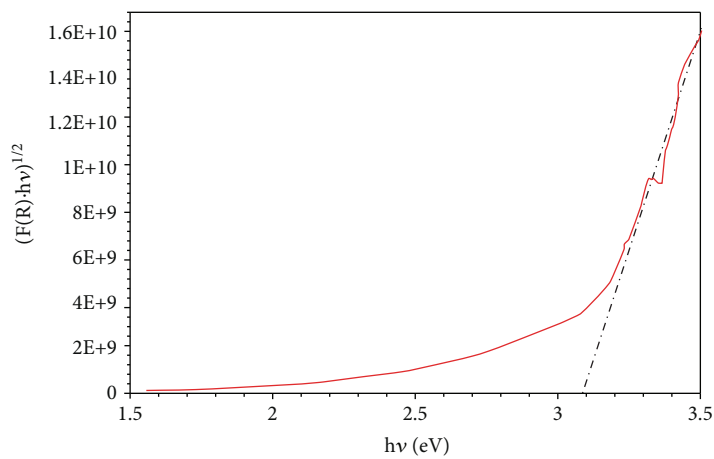
FIGURE 3: EDS patterns of nano 0.75 Ag-TiO₂ composite.



(a)



(b)



(c)

FIGURE 4: UV-vis absorption spectra of (a) the as-prepared nano-Ag-TiO₂ composites in powder. (b) Ag-TiO₂ photoanode films and (c) Kubelka-Munk plot for TiO₂ photoanode film.

Japan). The chemical composition of the materials was analyzed by EDS method using HITACHI S-4800 FE-SEM/EDS instrument.

2.5. I-V Characterizations. The photovoltaic characteristics (*I-V*) of the cells were recorded by Keithly 2400 source meter. The light source was a solar simulator from a 450 W halogen lamp with an infrared filter (AM 1.5). The incident light intensity was 1000 W/m² calibrated with a standard Si solar cell. Electrochemical impedance spectroscopy (EIS) of DSCs was carried out by an AUTOLAB 302N apparatus (Ecochemie, Netherlands) in the frequency range of 0.1 Hz-100 kHz and under illuminations of 1000 W/m².

3. Results and Discussion

3.1. Structural Characterization of Nano-Ag-TiO₂ Composites. Figure 1 illustrates the XRD patterns of commercial TiO₂ (Degussa P25) and nano-Ag-TiO₂ composites. All diffraction peaks can be indexed in the anatase phase (Tetragonal, space group *I41/amd*) and rutile phase (Tetragonal, space group *P42/mnm*). Structural conservation of TiO₂ indicates that the γ -irradiation with Co-60 irradiator does not affect the crystalline structure of TiO₂ as well as the ratio of anatase phase and rutile phase. No diffraction peak of Ag was observed in XRD patterns of the Ag-TiO₂ samples due to the low content of Ag nanoparticles (below 1%). To determine the existence of Ag nanoparticles in composites, other techniques (TEM, EDS, and UV-VIS) were applied.

Figure 2 exhibits the TEM images of the nano 0.75 Ag-TiO₂ composite. We observed the well-defined TiO₂ nanoparticles (bright color) in the range 10-25 nm and the nano-Ag (dark color) on the background of TiO₂ particles. The EDS pattern of 0.75 Ag-TiO₂ (Figure 3) composite powder confirms the existence of Ag on the composite.

Figure 4(a) shows the UV-vis spectra of the samples in powder. We observed that the band-edge absorption of nano-Ag-TiO₂ composites shifted towards the red wavelength (redshift) and the plasmon resonance effect of the silver nanoparticles appeared in the range of wavelength 500-550 nm. The results verified the formation of nano-Ag on TiO₂ by the gamma Co-60 irradiation. Based on the Kubelka-Munk plot, the bandgap energy (E_g) of nano-Ag-TiO₂ composite in powder (Table 2) dropped slightly as compared to TiO₂ ($E_g = 3.1$ eV) following the increase of Ag content.

Following the fabricating process of photoanodes, nano-Ag-TiO₂ composites were calcinated at 500°C for 30 minutes. We keep track of the photoproperties of photoanodes, with the UV-vis spectra visible in Figure 4(b). The UV-vis spectra of photoanodes in Ag-TiO₂ changed significantly. The disappearing of the plasmonic effect in nanosize, as well as the blueshift, was observed due to the agglomeration of Ag nanoparticles after the annealing process. The calculated bandgap of the four photoanodes was approximated in 3.1 eV. Many researches indicated the role of plasmon resonance effect of Ag nanoparticles to increase the performance of DSCs

TABLE 2: Bandgap energy (E_g) of the as-prepared nano-Ag-TiO₂ composites in powder and Ag-TiO₂ photoanode films, calculated by the Kubelka-Munk plot.

	Bandgap (eV)	
	As-prepared nano-Ag-TiO ₂ composites	Ag-TiO ₂ photoanode films
TiO ₂	3.1	3.1
0.25 Ag-TiO ₂	3.1	3.1
0.50 Ag-TiO ₂	3.0	3.1
0.75 Ag-TiO ₂	2.8	3.1

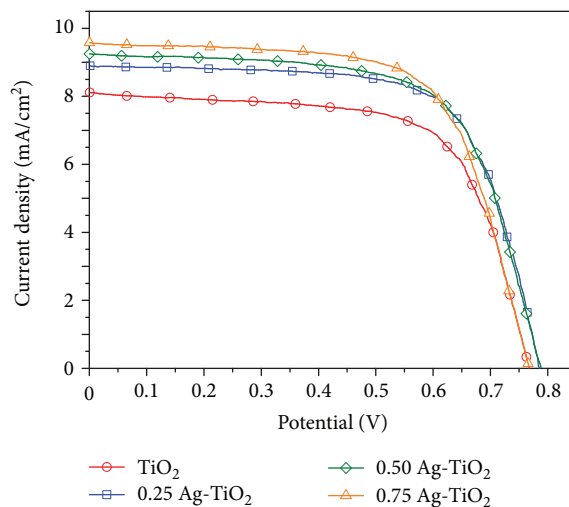


FIGURE 5: *I-V* curves of DSCs.

TABLE 3: Performance parameters of DSCs based on photoanodes nano-Ag-TiO₂ and TiO₂-P25.

Sample	V_{oc} (V)	I_{sc} (mA/cm ²)	FF	η (%)
TiO ₂	0.77	8.12	0.67	3.75
0.25 Ag-TiO ₂	0.79	8.90	0.67	4.83
0.50 Ag-TiO ₂	0.79	9.25	0.67	4.88
0.75 Ag-TiO ₂	0.77	9.56	0.64	4.86

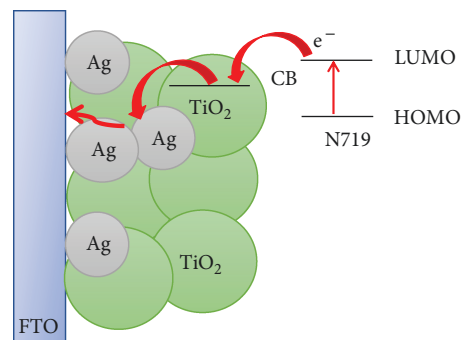


FIGURE 6: Electron transfer pathway in Ag-TiO₂ photoanode.

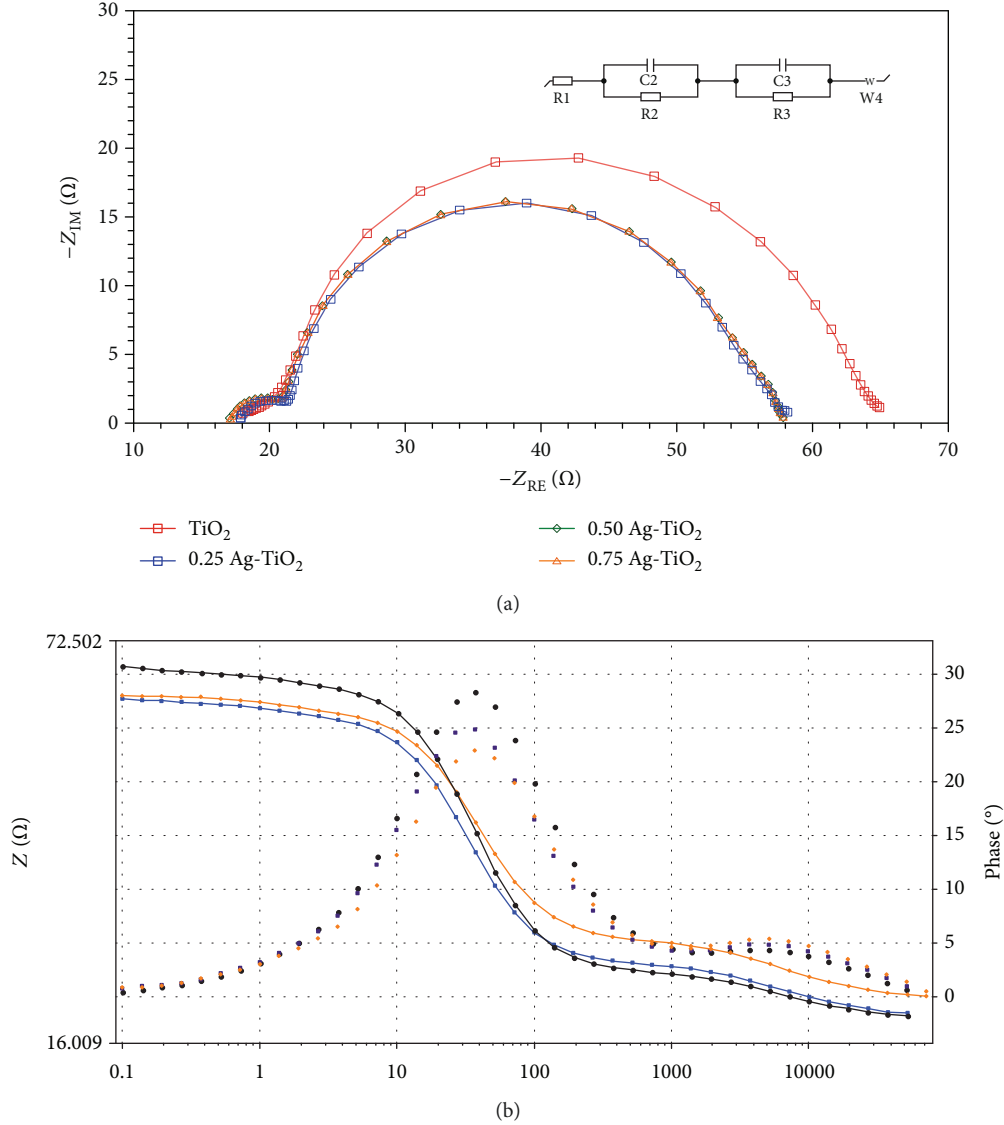


FIGURE 7: (a) Nyquist plot and (b) Bode-plot of DSCs based on photoanodes nano-Ag-TiO₂ and TiO₂-P25.

TABLE 4: Cathode charge transfer resistances (R_{ct}) and recombination resistances (R_r) of DSCs measuring at V_{oc} under 1 sun illuminate.

Sample	R_{Pt} (ohms)	R_r (ohms)	C_{μ} (μ F)	τ_n (mS)	f_{max} (Hz)
TiO ₂	2.9	43.1	210	7.4	37.3
0.25 Ag-TiO ₂	4.1	36.5	233	7.6	37.3
0.50 Ag-TiO ₂	4.5	36.6	230	7.2	37.3
0.75 Ag-TiO ₂	3.7	36.5	235	6.7	37.3

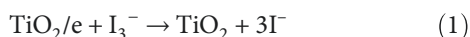
[11, 16, 19, 25]. The lack of plasmonic effect of low Ag content was detailed in DSCs Performance section.

3.2. DSCs Performances. We fabricated the DSCs using nano-Ag-TiO₂ composites as well as TiO₂-P25 as the photoanode and studied the photoperformance under the 1000 W/m² intensity light. The DSCs' performances' results

were gathered in Figure 5 and Table 3. The DSCs assembled from TiO₂-P25 photoanode receive a short-circuit current (I_{sc}) of 8.12 mA/cm², open-circuit voltage (V_{oc}) of 0.77 V, and fill factor (FF) of 67%; the overall photocurrent conversion efficiency (η) is calculated to be 3.75%. In the case of Ag-TiO₂ photoanodes, the photoperformance of DSCs essentially increased. It is noted that the open-circuit voltages (V_{oc}) were nearly unchanged and stabilized around 0.77 V, indicating that the energy structure of photoanodes (Fermi level) is unvaried. The short-circuit current (I_{sc}) enhanced gradually with the Ag content; particularly, the 0.75 Ag-TiO₂ photoanode exhibited the highest I_{sc} to 9.56 mA/cm² as compared to 8.12 mA/cm² with TiO₂-P25 photoanode. The photoefficiency (η) also improved significantly to 4.86%. We believed that the Ag nanoparticles at low content played as the electron-bridge between TiO₂ and the current collector FTO which limited the grain boundaries' effect across the TiO₂ matrix. We described the mechanism of photoelectron transfer of Ag-TiO₂ photoanodes in DSCs in

Figure 6. When the photoanodes Ag-TiO₂/N719 were illuminated under sunlight AM 1.5, N719 dye was excited and transformed to N719* following by ultra-fast electron injection from N719* to the conduction band (CB) of TiO₂ semiconductor. Due to the lower energy (Fermi level) of Ag-CB than TiO₂-CB, the photoelectrons can collect on Ag particles and transfer facilely in TiO₂ matrix to the current collector FTO. Moreover, the recombination of e_{CB}^- and h_{VB}^+ on TiO₂ particles can be restricted which also enhances the photocurrent in DSCs.

To clarify the role of Ag-TiO₂ photoanodes on the photoefficiency of DSCs, the electrochemical impedance spectroscopy (EIS) was performed at the V_{oc} under illuminations of 1000 W/m² in the frequency range of 0.1 Hz-100 kHz. The Nyquist plots and Bode plots are presented in Figure 7; the analysis of EIS spectra is detailed in Table 4. The equivalent circuit is given in the inset of Figure 7. The EIS spectra of DSCs in Nyquist plot (Figure 7(a)) show two semicircles, corresponding to two processes: (i) electron transfer in cathode platinum and (ii) electron transfer in TiO₂ network and from TiO₂-CB to triiodide in electrolyte *via* reaction (1), called recombination-process.



At high frequencies, we observed a negligible variation of electron transfer resistance (R_{Pt}) in cathode platinum. At intermediate frequencies, the recombination resistances (R_r) were decreased drastically (from 43.1 Ω for photoanode TiO₂ and 36.6 Ω for photoanodes Ag-TiO₂) that reveal the role of Ag electron-bridge to facilitate the electron transfer in TiO₂ network. According to the research of Wang et al. [4], the reducing recombination resistance R_r reflects the fast electron transfer in the photoanode whereby the photoperformances were beneficial. Moreover, the chemical capacitance of conduction band electron (C_{μ}) was also increased that indicated the electron lifetime (τ_n)—composed of resistance and capacitance ($\tau_n = R_r C_{\mu}$)—was slightly decreased. Furthermore, the characteristic frequency of R_r was stabilized at 37.3 Hz in Bode plots (Figure 7(b)), indicating stable free electron lifetime.

4. Conclusions

In conclusion, we demonstrate the direct preparation of nano-Ag-TiO₂ composites by the γ -irradiation method from a Co-60 irradiator and the Ag-TiO₂ showed a capability as photoanode in dye-sensitized solar cells. The DSCs—based on nano-0.75 Ag-TiO₂ composite photoanode—presented an encouraging performance with V_{oc} of 0.77 V, I_{sc} of 9.56 mA/cm², fill factor of 0.64, and photoefficiency of 4.86%. Studying the role of Ag by EIS, we observe only a reduction of recombination resistance in photoanode due to the formation of Ag electron-bridge that improves the electron transfer process but do not reduce electron lifetime.

Data Availability

The data used to support the findings of this study are included within the article.

Conflicts of Interest

The authors declare that there is no conflict of interest regarding the publication of this paper.

Acknowledgments

This research work was supported by Vietnam National University Ho Chi Minh City through grant number HS2015-18-01.

References

- [1] B. O'Regan and M. Grätzel, "A low-cost, high-efficiency solar cell based on dye-sensitized colloidal TiO₂ films," *Nature*, vol. 353, no. 6346, pp. 737–740, 1991.
- [2] T. Ma, M. Akiyama, E. Abe, and I. Imai, "High-efficiency dye-sensitized solar cell based on a nitrogen-doped nanostructured titania electrode," *Nano Letters*, vol. 5, no. 12, pp. 2543–2547, 2005.
- [3] X. Lü, X. Mou, J. Wu et al., "Improved-performance dye-sensitized solar cells using Nb-doped TiO₂ electrodes: efficient electron injection and transfer," *Advanced Functional Materials*, vol. 20, no. 3, pp. 509–515, 2010.
- [4] Y. F. Wang, J. H. Zeng, and Y. Li, "Silver/titania nanocable as fast electron transport channel for dye-sensitized solar cells," *Electrochimica Acta*, vol. 87, pp. 256–260, 2013.
- [5] R. Mori, T. Ueta, K. Sakai et al., "Organic solvent based TiO₂ dispersion paste for dye-sensitized solar cells prepared by industrial production level procedure," *Journal of Materials Science*, vol. 46, no. 5, pp. 1341–1350, 2011.
- [6] M. Grätzel, "Dye-sensitized solar cells," *Journal of Photochemistry and Photobiology C: Photochemistry Reviews*, vol. 4, no. 2, pp. 145–153, 2003.
- [7] Y. Li, M. Ma, W. Chen, L. Li, and M. Zen, "Preparation of Ag-doped TiO₂ nanoparticles by a miniemulsion method and their photoactivity in visible light illuminations," *Materials Chemistry and Physics*, vol. 129, no. 1-2, pp. 501–505, 2011.
- [8] S. P. Lim, A. Pandikumar, N. M. Huang, and H. N. Lim, "Enhanced photovoltaic performance of silver@titania plasmonic photoanode in dye-sensitized solar cells," *RSC Advances*, vol. 4, no. 72, pp. 38111–38118, 2014.
- [9] S. Ito, T. N. Murakami, P. Comte et al., "Fabrication of thin film dye sensitized solar cells with solar to electric power conversion efficiency over 10%," *Thin Solid Films*, vol. 516, no. 14, pp. 4613–4619, 2008.
- [10] Y. Duan, N. Fu, Q. Liu et al., "Sn-doped TiO₂ photoanode for dye-sensitized solar cells," *Journal of Physical Chemistry C*, vol. 116, no. 16, pp. 8888–8893, 2012.
- [11] W. Peng, Y. Zeng, H. Gong, Y. Leng, Y. Yan, and W. Hu, "Silver-coated TiO₂ electrodes for high performance dye-sensitized solar cells," *Solid-State Electronics*, vol. 89, pp. 116–119, 2013.
- [12] E. Schüler, A.-K. Gustavsson, S. Hertenberg, and K. Sattler, "Solar photocatalytic and electrokinetic studies of TiO₂/Ag

- nanoparticle suspensions,” *Solar Energy*, vol. 96, pp. 220–226, 2013.
- [13] E. Grabowska, A. Zaleska, S. Sorgues et al., “Modification of titanium(IV) dioxide with small silver nanoparticles: application in photocatalysis,” *Journal of Physical Chemistry C*, vol. 117, no. 4, pp. 1955–1962, 2013.
- [14] T. Harifi and M. Montazer, “Fe³⁺:Ag/TiO₂ nanocomposite: synthesis, characterization and photocatalytic activity under UV and visible light irradiation,” *Applied Catalysis A: General*, vol. 473, pp. 104–115, 2014.
- [15] H. Yu, S. Zhang, H. Zhao, B. Xue, P. Liu, and G. Will, “High-performance TiO₂ photoanode with an efficient electron transport network for dye-sensitized solar cells,” *Journal of Physical Chemistry C*, vol. 113, no. 36, pp. 16277–16282, 2009.
- [16] H. Zhang, G. Wang, D. Chen, X. Lv, and J. Li, “Tuning photoelectrochemical performances of Ag-TiO₂ nanocomposites via reduction/oxidation of Ag,” *Chemistry of Materials*, vol. 20, no. 20, pp. 6543–6549, 2008.
- [17] P. V. Kamat, “Manipulation of charge transfer across semiconductor interface. A criterion that cannot be ignored in photocatalyst design,” *Journal of Physical Chemistry Letters*, vol. 3, no. 5, pp. 663–672, 2012.
- [18] W. Tongon, C. Chawengkijwanich, and S. Chiarakorn, “Visible light responsive Ag/TiO₂/MCM-41 nanocomposite films synthesized by a microwave assisted sol-gel technique,” *Superlattices and Microstructures*, vol. 69, pp. 108–121, 2014.
- [19] Q. Xiang, J. Yu, B. Cheng, and H. C. Ong, “Microwave-hydrothermal preparation and visible-light photoactivity of plasmonic photocatalyst Ag-TiO₂ nanocomposite hollow spheres,” *Chemistry - An Asian Journal*, vol. 5, p. 1466, 2010.
- [20] F. Hossein-Babaei, M. M. Lajvardi, and F. A. Boroumand, “Large area Ag-TiO₂ UV radiation sensor fabricated on a thermally oxidized titanium chip,” *Sensors and Actuators A: Physical*, vol. 173, no. 1, pp. 116–121, 2012.
- [21] O. Tahiri Alaoui, A. Herissan, C. Le Quoc et al., “Elaboration, charge-carrier lifetimes and activity of Pd-TiO₂ photocatalysts obtained by gamma radiolysis,” *Journal of Photochemistry and Photobiology A: Chemistry*, vol. 242, pp. 34–43, 2012.
- [22] T. H. Nguyen, H. M. Tran, and T. P. T. Nguyen, “Application of electrochemical impedance spectroscopy in characterization of mass- and charge transfer processes in dye-sensitized solar cells,” *ECS Transactions*, vol. 50, no. 51, pp. 49–58, 2013.
- [23] T. H. Thanh, Q. V. Lam, T. H. Nguyen, and T. D. Huynh, “Performance of CdS/CdSe/ZnS quantum dot-sensitized TiO₂ mesopores for solar cells,” *Chinese Optics Letters*, vol. 11, no. 7, pp. 072501–072504, 2013.
- [24] N. V. Le, H. T. Nguyen, H. V. Le, and T. T. P. Nguyen, “Lead sulfide cathode for quantum dot solar cells: electrosynthesis and characterization,” *Journal of Electronic Materials*, vol. 46, no. 1, pp. 274–281, 2017.
- [25] S. P. Lim, Y. S. Lim, A. Pandikumar et al., “Gold-silver@TiO₂ nanocomposite-modified plasmonic photoanodes for higher efficiency dye-sensitized solar cells,” *Physical Chemistry Chemical Physics*, vol. 19, no. 2, pp. 1395–1407, 2017.